On the aerodynamics of a vertical axis wind turbine wake

An experimental and numerical study

Tescione, Giuseppe

DOI
10.4233/uuid:86ac7352-46b8-4c2d-9014-817472d80174

Publication date
2016

Document Version
Final published version

Citation (APA)
Tescione, G. (2016). *On the aerodynamics of a vertical axis wind turbine wake: An experimental and numerical study*. [Dissertation (TU Delft), Delft University of Technology].
https://doi.org/10.4233/uuid:86ac7352-46b8-4c2d-9014-817472d80174

Important note
To cite this publication, please use the final published version (if applicable).
Please check the document version above.

On the Aerodynamics of a Vertical Axis Wind Turbine Wake

An Experimental and Numerical Study

Giuseppe Tescione

On the Aerodynamics of a Vertical Axis Wind Turbine Wake

An Experimental and Numerical Study

On the Aerodynamics of a Vertical Axis Wind Turbine Wake

An Experimental and Numerical Study

Proefschrift

ter verkrijging van de graad van doctor
aan de Technische Universiteit Delft,
op gezag van de Rector Magnificus prof. ir. K.C.A.M. Luyben,
voorzitter van het College voor Promoties,
in het openbaar te verdedigen op dinsdag 25 oktober 2016 om 15:00 uur

door

Giuseppe Tescione

Laurea Magistrale in Ingegneria Aeronautica,
Università La Sapienza, Rome, Italy,
geboren te Rome, Italy.

Dit proefschrift is goedgekeurd door de

promotor: Prof. Dr. G.J.W. van Bussel
copromotor: Dr. C.J. Simão Ferreira

Samenstelling promotiecommissie:

Rector Magnificus,	voorzitter
Prof. Dr. G.J.W. van Bussel,	Technische Universiteit Delft
Dr. C.J. Simão Ferreira,	Technische Universiteit Delft
Onafhankelijke leden:	
Prof. Dr. S.G. Voutsinas	National Technical University of Athens
Prof. Dr. H.A. Madsen	DTU Wind Energy, Technical University of Denmark
Prof. Dr. T.A. Nygaard,	Norwegian University of Life Sciences
Dr. D. Micallef,	University of Malta
Prof. Dr. G. van Kuik,	Technische Universiteit Delft
Prof. Dr. S. Hickel,	Technische Universiteit Delft, reservelid

The research activity presented in this dissertation was performed in the Aerodynamics, Wind Energy and Propulsion department of the Faculty of Aerospace Engineering at the Delft University of Technology and was funded by the EU-FP7 DeepWind programme.

Printed by: Ridderprint, The Netherlands

Front & Back: Artistic render of the vorticity in the wake of a VAWT from PIV, by Anastasia Tsaparoglou.

ISBN 978-94-6299-462-1

This dissertation has been printed in recycled paper, saving 5kg of CO2 and 40kg of wood. Please consider the environment before printing; an electronic version is available at: http://repository.tudelft.nl/.

To my father, who taught me to open my eyes and to smile at life.
To my mother, who taught me to be patient and to give.

PREFACE

This book marks not only the end of my PhD at TUDelft, but also of my dutch experience. I would like to take advantage of this preface to acknowledge some people that contributed to the success of the first and to thank some other who made the latter a great experience.

First I'd like to thank who made all this possible. My promoter, Gerard, from whom I learned (I hope!) to be a better communicator and who helped me greatly in the last phase when I was getting lost and failing to see the path to the end. My co-promoter, Carlos, who believed in me at the beginning and who never ceased to challenge me to become an independent and better researcher. Thank you both for your support and dedication.

I'd like to thank my committee members who agreed with enthusiasm to the task and contributed to the final version with important feedback, and who, I am sure, will make the defense and interesting event. A special thank to Daniel, who went through every page meticulously and helped me to achieve a better text and a clearer content. I am glad you are going to be there at the end, considering that we were together at the start, sharing precious time inside and outside the wind tunnel. A big thank also to Nando who offered to translate my summary in dutch last minute, despite being very busy: I could not hope for a better man for the job!

In my years at the Wind Energy group of TUDelft and as an occasional visitor of the Aerodynamics group, first as a guest researcher then as a PhD, many people have shared with me coffees and rooms, long working days and pleasant trips, days out and Fridays beers, hours in front of monitors or in the wind tunnels. I would like to thank each and everyone of you, but I would surely forget someone, so I will not even try to. There are, however, some people I could never forget.

Daniele is surely the first I can think of; it is not a coincidence you end up often in acknowledgments of PhD thesis: you give without asking and without reserve. I am very much indebted to you for your support in and out of the wind tunnel, for your being a constant source of inspiration on how research should be made, and for being a good friend before an awesome colleague. My only regret is that our paths did not cross earlier, but I hope they will cross again in the future. To Ben and Busra, who were my first roomies and made me feel at home from the start: we had a great time, thank you and all the best for your future! Thanks to Lorenzo, Ricardo, Francesco, Jacopo, Artur and Lars because you made spending time inside the faculty a much more enjoyable experience and the time outside the faculty an even better one! To Sylvia I owe making my everyday life in the faculty much easier and much warmer, heel hartelijk bedankt!

Since being a PhD is not a full-time job, but a 24/7 state of being, I would not be writing this preface it it wasn't for many people supporting me beyond the University. Being a PhD in a country different from your own one, you need double the people to support you, and I was lucky to have them.

Alla mia famiglia, devo tantissimo. A mia madre e mio padre, a cui questa tesi é dedicata, non devo solo (semplicemente) chi sono, ma la forma piú altruista di amore: il supporto incondizionato nelle mie scelte, anche quando queste mi allontanano da loro. A mia sorella, devo un affetto infinito, pari solo alla mia stima per lei.

At the end of my dutch experience, although some left the Netherlands before I did, I can count a handful of people to whom I am grateful, for sharing with me the sometimes difficult experience of being abroad, and for making me feel at home. The first and most important is surely Andrea, my acquired brother who has been for me family here. You know, there is no need for words between us, or maybe just one: grazie! I also want to show my gratitude and my affection to Arianna, Alberto and Tanyi, Ricardo and Vicky, Diego and Mary, Nicoletta and Bob, Athina and Ciccio, Marco and Paola, Ivan and Giorgia, Maga, Dani, Artur and Efi. With some of you we share a long history, you made my early days in Delft and my late days in Rotterdam never lonely, always full and joyful.

Non posso non includere nei miei ringraziamenti chi ha rappresentato un punto fermo a Roma e mi ha dato forza e supporto da lontano, insieme alla consapevolezza che la distanza non é e non sará un ostacolo ad una profonda amicizia. Peppone, Fabrizio, Giorgio, Manuel, Daniele, Luca e Laura, per cui non esiste distanza in grado di separarci. Voi siete i primi che cerco ogni volta che torno, i primi a cui penso quando penso a casa, grazie!

My last paragraph is dedicated to Tia. For what you have endured in my last (nervous) years of my PhD, and for the support and the love you gave to me you should be a Doctor today as well. I was so lucky to find you and so lucky to have you, Manulaki!

Giuseppe Tescione
Munich,
few hours before sending to the prints,
October 2016

SUMMARY

THE recent trend in wind energy industry, with the increasing deployment of offshore wind farms, has revived the interest in the concept of a vertical axis wind turbine. The scientific, technological and economical challenges of the next generation of wind turbines indicate that a transformative approach is the key for the reduction of the cost of energy. The adaptation of current designs and practice may not be the best solution to face rotor up-scaling, wind farm losses, floating support structures and improved reliability.

In this context, the vertical axis wind turbine has the potential to respond to some of the new environment's challenges. The new interest has to face a lack of knowledge and proper models; the tendency to adapt both from the more developed horizontal axis wind turbine research field is often inaccurate.

This research addresses the aerodynamic phenomena in the wake of a vertical axis wind turbine. While past and present researchers have focused on the flow inside the rotor volume and how to proper model the blade loadings, what happens in the wake has been poorly explored. The result is the use of wake models from horizontal axis wind turbines, without considering the inherent differences the two systems bear.

The study combines an experimental and numerical approach, where the wake is analyzed in terms of the dominant vortical structures, their evolution and interactions. The use of a numerical model based on a vortex element method is then investigated with respect to the level of fidelity in representing the complex flow in the wake. Finally, the analysis is shifted to an up-scaled turbine and the energy available in its wake is compared to the case of an offshore horizontal axis wind turbine.

The experiments are performed with a stereoscopic particle image velocimetry to obtain detailed flow quantities in the wake of an H-shaped vertical axis wind turbine model. The measurement domain scans the flow in the horizontal symmetry plane and in several vertical planes in the cross-stream direction from the rotor volume up to three diameters downwind.

The analysis reveals the different vorticity dynamics happening in the horizontal and in the vertical planes. First, the vorticity shed by the blade as a result of the change in its circulation during the rotation, organizes in counter-rotating concentrated structures at the horizontal edges of the wake. The roll-up of such structures is triggered by the blade-wake interactions as the blade hits multiple previously shed wakes during its rotation. The resulting shed vortices create a stable system visible all through the measured domain.

In the vertical planes, vorticity trailed from the tip of the blades organizes in a complex system. A cycloidal vortex curve with a convex and a concave segment released by the blade in its upwind and downwind passage rapidly undergoes instability and breaks

down under the mutual induction of the two segments. The break down of the tip vortices triggers a vertical contraction of the wake and entrapment of the outer flow with a wake recovery.

The experiments also showed a high degree of asymmetry of the wake. Both in the horizontal and in the vertical direction the wake expansion is higher at the windward side, while a vertical contraction is observed in the central part of the wake.

Given the high vorticity content of the vertical axis wind turbine wake, the use of a numerical model based on vortex element methods has been investigated with a verification and validation analysis, comparing the simulated results to the experimental measurements. The model is capable of capturing the main vorticity dynamics and the induction levels are predicted with good accuracy up to three diameters.

The use of the validated numerical model allows to overcome the limitation of the experimental approach, increasing both the size and Reynolds number of the turbine and the extent of the measurements. An up-scaled 5-MW machine is investigated and its wake evolution is compared with the one of an equivalent horizontal axis wind turbine until six diameters downstream, at distances typical of wind farm deployment.

The kinetic energy available in the flow to a downwind turbine of same size placed at varying stream-wise and cross-stream positions has been evaluated for the two systems. In order to account for the high three-dimensionality of the flow in the wake of a vertical axis wind turbine and the lack of the cylindrical symmetry characterizing the horizontal axis wind turbine wake, a new method to evaluate equivalent velocity profile and kinetic energy content has been proposed valid for both systems.

The comparison showed an increase in the energy content for the vertical axis wind turbine case already after three diameters, thanks to the vertical contraction of the wake, and leading to a reduced stream-wise inter-turbine spacing in a wind farm scenario. At the same time a larger horizontal wake expansion is observed with an increased cross-stream turbine spacing.

The research contributes to improve the knowledge on the aerodynamics of vertical axis wind turbines, by identifying and documenting the dominant vorticity dynamics in the wake. It provides an aerodynamic database with local quantities for the validation of numerical models and shows the feasibility of a vortex element method approach for the numerical simulation. Furthermore, it compares the wake development to that of an equivalent horizontal axis wind turbine, showing the need of dedicated models for the wake study.

SAMENVATTING

ALS gevolg van de huidige trend in de windenergie-industrie, de voortschrijdende realisering van windparken op zee, is hernieuwde belangstelling ontstaan voor de toepassing van het verticale-as concept bij wind turbines. Bij verdergaande schaalvergroting is aanpassing van bestaande ontwerpen en ontwerppraktijk wellicht niet de juiste methode om problemen rond opschaling, windparkverliezen, drijvende ondersteuningsconstructies, verbeterde betrouwbaarheid en verlaging van de energieprijs het hoofd te kunnen bieden. De wetenschappelijke, technische en economische uitdagingen die het realiseren van een volgende generatie windturbines met zich mee brengt duiden op de noodzaak van een geheel andere aanpak met het oog op verdere verlaging van de energieprijs.

In potentie kan de toepassing van de verticale-as windturbine in deze situatie een oplossing zijn. De hernieuwde aandacht voor dit type turbines legt echter ook meteen een gebrek aan kennis en aan de juiste rekenmodellen bloot, welke niet zonder verlies aan nauwkeurigheid kunnen worden ontleend aan de onderzoeksresultaten rond de meer ontwikkelde horizontale-as wind turbine.

Het huidige onderzoek richt zich op de aerodynamische fenomenen in het zog van een verticale-as wind turbine. In het verleden is de aandacht van onderzoekers uitgegaan naar de stroming in het rotorvolume en naar de juiste voorspelling van bladbelastingen. Echter, wat er precies in het zog gebeurt is nog nauwelijks onderzocht. Het resultaat is dat er nu zogmodellen worden gebruikt, ontwikkeld voor horizontale-as turbines, zonder de wezenlijke verschillen van de twee type turbines in aanmerking te nemen.

Het onderzoek combineert een experimentele met een numerieke benadering, waarbij de ontwikkeling van de dominante wervelstructuren in het zog en hun interacties worden geanalyseerd. Vervolgens wordt een rekenmodel gebaseerd op een “vortex element method” onderzocht op de mate van betrouwbaarheid waarmee het model de complexe stroming in het zog kan representeren. Tenslotte richt de aandacht zich op de beschikbare energie in het zog van een opgeschaalde verticale-as turbine in vergelijking met dat van een offshore horizontale-as turbine.

Met “stereoscopic particle image velocimetry” zijn gedetailleerde metingen verricht van de stromingsparameters in het zog van een verticale-as turbinemodel met een H-vormige rotor. Het experiment omvat stromingsmetingen in het horizontale symmetrievlak en in diverse verticale vlakken loodrecht op de stroming gesitueerd tussen het rotorvolume en een locatie drie diameters stroomafwaarts. De analyse laat de verschillen in werveldynamiek zien die in het horizontale en het verticale vlak plaatsvindt. Allereerst ontstaan geconcentreerde contra-roterende structuren aan de horizontale randen van het zog uit door het blad afgeschudde wervels, die weer samenhangen met de verandering in circulatie ten gevolge van de rotatie van het blad. Gedurende de rotatie doorsnijdt het blad diverse reeds eerder afgeschudde zoggen, waardoor dit oprollen van de wervels

wordt versterkt. Het resultaat is een systeem van stabiele wervels dat in het hele stromingsveld stroomafwaarts zichtbaar is.

In het verticale vlak ontstaat een complex wervelsysteem gevoed door de tipwervels van de roterende bladen. Een cyclische tipwervelbaan komend van het stroomopwaartse blad interfereert met dat afgegeven door het blad als het zich stroomafwaarts bevindt. Door deze wederzijdse beïnvloeding worden de wervels opgebroken en ontstaat een verticale contractie van het zog, waarbij energie uit de buitenstroming wordt opgenomen.

Het experiment laat eveneens een grote asymmetrie van het zog zien. Zowel in horizontale als in verticale richting expandeert het zog meer aan de bovenwindse zijde, terwijl in het centrale deel van het zog een contractie in verticale richting zichtbaar is.

Gezien de hoge mate van wervelactiviteit in het zog is een numeriek model gebruikt gebaseerd op “vortex element” methoden, waarbij verificatie en validatie van de code heeft plaatsgevonden door de simulaties te vergelijken met de experimenteel verkregen waarden. De belangrijkste wervelactiviteiten worden door het model beschreven en de waarde van de inductie wordt met goede nauwkeurigheid voorspeld tot op een afstand van drie rotordiameters stroomafwaarts.

Een gevalideerd numeriek model kent niet de beperkingen van modelexperimenten, in termen van rotordiameter en te bereiken Reynoldsgetallen, zodat ook grote turbines kunnen worden bestudeerd. Zowel voor een opgeschaalde 5 MW verticale-as machine als voor een horizontale-as turbine met hetzelfde vermogen is een analyse gemaakt van de in de stroming aanwezige kinetische energie beschikbaar voor een even grote turbine die op diverse afstanden stroomafwaarts dan wel zijwaarts is opgesteld.

Om de grote mate van drie-dimensionaliteit van de stroming in het zog van een verticale as turbine en de afwezigheid van cilindrische symmetrie in dat van een horizontale-as turbine op een juiste manier in rekening te brengen wordt een nieuwe methode voorgesteld, waarmee voor beide machines het equivalente snelheidsprofiel en daarmee de kinetische energie in het zog kan worden berekend. Dankzij de verticale contractie van het zog laat de verticale-as turbine reeds een vergroting van de energie-inhoud zien na drie rotordiameters, zodat in een windpark de turbines stroomafwaarts dichterbij kunnen worden geplaatst. Echter, door de grotere horizontale expansie van het zog moet de afstand tot de zijwaarts geplaatste turbines groter zijn dan bij horizontale-as turbines.

Door de dominante wervelstructuren en hun interactie in het zog in kaart te brengen draagt deze studie bij tot een beter begrip van de stroming rond verticale-as turbines. Een data base met lokale stromingsgrootheden is beschikbaar gekomen waarmee numerieke modellen kunnen worden gevalideerd . De studie laat zien dat een vortex element methode geschikt is voor numerieke simulatie van de stroming in het zog van een verticale-as turbine. Tenslotte is het mogelijk gebleken de ontwikkeling van het zog van een verticale-as turbine te vergelijken met dat van een equivalente turbine met horizontale-as, waarbij de noodzaak van toegepaste zogmodellen is aangetoond.

CONTENTS

GLOSSARY

GREEK LETTERS

$\Delta\theta$	azimuth step.
λ	tip speed ratio, $\Omega R/V_\infty$.
$\alpha_{z0}(\theta)$	perceived angle of attack of the middle section of the blade.
μ	doublet singularity strength.
σ	source singularity strength.
ϕ	velocity potential.
ϕ_∞	undisturbed velocity potential.
Ω	rotational velocity.
$\vec{\omega}$	vorticity vector.
Γ_{TE}	circulation on the trailing edge segment.
γ	vortex filament strength.
γ_S	shed vorticity (wake filament).
γ_T	trailing vorticity (wake filament).
ϵ_R	simulation uncertainty on the velocity inside the rotor volume (constant).
$\epsilon_W(x)$	simulation uncertainty on the velocity inside the wake volume (function of downstream distance).
θ	azimuth angle.

LATIN LETTERS

$\mathcal{AR}$	Aspect Ratio, H/D.
A_F	Frontal area.
A_S	Swept area.
c	blade chord.
C_P	power coefficient.
C_T	thrust coefficient.
D	rotor diameter.
H	rotor height.
h	blade thickness.
M	Mach number.
N	number of blades.
$\vec{n}$	normal vector (to body/wake surface).
P_{rated}	rated power.
R	rotor radius.
Re_c	chord-based Reynolds number.
Re_{MAX}	max Reynolds number.
S_D	Area of a downwind turbine.

$\vec{s}$	trailing edge segment vector.
t	time.
$\vec{u}$	velocity vector (general form).
$\vec{u}_i$	induced velocity vector (general form).
V_∞	free-stream velocity.
V_{REL}	relative velocity (to the blade).
V_x	stream-wise velocity component.
V_y	cross-stream velocity component.
V_z	vertical velocity component.
x	stream-wise spatial coordinate.
X_D	center of a downwind turbine, in x.
y	cross-stream spatial coordinate.
Y_D	center of a downwind turbine, in y.
z	vertical spatial coordinate.

ACRONYMS

AoA	Angle of Attack.
BoS	Balance of System.
BVI	Blade-Vortex Interaction.
BWI	Blade-Wake Interaction.
CAPEX	Capital Expenditure.
CFD	Computational Fluid Dynamics.
CPAN	Chord-wise Panels.
DMST	Double-Multiple Streamtube Model.
EKE	Equivalent Kinetic Energy.
EVP	Equivalent Velocity Profile.
EWEA	European Wind Energy Association.
FOV	Field of View.
GPGPU	General Purpose GPU.
GPU	Graphic Processing Unit.
HAWT	Horizontal Axis Wind Turbine.
H-VAWT	H-shaped VAWT (straight blades).
LES	Large Eddy Simulation.
NACA	National Advisory Committee for Aeronautics.
NRC	National Research Council (of Canada).
NREL	National Renewable Energy Laboratory.
O&M	Operational & Maintenance.
OJF	TUDelft Open Jet Facility.
OOP	Object Oriented Programming.
OPEX	Operational Expenditure.
PIV	Particle Image Velocimetry.
SNL	Sandia National Laboratories.
SOWFA	Simulator for Offshore Wind Farm Applications.
SPAN	Span-wise Panels.

SPIV	Stereoscopic PIV.
SROT	Simulated Rotations.
VAWT	Vertical Axis Wind Turbine.
Φ-VAWT	Φ-shaped VAWT (curved blades, Troposkein or similar).
VEM	Vortex Element Method.

List of Figures

LIST OF TABLES

1

INTRODUCTION

THE rationale behind the research is presented in this chapter. The current wind energy trends and technological challenges and the role of vertical axis wind turbines are first introduced. A summary overview of the main elements of rotor flow and wake aerodynamics and of the history of research is then presented, highlighting the open issues and the unexplored topics which still characterize the field. Finally, the objective of the investigation with the research questions and the methodology used to answer them is addressed.

The chapter also includes a section describing the terminology used in order to clarify the following presentation of results and discussions and an outline of the dissertation.

1

1.1. VAWT IN PRESENT WIND ENERGY SCENARIO

Present trends in the wind energy industry show the development of offshore wind farms of multi-MW turbines in large clusters.

The first aspect is the growing development of offshore wind power. The marine environment offers higher capacity factors, with more strong and consistent winds, less turbulence and lower wind shear (Boyle, 2006). Moreover, onshore wind energy suffers from saturation effects and higher environmental impacts (Esteban *et al.*, 2011). In the first half of 2015, 2.3 GW of offshore wind power were installed in Europe; an increment of 100% from the same period the previous year, reaching a total capacity of 10.4 GW, over 7% of Europe total wind energy capacity[1] (Ho & Mbistrova, 2015).

The second aspect of such trend is the tendency to up-scaling. Recent studies showed that increasing the rotor size while reducing the induction factor leads to an increase in wind farm capacity factors (Chaviaropoulos *et al.*, 2014b). Moreover, the increase of rotor size of the turbine can lead to a decrease in Capital Expenditure (CAPEX)[2] and Operational Expenditure (OPEX)[3] per unit power in the offshore environment (Chaviaropoulos *et al.*, 2014a). The latest generation of wind turbines has rotor diameters (D) up to 180 m and rated capacity (P_{rated}) up to 8 MW[4]; while research is focusing on 10-20 MW machines (Sieros *et al.*, 2012), (Peeringa *et al.*, 2011), (Ceyhan & Grasso, 2014), (Chaviaropoulos *et al.*, 2014b), (Schepers *et al.*, 2015).

The third aspect is the creation of wind farms of larger sizes. The deployment of multiple turbines in clusters allows to decrease the BoS (foundations, installation, assembly, logistics, grid connection and development costs) and Operational & Maintenance (O&M) unit cost, in order to counteract the increase in CAPEX and OPEX of offshore wind energy. The past three years saw the construction of 5 wind farms with hundreds of wind turbines and a total power above 500 MW[5]; while plans for combined farms of 2.4+ GW have been proposed[6].

At the same time, offshore wind farm development trends towards farms built in deeper waters. Going beyond the current limit of 50 m of water depth for fixed substructure concepts will allow to expand the market in deeper seas, as the remaining 66% of the North Sea, the Mediterranean and the Atlantic basins in Europe, or the oceanic coasts of US, China, Japan, Latin America and India. Within these waters, floating sup-

[1] As a reference in 2001 offshore wind was 1.15% of annual wind power installed while in 2014 it reached 12.7% of annual installation (Corbetta & Mbistrova, 2015). Future scenarios by European Wind Energy Association (EWEA) see an offshore installed capacity of 40 GW in 2020 (4% of EU electricity demand) and a 150 GW offshore wind capacity in 2030 (meeting 14% of EU's total electricity consumption (Arapogianni & Genachte, 2013)).

[2] The reduction of CAPEX per unit power interests mainly the Balance of System (BoS) portion (assembly, transport & installations, and electrical infrastructure); for the turbine part the reduction with the up-scaling above a certain limit is subject to technological improvements (Sieros *et al.*, 2012).

[3] The reduction of OPEX is only achieved if failure rates and maintenance durations are not increased as well (Hofmann & Sperstad, 2014).

[4] E.g.: Adwen AD 8-180 [$D = 180m$, $P_{rated} = 8MW$]; Samsung S7-171 [$D = 171m$, $P_{rated} = 7MW$]; MHI Vestas V164 [$D = 164m$, $P_{rated} = 8MW$]; Siemens SWT-7.0-154 [$D = 154m$, $P_{rated} = 7MW$].

[5] London Array, UK, 630 MW (operational since 2012); Gemini, NL, 600 MW (expected by 2017); DGode Wind, GE, 582 MW (expected by 2016); Gwynt y Mor, UK, 576 MW (operational since 2015); Greater Gabbar, UK, 504 MW (operational since 2012).

[6] Bleking, SW, 2.5 GW; East Anglia 3&4, UK, 2.4 GW; Creyke Beck A&B, UK, 2.4 GW; Teeside A&B, UK, 2.4 GW.

port structures proved to be economically competitive (Arapogianni & Genachte, 2013), (Myhr *et al.*, 2014).

The development of large offshore wind farms of multi-MW (floating) turbines has made Vertical Axis Wind Turbines (VAWTs) recently gain new popularity in the wind energy community. Adapting onshore wind turbine design to the new offshore sites may not be economically viable and a new approach might be needed. VAWTs present great potential of cost reduction and advantages in areas (e.g. BoS, O&M, up-scaling, wind farm wake losses) critical for future offshore wind energy development (fig. 1.1). Several research projects in Europe and US focus on floating large VAWTs[7]. Preliminary results (Paquette & Barone, 2012) estimate a potential reduction in the cost of energy of 28% and 21% from a baseline fixed-bottom and floating Horizontal Axis Wind Turbine (HAWT).

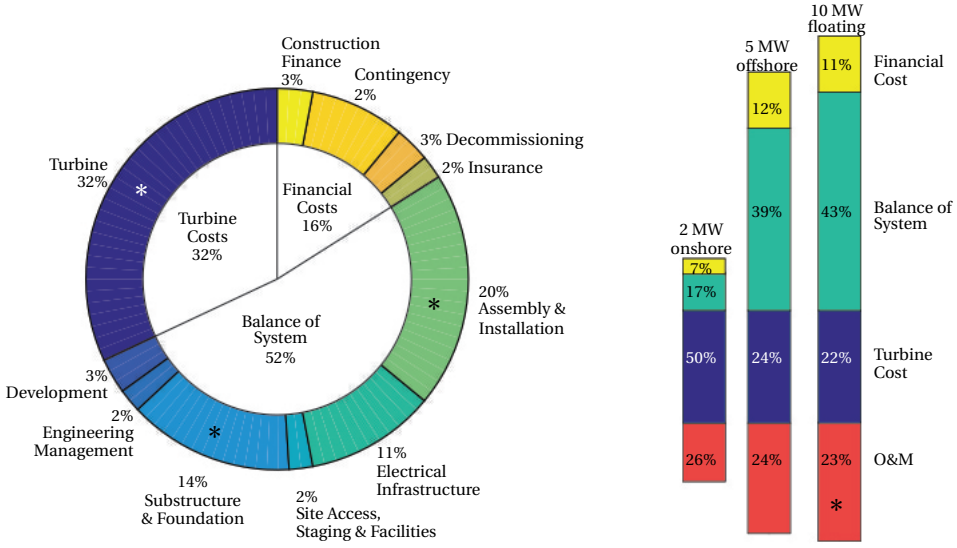

Figure 1.1: CAPEX breakdown for a typical offshore wind turbine (left) and contribution to the cost of energy for different classes of wind turbines (right). The asterisks highlight areas of potential cost reduction with the use of VAWT, data from Mone *et al.* (2015); Myhr *et al.* (2014); Paquette & Barone (2012).

Figure 1.2 highlights some of the advantages of the VAWT architecture over the HAWTs for (floating) offshore deployment. VAWTs have a simple mechanical design with no yaw or pitch mechanisms and no need for tapered and twisted blades. This leads to a reduction in production costs, rotor weight and especially O&M[8]. The vertical orientation of

[7] EU FP7 DeepWind (see Paulsen *et al.* (2013)), EU FP7 Inflow (with the predecessor VertiFlow and VertiWind), EU FP7 H2Ocean (see Borg *et al.* (2014)), Innovative Offshore VAWT Rotor by Sandia National Laboratories (see Fowler *et al.* (2014)), Aerogenerator X by WindPower Ltd. (see Blusseau & Patel (2012)), Spinfloat by Eolfi, SpinWind by Gwind, VertAX by Vertax Ltd., Skwid by Modec.

[8] The pitch and yaw systems combined account for a 33% failure rate and a 31% of total downtime in offshore

the shaft allows to place the heavy generator at sea level, lowering the center of gravity, decreasing the stress on the support structure, easing installation and access for maintenance. Moreover, VAWTs show a higher potential in overcoming some of the limits for HAWT up-scaling (Sieros *et al.*, 2012): the rotation around a vertical axis mitigates low-cycle fatigue from weight-induced loads, while the insensitivity to the wind direction avoids losses due to vertical yaw misalignment[9].

In addition, recent studies (Araya, 2016; Dabiri, 2011) hypothesized potential advantages of using VAWTs in a wind farm cluster as downwind turbines could experience an increased amount of energy in the flow in comparison with HAWTs. This could translate in lower wind farm wake losses [10], or in a smaller spacing of the cluster decreasing costs associated with grid connection or land use. The need to decrease wind farm losses has already led researchers and manufacturers to consider decreasing the power coefficient of single turbines to increase the capacity factor and power density of wind farms (Chaviaropoulos *et al.*, 2014b).

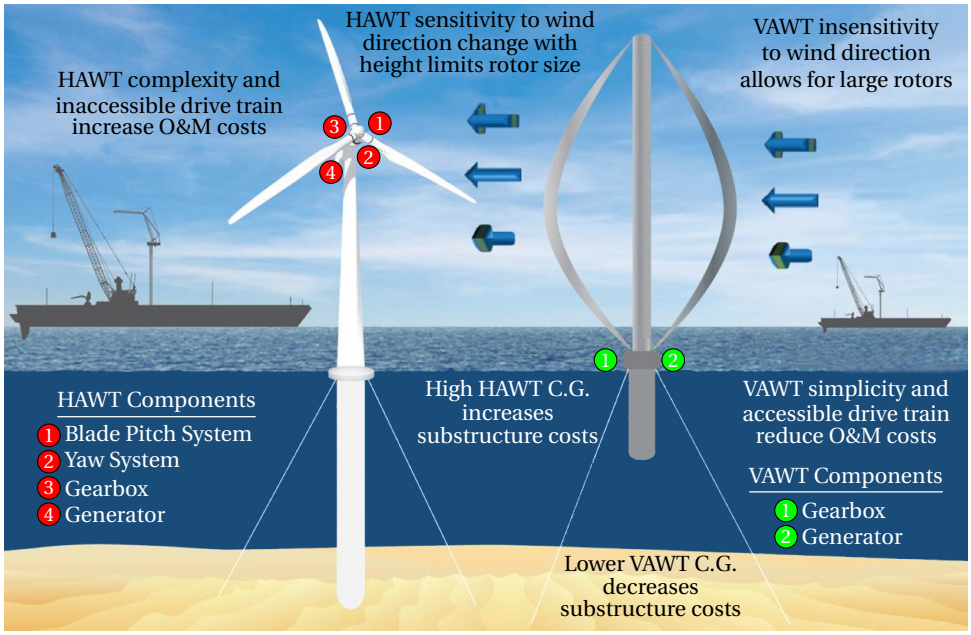

Figure 1.2: Comparison of HAWT and VAWT devices for (floating) offshore deployment, figure from Paquette & Barone (2012).

The use of VAWTs poses significant challenges to overcome, mainly due to the unsteady nature of its aerodynamics (cyclic torque output and fatigue loads on blades).

wind farms (Wilkinson & Hendriks, 2011).

[9] A recent measurement campaign in a wind farm highlighted an average yaw misalignment error of 10 degrees with a 1.6% loss in annual energy production (Pedersen *et al.*, 2011).

[10] Average power losses due to wind turbine wakes are of the order of 10 to 20% of total power output in large offshore wind farms (Barthelmie *et al.*, 2009; Schepers, 2012)

Moreover aspects such as theoretical and real aerodynamic efficiency of a single rotor and wind farm wake losses have not been sufficiently addressed yet.

The renewed interest in the VAWT technology faces an overall lack of understanding some physical phenomena governing the VAWT aerodynamics and of proper aerodynamic modeling. The underdevelopment of advanced models for VAWT aerodynamic analysis reflects the situation of a fragmented research field: after its peak during the '70s and the '80s, VAWT research was discontinued when the commercial success of the HAWT drove most of the research effort of the wind energy community.

1.2. INTRODUCTION ON VAWT AERODYNAMICS & RESEARCH

The complexity of the physical phenomena behind a VAWT wake and the scarcity of the related research activity create a scientific gap that this work contributes to fill. The following section provides a brief overview of the main elements of VAWT wake aerodynamics and a summary of its research history. For an extended reviews of VAWT blade and rotor aerodynamics, performance and design considerations, theoretical, numerical and experimental research on VAWT aerodynamics, the reader is referred to the doctoral dissertations of Ferreira (2009, p.11-24), Deglaire (2010, p.19-34), Danao (2012, p.30-75), Ferrari (2012, , p.12-22), Pearson (2013, p.35-55), Beaudet (2014, p.15-92), the retrospective on VAWT technology of Sutherland *et al.* (2012) by Sandia National Laboratories (SNL), and the book by Paraschivoiu (2002).

VAWT is a type of wind turbine with the axis of rotation perpendicular to the wind direction (commonly vertical, hence the name), which differs it from the widely used HAWT where the axis is parallel to the wind.

The present research investigates the wake behavior of the simplest configuration of lift-driven VAWT devices[11], called H-shaped VAWT (H-VAWT), which has straight, untwisted blades with the same orientation of the axis, placed symmetrically on the surface of a cylinder of radius R centered on the shaft. The reason for such choice lies in the need to isolate the basic common aerodynamic phenomena from specific design-driven effects.

Several other configurations exist with diverse and more complex blade geometries (fig. 1.3), where the increased complexity is introduced to alleviate some critical issues of the simpler design: a blade twisted helically on the cylinder surface leads to an helical-VAWT which alleviates the torque ripple; while a curved blade (in one or a combination of Troposkien, catenary or parabolic shapes) leads to a Φ-shaped VAWT (Φ-VAWT) which alleviates the bending moment on the blades.

The first consideration on VAWT wake aerodynamics relates to its dimensionality and symmetry which represent important elements of distinction with the wake of a HAWT. Due to the perpendicularity of the rotational axis and the wind direction, the turbine blades experience a periodic asymmetric change of the incoming flow vector (see

[11] Lift-driven VAWTs, known also as Darrieus turbine from the name of the French engineer who first patented them in 1931, differentiate from the drag-driven devices exploiting the aerodynamic lift as the main force for torque production.

Figure 1.3: Different configurations of lift-driven VAWTs: a 2 blades H-VAWT (left); a 2 blades Φ-VAWT in a Troposkien shape (center); a 3 blades Helical VAWT (right)

fig. 1.4). In the simplified hypothesis of an infinite straight blade and a uniform flow, the aerodynamics of the VAWT is 2D in space and 1D in time: each blade section experiences the same unsteady 2D flow field and generates the same wake. When in reality the hypothesis of infinite blades is lost, span-wise gradients arise. The wake is characterized then by unsteady 3D phenomena and the only symmetry present is the one about its equatorial plane (if one neglects the tower and any vertical shear layer).

In comparison in HAWT, the parallelism of the flow direction and the rotational axis makes its aerodynamics 3D in space (even without considering a finite blade): each section experiences a different steady 2D flow and generates a different wake with an helical symmetry. The unsteadiness, inherent in the VAWT wake, is here the consequence of an unsteady or non uniform inflow, or a yawed operation.

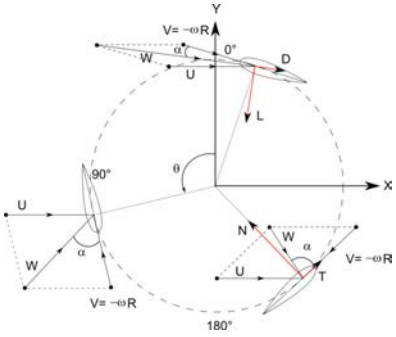

(a) Forces, velocities and incident angles in the equatorial plane of a VAWT

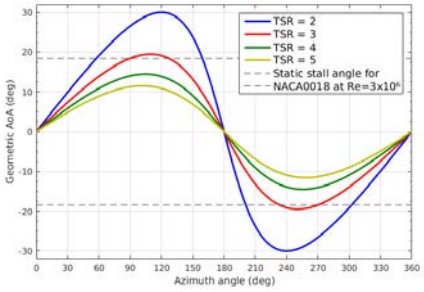

(b) Variation of geometric angle of attack.

Figure 1.4: VAWT geometry and unsteady operation

Two main inherent and distinctive effects of the vertical axis can be identified in the aerodynamics of VAWT wakes. The first is a consequence of the blade rotating in the same plane as the wake convects, which leads to the blade operating in its own, and

other blades, previously generated wakes. Such phenomenon, referred to as Blade-Wake Interaction (BWI)[12], affects both the loading of the blade in the downwind passage as well as the evolution of the wake after impinging on the blade (see fig. 1.5).

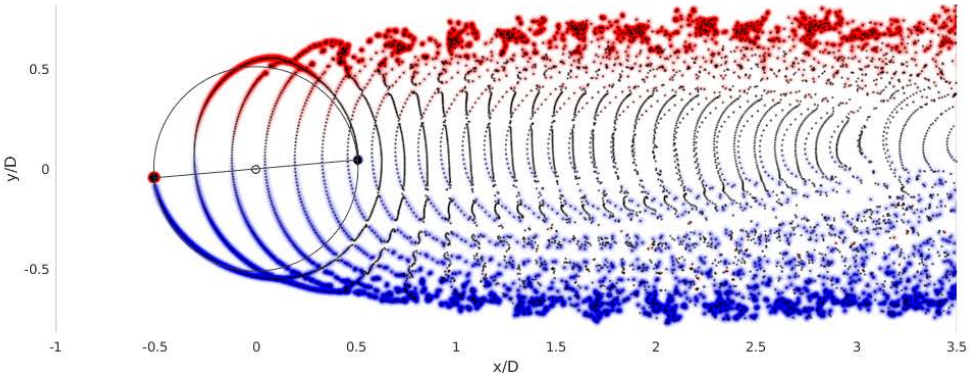

Figure 1.5: VAWT wake in the equatorial plane from a vortex particle simulation showing multiple BWI (vortex particles in black, blue and red color levels for positive and negative vorticity)

The second is a consequence of the periodic change in the blade's relative flow vector and thus in its bound circulation, which implies a continuous release of vorticity from the blade trailing edge (as per Kelvin's circulation theorem). This vorticity, initially parallel to the rotor axis, is usually (and later in this dissertation) referred to as *shed vorticity*.

The main three-dimensional effect in VAWT aerodynamics, a consequence of the finite blade span, is the span-wise distribution of blade's bound circulation and the occurrence of tip vortices. These are the result of the rolling up of the *trailing vorticity* released (as per Helmholtz's second theorem) perpendicular to the blade span. Tip vortices are not unique to VAWTs but common to any finite lifting surface, included the blades of a HAWT. However, as the VAWT blade's bound circulation change with the azimuth, VAWT tip vortices are characterized by a varying vorticity and retain the same cycloidal pattern of the blades wake. Moreover, in VAWTs the tip vortex released in the upwind blade passage may impinge on the downwind blade passage leading to an orthogonal BVI.

Despite their simpler mechanical design, their more complex and unsteady aerodynamics contributed to the early failure of VAWTs during the initial years of the development of modern wind energy. In the '70s and the '80s, the concept received substantial attention, with considerable research programs in US, Canada and UK and the realization of a few commercial turbines[13] (Paraschivoiu, 2002).

[12] In the present work a distinction is made between BWI and Blade-Vortex Interaction (BVI). The first is a more general phenomenon of mutual interaction between the solid blade and a wake region characterized by a high content of vorticity, while in the latter a coherent and identifiable vortex exists in the flow interacting with the blade.

[13] In US the SNL 34-m VAWT Test Bed (Berg *et al.*, 1990; Dodd *et al.*, 1989) and the commercial turbines of FloWind Corp. and Vawtpower; in Canada the National Research Council (NRC) Eole project (Veilleux & Tinawi, 1988) and Indal Technologies Inc., Lavalin Inc. and Adecon Inc; in UK the DoE H-VAWT project

The aerodynamic research focused on the creation of models to assist analysis and design, culminating in the Double-Multiple Streamtube Model (DMST) of Paraschivoiu (1981) and the 3D unsteady Vortex Element Method (VEM) of Strickland *et al.* (1981). Fatigue issues (exacerbated by the combination of the unsteady aerodynamics and the use of aluminum blades) and the higher CAPEX of the longer blades hindered the acceptance of the concept as a viable economic solution for MW-scale onshore applications. The HAWT soon became the standard of the growing wind energy industry, driving almost the totality of the research by the beginning of the '90s.

Though some research in VAWTs partially continued in the '90s and early 2000[14] the interest for this concept rose again in the mid-2000 with the new challenges emerged from the growing offshore environment, followed by the first studies on floating wind turbines (see fig. 1.6). Most of the challenges that hindered VAWTs development in the past decades can now be adequately addressed by technological advances in materials and production techniques (Paquette & Barone, 2012).

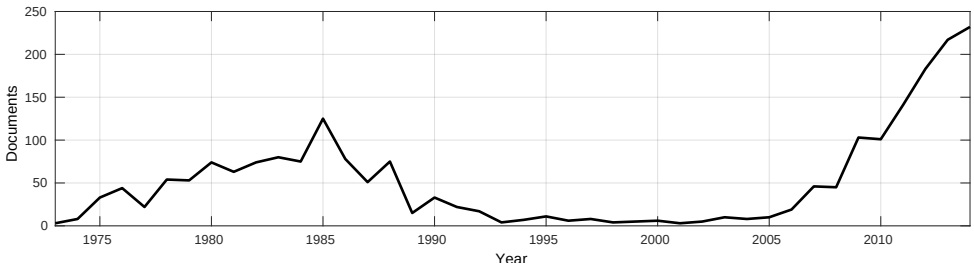

Figure 1.6: Published documents (journal articles and conference papers) on the topics of VAWTs from 1973 to 2014 [data from Scopus, keywords: VAWT, Vertical Axis Wind Turbine, Darrieus]

In the past ten years the focus of this renewed VAWT research has mainly been directed to define the design space of the rotor, and the aerodynamic optimization is still an open issue. More than one third of the recent literature deals with performance analysis for different configurations (rotor shape, number of blades, solidity, tip speed ratio) and blade design, with the DMST being the main numerical aerodynamic model used.

The advances in computational capabilities allowed refinement of vortex methods and the first full 3D Computational Fluid Dynamics (CFD) calculations, and part of the current research activity deals with more complex operations (effect of turbulent, unsteady or tilted flow) or configurations (active control, variable pitch, flexible geometry). For a comparison of recent developed numerical models and DMST the reader is referred to the blind comparison of Ferreira *et al.* (2014). However, the lack of significant and detailed experiments for validation purposes limits the development of numerical models.

Extended experimental analysis is also needed to improve the understanding of the blades, rotor and wake flow to develop new design methods. Some of the physical phenomena behind VAWT aerodynamics are not yet fully understood and some aspects, like the theoretical and practical maximum efficiency of the rotor or the stability and recovery

(Musgrove, 1987; Price, 2006) and VAWT Ltd.

[14] for their advantageous use as small turbines in the built environment.

process in the wake, have not yet had an exhaustive and unambiguous answer (Ferreira, 2009; Madsen, 1983).

The main focus of VAWT research remains directed, however, to the rotor volume, and the interest in the wake aerodynamics relates to the effects of BVI, in the case of dynamic stall or 3D evolution of the tip vortices inside the rotor, to better assess the blade loading in the downwind passage. Few researchers have extended their view past the rotor volume and the behavior of the wake at distances typical of wind farm scenarios have only started to be explored.

1.3. RESEARCH OBJECTIVE AND METHODOLOGY

In this section the three main questions guiding the research are presented in their general formulation and analyzed in more detail together with the methodology used to address them.

RQ1: WHAT ARE THE DYNAMICS THAT CHARACTERIZE THE EVOLUTION OF THE WAKE OF A VAWT?

A deeper understanding of the flow phenomena behind the VAWT wake is needed to develop accurate models for the analysis and design.

The methodology used in the present research to address such question is combined experimental investigations of the flow of a model turbine in a wind tunnel together with numerical simulations of a scaled-up turbine. Stereoscopic PIV (SPIV) is used for the experimental analysis of the flow structures by providing instantaneous velocity fields over large domains, while a Vortex Element Method (VEM) is used for the numerical analysis.

The *dynamics* refers to the study of the motion of the flow and its underlying causes. Special attention is given to the vorticity dynamics which are considered to be responsible for the main distinctions between the wake of VAWTs and HAWTs.

The *evolution* of the wake is considered as the generation of the vorticity field, the development in different coherent vortical structures, their motion and mutual interaction and the effect on the velocity field. The research question does not explicitly differentiate between *near*, *mid* or *far* wake[15], although the focus in this part of the research is mainly directed at the first two parts. The present study classifies also this distinction which for VAWTs is not clear until now.

Finally the generic term of *VAWT* is used, although the present analysis addresses only the H-VAWT configuration in a specific operational point with no dynamic stall involved. Some of the conclusions on the vorticity evolution, such as the ones referring to the horizontal plane, can be easily extended to other types of VAWTs, while other, such as the evolution of the tip vortices, are strongly dependent on the 3D geometry of the blades

[15] Researchers of HAWTs distinguish the near wake as the initial part where the presence of the individual blades and of the operation of the turbine can be identified, the far wake as the last part where details of the rotor geometry are no longer recognizable, and the mid or intermediate wake as the transition part between the two.

and their extension to other configurations needs caution. Moreover, the presence of dynamic stall affects the wake dynamics in such a way that this should be considered as a separate regime, not addressed in the present research[16].

RQ2: HOW DOES THE WAKE OF A VAWT DIFFER FROM THAT OF A HAWT AND WHAT DOES THIS IMPLY FOR FAR WAKE DEVELOPMENT?

The increasing deployment of turbines in clusters calls for a different approach in wind turbine design where the combined rotor-plus-wake system is considered, implying the need for more accurate wake models. The use of generic models based on HAWT wake knowledge for VAWT wakes raises doubts on their suitability given the fundamental differences in the two turbines aerodynamics.

The way this research deals with the research question is by comparing the wake development and associated energy levels of equivalent sized HAWT and VAWT. For the HAWT a reference turbine with available wake data is used, while for the VAWT a numerical analysis is performed on a scaled-up version of the experimental turbine. The comparison is made based on averaged stream-wise velocity and kinetic energy profiles. New quantities are introduced enabling a straightforward comparison none withstanding the dimensional differences of the two systems, and dissimilarities are linked to the wake topology.

RQ3: WHAT IS THE LEVEL OF ACCURACY OF A VORTEX ELEMENT METHOD FOR VAWT WAKE SIMULATIONS?

While the experimental approach gives valuable insight into the physics of the wake, the need to overcome its limitations, such as reduced Reynolds number or the cost associated to the extent and details of the measurements, leads to the use of a numerical model. As vorticity plays an important role in VAWT wakes, a Vortex Element Method (VEM) is chosen for its ability to represent vortical structures with minimal numerical dissipation.

A *VEM* is an aerodynamic numerical model for the solution of the Navier-Stokes (or Euler) equations which makes use of a vorticity-velocity formulation and a Lagrangian mathematical approach. Although several implementations of models based on VEM exist, the present study deals with a specific class where the wake is discretized with vortex filaments. Viscosity effects such as vorticity diffusion or dissipation are not modeled, thus dealing with the Euler equations and leading to a potential flow solver. The model is considered the simplest implementation of VEM retaining the fundamental nature of a vorticity/Lagrangian approach, so that the question deals with the extent to which such approach is able to represent VAWT wake aerodynamics.

[16] The lack of dynamic stall in the present research has been obtained by operating the turbine at a relative high tip speed ratio ($\lambda = 4.5$). The absence of the characteristic large vortical structures in the experimental observations, and a blade Angle of Attack (AoA) below known static stall angles in the simulations ensured dynamic stall was avoided.

The methodology to address the accuracy of this vortex model passes through a verification analysis on the numerical implementation and a validation of the model with experimental data.

1.4. TERMINOLOGY

Some common terminology will be defined in order to make the discussion clearer and easier to follow. A result of fragmented research field in VAWT is reflected in a ambiguous and non homogeneous semantics. The following sections present the nomenclature, dimensions, directions used through the whole dissertation and refers to the H-VAWT rotor and its wake.

ROTOR SYSTEM

The rotor is composed of N number of blades (two in this study) with chord c, span H and thickness h which are mounted at a distance R from the central vertical shaft with connecting struts. The rotating blades encircle a cylindrical rotor volume of diameter D and height H. For an H-VAWT the *swept area* is equal to the lateral cylindrical surface swept by the blade during its revolution ($A_S = 2\pi RH$), while the *frontal area* is the planar surface offered to the wind ($A_F = DH$)[17]; the latter is used as reference area for non-dimensional power or force coefficients. For the rotor the geometric quantities *solidity* ($\sigma = Nc/R$) and *rotor aspect ratio* ($\mathcal{AR} = D/H$) are defined.

The coordinate system is a Cartesian frame with origin at the rotor center. The x-axis is directed as the free stream velocity vector ($\vec{V_\infty}$) with the same orientation, the z-axis is directed as the vertical shaft oriented as the rotational velocity ($\vec{\Omega}$), and the y-axis results from the cross-product of the z and x-axes.

With this convention a positive rotation of the turbine is counter-clockwise seen from top. The blade position is defined by the vector $\vec{R}$ which forms with the axis $\vec{y}$ the *azimuth angle* (θ); a $\theta = 0°$ results in $\vec{R}$ being aligned with $\vec{y}$ while a $\theta = 270°$ results in $\vec{R}$ being aligned with $\vec{x}$. Following the work of Ferreira (2009), the blade orbit is divided in 4 regions:

- upwind: $45° < \theta < 135°$;
- leeward: $135° < \theta < 225°$;
- downwind: $225° < \theta < 315°$;
- windward: $315° < \theta < 45°$;

The blades experience a relative velocity $\vec{V_{REL}}$ (the vector sum of the free stream velocity $\vec{V_\infty}$, the induced velocity $\vec{u_i}$ and the relative rotational velocity $-\vec{\Omega} \times \vec{R}$) which forms, with the blade chord axis, the Angle of Attack (AoA) (which is a function of the azimuth angle). For the rotor operation the quantity *tip speed ratio* ($\lambda = \Omega R/V_\infty$) is defined. Figure 1.7 shows a schematic of the VAWT rotor with the system of reference and the terminology used.

[17] For a HAWT in non-yawed operations the two areas are the same

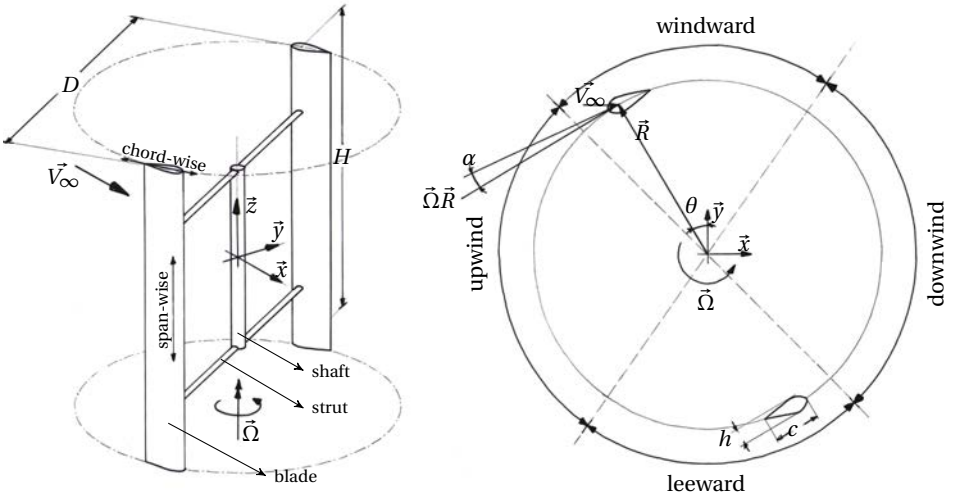

Figure 1.7: Schematic of the rotor with the system of reference and the terminology.

WAKE SYSTEM

The wake of VAWTs covers the area inside the rotor volume and downwind of it, with a main transport velocity directed in the free stream direction and secondary motions in both y and z directions. For the sake of simplicity the wake of the H-VAWT will be often represented with planar sectional views. Such planes are either vertical/stream-wise (*S-planes*), vertical/cross-stream (*C-planes*) or horizontal (*H-planes*). Figure 1.8 on page 14 shows a representation of the sectional planes used in the wake description from the numerical data.

The H-plane defined by $z = 0$ is also called *equatorial* plane, while the S-plane defined by $y = 0$ and the C-plane defined by $x = 0$ are referred as *meridian* planes. The *center line* is the intersection between the equatorial H-plane and the meridian S-plane, coincident with the x-axis.

To define the wake kinematics unequivocally the following regions and directions are defined:

- the meridian C-plane ($x = 0$) divides the domain in a *upwind* ($x < 0$) and a *downwind* ($x > 0$) region;
- the meridian S-plane ($y = 0$) divides the domain in a *leeward* ($y < 0$) and a *windward* ($y > 0$) region[18];

[18] the terms windward and leeward are here used as an extension from the rotor system to define the half domains corresponding to the windward and leeward sides of the blade orbit. They are not meant to be intended as motions, for which they would retain a different meaning. The reason for the extension of the term into the wake system, instead of a more straightforward *port* and *starboard*, derives by their taking into account also the blade rotation, essential to define uniquely the wake evolution. The starboard portion of the wake would behave differently if the turbine had a negative instead of a positive rotation, while the windward region of the wake is rotation invariant.

- the equatorial H-plane ($z = 0$) divides the domain in a *bottom* ($z < 0$) and a *top* ($z > 0$) region;
- in the direction parallel to the free stream ($\vec{x}$) a motion concordant to $\vec{V_\infty}$ is *downstream* while an opposite is *upstream*,
- in the two directions perpendicular to the free stream ($\vec{y}, \vec{z}$) *outward* is a divergent motion from the inside towards the outside of the wake resulting in a expansion of the wake area while *inward* is a convergent motion from the outside to the inside resulting in a contraction of the wake.

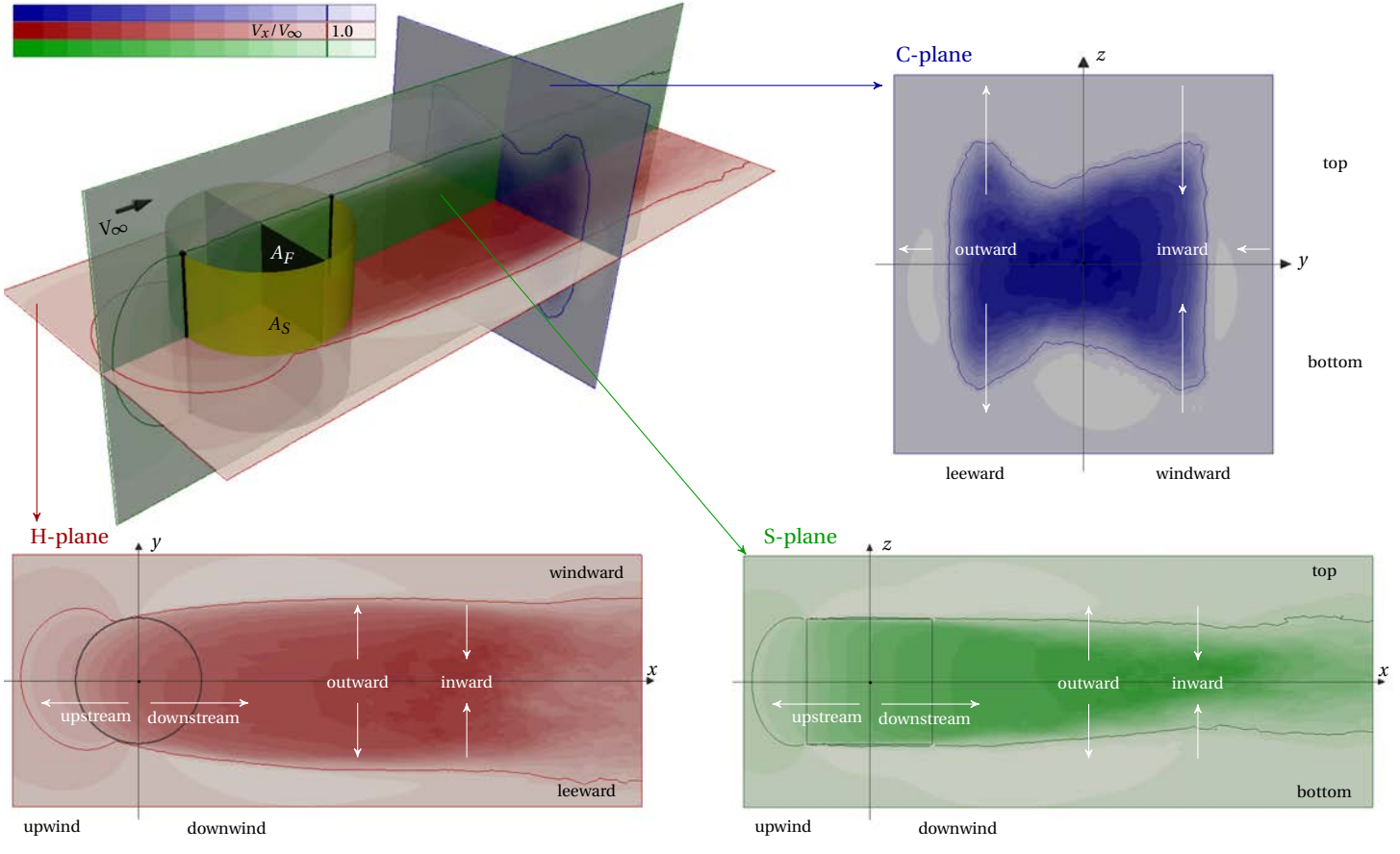

Figure 1.8: Schematic of the wake with the system of reference and the terminology for the domain (black) and the kinematics (white). 3D view (top left); cross-stream section in the C-plane (top right); horizontal/stream-wise section in the H-plane (bottom left); vertical/stream-wise section in the S-plane (bottom right)

VORTICITY SYSTEM

As introduced in section 1.2, the vorticity released in the wake of a H-VAWT is divided into a component initially parallel (*shed vorticity*) and one initially perpendicular (*trailing vorticity*) to the rotor axis.

The two components not only have diverse axis orientations but different origins and evolutions. The trailing vorticity originates from spatial derivatives of blade bound circulation and rolls-up in a system of *tip vortices* at the blade extremities. The shed vorticity derives from temporal variations of blade bound circulation and organizes in concentrated structures at the horizontal edges of the wake. Such structures are referred to as *edge vortices* in order to differentiate them from the tip vortices. Chapter 2 provides experimental observation and detail explanation of the dynamics of both systems.

1.5. THESIS OUTLINE

This dissertation is divided in 5 main chapters, each identifying and addressing a specific stage of the research performed (see Figure 1.9 on page 16). Chapters 2, 3 and 4 are extended and revised versions of research articles published or submitted to scientific journals during the course of the research.[19] The content of some of the chapters has been updated following the progress of the research achieved after the publication. They are also extended versions, particularly concerning the presentation of the results, given the space limitations of journals. The introductory section of each paper has been removed in favor of the more comprehensive introduction just presented in chapter 1, and the terminology has been unified.

Chapter 2 presents the phenomenological and topological study on the wake of an H-VAWT conducted through an experimental approach. A Stereoscopic PIV (SPIV) technique is used, focusing on the vorticity dynamics of the flow in the rotor volume and in the first three diameters from the shaft of a wind tunnel model. The wake evolution is highlighted and explained in terms of production, development and interaction of the main coherent vortical structures and of the consequent induction velocity field. The chapter addresses mainly RQ1 and partly RQ2, but creates the necessary basis for answering RQ3.

Chapter 3 focuses on the verification and validation of a numerical model for the simulation of VAWT aerodynamics, based on a Vortex Element Method (VEM). Issues as discretization effects, sensitivity analysis and convergence are addressed and the results

19

- G. Tescione, D. Ragni, C. He, C. Ferreira, and G. van Bussel, *Near Wake Flow Analysis of a Vertical Axis Wind Turbine by Stereoscopic Particle Image Velocimetry*, published on *Renewable Energy* (vol. 70, pp. 47-71, 2014), extended and revised in chapter 2.
- G. Tescione, C. Ferreira, and G. van Bussel, *Analysis of a Free Vortex Wake Model for the Study of the Rotor and Near Wake Flow of a Vertical Axis Wind Turbine*, published on *Renewable Energy*, (vol. 87, pp. 552-563, 2016), extended and revised in chapter 3.
- G. Tescione, C. Ferreira, and G. van Bussel, *A Comparison of the Wake Evolution for 5-MW Vertical and Horizontal Wind Turbines*, submitted to *Journal of Wind Engineering and Industrial Aerodynamics* on February 2016, extended and revised in chapter 4.

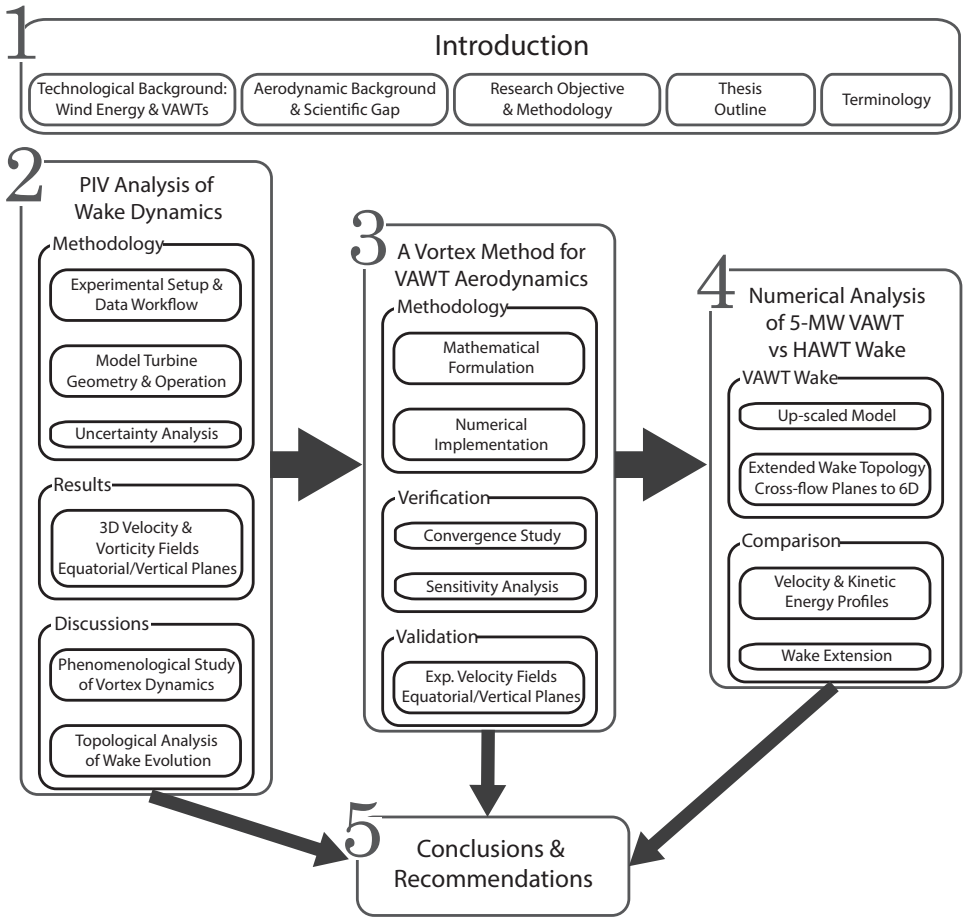

Figure 1.9: Schematic of the structure of the dissertation showing the work-flow and the connections between the different parts

of the verified model are validated against the experimental data in order to quantify the accuracy of the model and its limit of applicability. The chapter addresses RQ3.

Chapter 4 turns back to the study of the physical phenomena in the wake, completing and extending the results of the experimental analysis, by the use of the validated numerical model. The turbine is up-scaled to a 5-MW machine and the domain of investigation extended to the whole volume up to 6 diameters downwind the shaft. The wake evolution and energy content available for a downwind turbine is analyzed and compared with the wake of a HAWT, with the objective to highlight differences in the far wake development. This chapter addresses RQ1 and RQ2.

The last chapter presents the conclusions (chapter 5) and answers the formulated research questions, combining the observations from the experimental investigation and the results of the numerical analysis. Finally, recommendations for further investigation are given.

1

CHAPTER REFERENCES

Arapogianni, A., & Genachte, A. 2013. *Deep water - The next step for offshore wind energy*. Tech. rept. European Wind Energy Association (EWEA).

Araya, D.B. 2016. *Aerodynamics of vertical-axis wind turbines in full-scale and laboratory-scale experiments*. Ph.D. thesis, California Institute of Technology.

Barthelmie, R.J., Hansen, K., Frandsen, S.T., Rathmann, O., Schepers, J.G., Schlez, W., Phillips, J., Rados, K., Zervos, A., Politis, E.S., & Chaviaropoulos, P.K. 2009. Modelling and measuring flow and wind turbine wakes in large wind farms offshore. *Wind Energy*, **12**(5), 431–444.

Beaudet, L. 2014. *Etude éxperimentale et numérique du décrochage dynamique sur une eolienne á axe vertical de forte solidité*. Ph.D. thesis, Université de Poitiers. in french.

Berg, D.E., Klimas, P.C., & Stephenson. 1990. Aerodynamic design and initial performance measurements for the Sandia 34-m diameter vertical-axis wind turbine. *In: Proceedings of the ninth ASME Wind Energy Symposium*.

Blusseau, P., & Patel, M.H. 2012. Gyroscopic effects on a large vertical axis wind turbine mounted on a floating structure. *Renewable Energy*, **46**, 31 – 42.

Borg, M., Shires, A., & Collu, M. 2014. Offshore Floating Vertical Axis Wind Turbines, Dynamics Modeling State of the Art. Part I: Aerodynamics. *Renewable and Sustainable Energy Reviews.*, **39**, 1214–1225.

Boyle, G. 2006. UK offshore wind potential. How offshore wind could supply a quarter of UK electricity by 2024. *Refocus*, **7**(4), 26–29.

Ceyhan, O., & Grasso, F. 2014. Investigation of Wind Turbine Rotor Concepts for Offshore Wind Farms. *Journal of Physics: Conference Series*, **524**(1), 12–32.

Chaviaropoulos, P., Natarajan, A., & Jensen, P.H. 2014a. *Key Performance Indicators and Target Values for Multi-Megawatt Offshore Turbines*. Sound/Visual production (digital) in European Wind Energy Conference & Exhibition 2014, Barcelona, Spain.

Chaviaropoulos, P., Beurskens, H.J.M., & Voutsinas, S.G. 2014b. *Moving Towards Large(r) Rotors Is that a good idea?*

Corbetta, G., & Mbistrova, A. 2015. *The European offshore wind industry - key trends and statistics 2014*. Tech. rept. European Wind Energy Association (EWEA).

Dabiri, J.O. 2011. Potential order-of-magnitude enhancement of wind farm power density via counter-rotating vertical-axis wind turbine arrays. *Journal of Renewable and Sustainable Energy*, **3**(4).

Danao, L.A.M. 2012. *The Influence of Unsteady Wind on the Performance and Aerodynamics of Vertical Axis Wind Turbines*. Ph.D. thesis, The University of Sheffield, Department of Mechanical Engineering.

Deglaire, P. 2010. *Analytical Aerodynamic Simulation Tools for Vertical Axis Wind Turbines*. Ph.D. thesis, Uppsala University.

Dodd, H.M., Ashwill, T.D., Berg, D.E., Ralph, M.E., Stephenson, W.A., & Veerw, P.S. 1989. Test results and status of the DOW/Sandia 34-m VAWT test bed. *In: Proceedings of the Canadian Wind Energy Association Conference, 18-21 September 1989*.

Esteban, M. D., Diez, J. J., López, J. S., & Negro, V. 2011. Why offshore wind energy? *Renewable Energy*, **36**(2), 444 – 450.

Ferrari, G.M. 2012. *Development of an Aeroelastic Simulation for the Analysis of Vertical-Axis Wind Turbines*. Ph.D. thesis, The University of Auckland.

Ferreira, C. 2009. *The Near Wake of the VAWT, 2D and 3D Views of the VAWT Aerodynamics*. Ph.D. thesis, Delft University of Technology.

Ferreira, C., Aagard Madsen, H., Barone, M.F., Roscher, B., Deglaire, P., & Arduin, I. 2014. Comparison of Aerodynamic Models for Vertical Axis Wind Turbines. *Journal of Physics: Conference Series*, **524**(1).

Fowler, M., Bull, D., & Goupee, A. 2014. *A Comparison of Platform Options for Deep-water Floating Offshore Vertical Axis Wind Turbines: An Initial Study*. Tech. rept. SAND2014-16800. Sandia National Laboratories (SNL).

Ho, A., & Mbistrova, A. 2015. *The European offshore wind industry - key trends and statistics 1st half 2015*. Tech. rept. European Wind Energy Association (EWEA).

Hofmann, M., & Sperstad, I.B. 2014. Will 10 MW Wind Turbines Bring Down the Operation and Maintenance Cost of Offshore Wind Farms? *Energy Procedia*, **53**, 231–238. EERA DeepWind' 2014, 11th Deep Sea Offshore Wind R&D Conference.

Madsen, H.A. 1983. *On the Ideal and Real Energy Conversion in a Straight Bladed Vertical Axis Wind Turbine*. Ph.D. thesis, Aalborg University Centre, Institute of Industrial Constructions and energy Technology.

Mone, C., Smith, A., Maples, B., & Hand, M. 2015. *2013 Cost of Wind Energy Review*. Tech. rept. NREL/TP-5000-63267. {N}ational {R}enewable {E}nergy {L}aboratory.

Musgrove, P.J. 1987. Wind Energy Conversion: Recent Progress and Future Prospects. *Sol. Wind Technol.*, **4**(1), 37–49.

Myhr, A., Bjerkseter, C., Ågotnes, A., & Nygaard, T. A. 2014. Levelised cost of energy for offshore floating wind turbines in a life cycle perspective. *Renewable Energy*, **66**, 714 – 728.

Paquette, J., & Barone, M. F. 2012. *Innovative Offshore Vertical-Axis Wind Turbine Rotor Project* . Tech. rept. SAND2012-3295C. Sandia National Laboratories.

Paraschivoiu, I. 1981. Aerodynamic Loads and Performance of the Darrieus Rotor. *Journal of Energy*, 406–412.

Paraschivoiu, I. 2002. *Wind Turbine Design: With Emphasis on Darrieus Concept.* Polytechnic International Press.

Paulsen, U.P., Madsen, H.A., Hattel, J.H., Baran, I., & Nielsen, P.H. 2013. Design Optimization of a 5 {MW} Floating Offshore Vertical-axis Wind Turbine. *Energy Procedia*, **35**, 22–32. DeepWind'2013 - Selected papers from 10th Deep Sea Offshore Wind R&D Conference, Trondheim, Norway, 24 - 25 January 2013.

Pearson, C. 2013. *Vertical Axis Wind Turbine Acoustics.* Ph.D. thesis, Cambridge University, Engineering Department.

Pedersen, T.F, Gottschall, J., Kristoffersen, J.R., & Dahlberg, J-A. 2011. Yawing and performance of an offshore wind farm. *In: Proceedings.* European Wind Energy Association (EWEA).

Peeringa, J., Brood, R., Ceyhan, O, Engels, W., & de Winkel, G. 2011. *Upwind 20MW Wind Turbine Pre-Design.* Tech. rept. ECN-E–11-017. Energy research Centre of the Netherlands (ECN).

Price, T.J. 2006. UK Large-scale Wind Power Programme from 1970 to 1990: the Carmarthen Bay experiments and the Musgrove Vertical-Axis Turbines. *Wind Engineering*, **30**(3), 225–242.

Schepers, G. 2012. *Engineering Models in Wind Energy Aerodynamics.* Ph.D. thesis, Delft University of Technolo.

Schepers, G., Ceyhan, O., Savenije, F.J., Stettner, M., Kooijman, H.J., Chaviarapoulos, P., Sieros, G., Ferreira, C., Sorensen, N., Wachter, M., Stoevesandt, B., Lutz, T., & Gonzalez, A. 2015. AVATAR: AdVanced Aerodynamic Tools of lArge Rotors. *In: 33rd Wind Energy Symposium, AIAA ScitTech, Kissimmee, FL.*

Sieros, G., Chaviaropoulos, P., Sørensen, J. D., Bulder, B. H., & Jamieson, P. 2012. Upscaling wind turbines: theoretical and practical aspects and their impact on the cost of energy. *Wind Energy*, **15**(1), 3–17.

Strickland, J. H., Webster, B. T., & van Nguyen, T. 1981. *A Vortex Model of the Darrieus Turbine: An Analytical and Experimental Study.* Tech. rept. SAND81-7071. Sandia National Laboratories (SNL).

Sutherland, H.J., Berg, D.E., & Ashwill, T.D. 2012 (January). *A Retrospective of VAWT Technology.* Tech. rept. Sandia National Laboratories.

Veilleux, M., & Tinawi, R. 1988. Comportement dynamique d'une éolienne á axe vertical (application pratique). *Canadian Journal of Civil Engineering*, **15**, 369–381.

Wilkinson, M, & Hendriks, B. 2011. *Report on Wind Turbine Reliability Profiles.* ReliaWind Deliverable D.1.3.

2

PIV Analysis of H-VAWT Wake Dynamics

A non-complete understanding of the physics of VAWT wake and the scarcity of proper validated models for their simulation have been identified in the introduction as the main motivations of the present research. The limited experimental activity in the field is mainly responsible for this lack of theoretical knowledge and analysis tools. Detailed measurements of local flow quantities provide the necessary insight for the phenomenological analysis and the means for model validation and refinement.

The following chapter presents the experimental activity performed as the first step of the research. The measurements are obtained in the open-jet wind tunnel of the Delft University of Technology on an H-shaped VAWT wake flow at a chord-based Reynolds number of 1.7×10^5. *Phase-locked velocity and vorticity fields are acquired with an orthogonal and stereoscopic particle image velocimetry technique in the equatorial H-plane and several S-planes up to three diameters downwind the turbine shaft, in order to study the wake dynamics in the different dimensions.*

A thorough examination of the velocity fields and of the vorticity dynamics leads to a detailed phenomenological analysis of the mechanisms governing the H-shaped VAWT (H-VAWT) wake evolution. Results show the different vortical structures evolving in the horizontal and vertical planes, their mutual interaction and the effect they have on the asymmetry of the wake flow.

This chapter is a revised and extended version of the paper *Near Wake Flow Analysis of a Vertical Axis Wind Turbine by Stereoscopic Particle Image Velocimetry*, by G. Tescione, D. Ragni, C. He, C. Ferreira, G.J.W. van Bussel, published on *Renewable Energy* 70 (2014) 47-61, on October 2014.

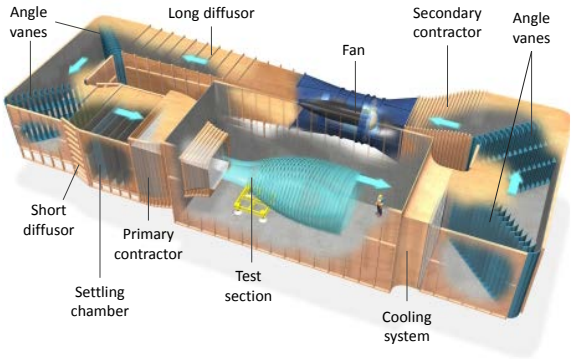

Figure 2.1: Schematic of the TUDelft OJF.

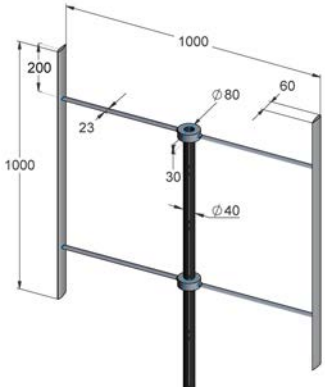

Figure 2.2: Wind turbine model (dimensions in mm).

2.1. METHODOLOGY

2.1.1. WIND TUNNEL AND VAWT MODEL

The experimental activity has been performed in the Open Jet Facility (OJF) which is the closed-circuit, open-jet wind tunnel of the Delft University of Technology. The OJF produces an octagonal jet with a cross-section of 2.85 m × 2.85 m, following a contraction ratio of 3:1, and free to expand in a 13.7 m × 6.6 m × 8.2 m test section. The wind tunnel is powered by a 500 kW electric fan allowing for a free stream velocity range from 3 m/s to 34 m/s with a maximum 0.5% of turbulent intensity. A 350 kW heat exchanger maintains a constant temperature (20 °C, in the present experiment) in the test section. Previous studies (Lignarolo *et al.*, 2014) showed a uniform free stream flow (uniformity of ±0.5% in area) up to 6 m from the jet exit. Figure 2.1 shows a schematic of the facility.

The turbine model is a two-blades H-VAWT, shown in fig. 2.2. The rotor blades are generated by straight extrusion of a National Advisory Committee for Aeronautics (NACA) 0018 aluminum section with two inner spars and a constant chord of $c = 0.06$ m, resulting in a untwisted, untapered blade of $H = 1$ m span. The turbine has a diameter of $D = 1$ m, leading to an aspect ratio of $\mathcal{AR} = 1.0$ and a blade solidity of $\Sigma = 0.11$. The wind tunnel blockage ratio is 14%, which requires no blockage factor corrections for open-jet wind tunnels[1]. The blade-tower connection is obtained with two aerodynamically profiled struts (NACA 0030, chord 0.023 m) per blade, installed at 0.2 m from the blade tips. The location of the connections minimizes the maximum deformation at blade mid-span and tips due to centrifugal effects. The strut-blade connection has been shaped to minimize the flow interference. Both blades and struts, as well as the central part of the tower, have been painted in black to minimize laser reflections. The tower is a 3 m steel shaft of 0.04 m diameter, connected to a Faulhaber© brushless DC Motor 4490 BS providing a 202 W maximum output power, driving the turbine at low wind speeds and maintain-

[1] Chen & Liou (2011) found there is no need for blockage factor corrections for wind turbines with blockage ratio below 10% in closed-jet wind tunnel and Garner *et al.* (1966) found the blockage factor correction to be half in magnitude and opposite in sign for open-jet wind tunnels

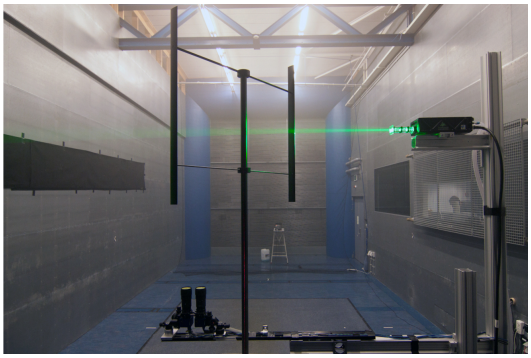

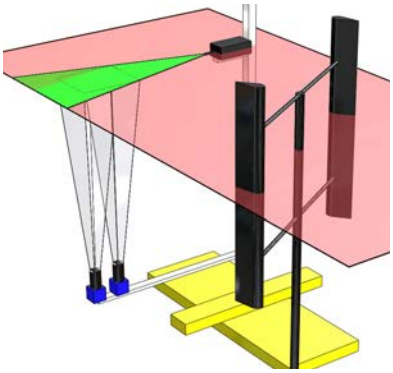

Figure 2.3: Orthogonal PIV configuration.

ing a constant rotational speed. A Faulhaber© gearbox with 5:1 gear ratio is coupled to the electrical engine to obtain sufficient torque at the operating regimes. The motor operates within a measured accuracy of ± 0.02 Hz. A photo diode is installed on the shaft to obtain a 1 pulse per revolution trigger signal to synchronize the Particle Image Velocimetry (PIV) system in phase-locked acquisition. The turbine model is operated at a tip speed ratio of $\lambda = 4.5$, under a free stream velocity of $V_\infty = 9.3\,\mathrm{m/s}$ and at a rotational speed of $\Omega = 800\,\mathrm{RPM}$, in a range of chord-based Reynolds numbers from 1.3×10^5 to 2.1×10^5. The high tip speed ratio has been chosen after 2D numerical simulations to limit the Angle of Attack (AoA) experienced by the blade below the static stall, in order to avoid dynamic stall. Considering the chord-based Reynolds number range of the tests, the airfoil has been tripped, to avoid the occurrence of laminar separation bubbles (Gerakopulos *et al.*, 2010; Nakano *et al.*, 2007; Timmer, 2008), in order to avoid adding a further level of unsteadiness to the wake flow. A 3D-turbulator tape developed by Glasfaser Flugzeug© (6 mm point distance, 0.20 mm thickness, 12 mm width, 60° zig-zag tape) at 8% of the chord on both sides has been applied, following the recommendations of Selle (1997).

2.1.2. PIV EXPERIMENTAL SETUP

The velocity fields in the near wake of the turbine have been obtained by PIV, adopted in an orthogonal 2D-2C configuration (two velocity components in a two-dimensional domain) for the equatorial H-plane and in a stereoscopic 3C-2D configuration (three velocity components in a two-dimensional domain) for the measurements on the S-planes.

A Quantel Evergreen© double-pulsed Nd:YAG laser with 200 mJ per pulse provides green light of wavelength 532 nm to create a laser sheet of approximately 2 mm width. A SAFEX© MIX diethyl glycol based fog of seeding particles of less than 1 µm mean diameter were produced by a SAFEX© TWIN FOG generator located downstream of the model. The seeding particles convected through the test section were imaged by two LaVision© Imager Pro LX 16M cameras (12 bit) having an image resolution of 4870 px × 3246 px and a pixel pitch of 7.4 µm/px.

The first adopted configuration has been realized by acquiring particle images on

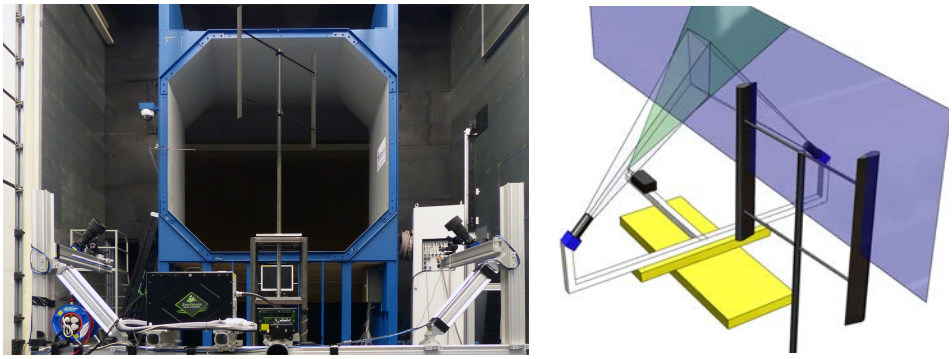

Figure 2.4: Stereoscopic PIV configuration.

the equatorial H-plane as shown in fig. 2.3. Given the vertical symmetry of the flow, and that no relevant out of plane component has been detected across the equatorial plane, an orthogonal PIV setup has been used by placing the two cameras side by side at 90° viewing angle with the measurement plane. The cameras have been equipped with Nikon© lenses of focal length $f = 105\,\text{mm}$, at an aperture of $f\# = 4$ and placed at about 1.5 m from the laser sheet, out of the jet flow to avoid flow interference and camera vibrations. This setup resulted in a magnification factor $M = 0.09$, a single camera Field of View (FOV) of 0.266 m × 0.399 m, a combined FOV of 0.266 m × 0.755 m, and a 11% FOV overlap.

A second stereoscopic PIV setup has been employed to acquire velocity fields in the S-planes (fig. 2.4). The cameras are in this configuration equipped with $f = 180\,\text{mm}$ Nikon© lenses with aperture $f\# = 4$ and placed at about 2 m from the measurement plane with a relative viewing angle of 96°. The resulting magnification factor is $M = 0.07$ and the stereoscopic FOV consists of 0.365 m × 0.430 m. Both setups have been installed on a two degrees of freedom traversing system, with a range of 1.4 m × 1.0 m, allowing for automated acquisitions of several FOVs with a single calibration.

2.1.3. DATA ACQUISITION AND MEASURING DOMAINS

In both adopted configurations, ensembles of 150 image pairs have been acquired in phase with the rotor motion. Considering the different setups, in order to minimize the shadow effects from the blockage of the laser light by the blade, the orthogonal measurements are in phase with the blades at $\theta = 90°$ and $\theta = 270°$ (most upwind and downwind positions), while for the stereoscopic measurements the blades are at $\theta = 0°$ and $\theta = 180°$ (most windward and leeward positions).

The ensembles of the individual FOVs have been processed to obtain averaged velocity and vorticity fields. They have been later combined in a single field for each plane, employing a common coordinate system with the origin at the turbine center. Both acquisition and processing of the PIV images were done with LaVision© Davis 7.2.2 and 8.1.4.

In the orthogonal measurement setup (fig. 2.5 left) the area covered by the measurement ranges from $-1.85 < x/R < 4.30$ and $-1.75 < y/R < 1.75$. In the stereoscopic mea-

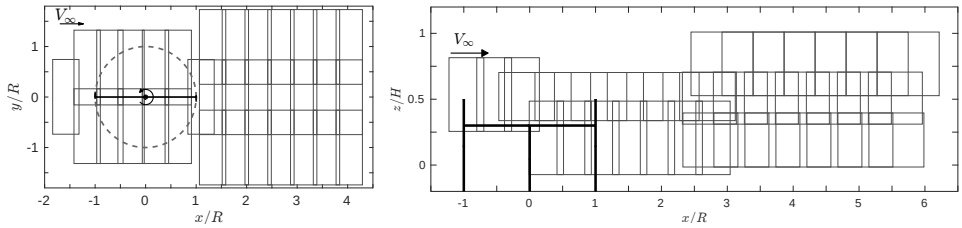

Figure 2.5: Measurement domains for the orthogonal (left) and stereoscopic (right) configurations.

surement setup (fig. 2.5 right), 7 different S-planes were measured (y/R = -1.0, -0.8, -0.4, 0, 0.4, 0.8 and 1.0), in an area ranging from $-1.22 < x/R < 6.22$ and $0 < z/H < 1$.

2.1.4. DATA PROCESSING AND UNCERTAINTY ANALYSIS

In the present study a forward uncertainty propagation approach with linear error propagation equations (Gaussian distribution and uncorrelation of errors) is used (Stern *et al.*, 1999). Given the complexity of the experimental setup and the fact that not all the sources of error can be quantified, the analysis aims at providing a rough estimate of the uncertainties associated with the measurements. Since the experimental data originate from PIV, the measurement uncertainties are associated with velocity and consist of random and bias components.

With a relatively low free-stream of 9.3 m/s and the low magnification factors obtained, the most relevant sources of bias components in the PIV measurements are the particle peak-locking and the lack of spatial resolution. With a magnification of 0.09 (standard PIV) and 0.07 (stereoscopic PIV) and an aperture of $f\#4$, the imaged diffraction of the particle diameter is 5.7 µm and 5.5 µm, corresponding to less than 1 px (Raffel *et al.*, 2013). In order to reduce the effect of peak-locking the focus has been slightly offset with respect of the laser plane (de-focusing) to ensure particles of about 2 px (Westerweel, 1997). A subsequent 3x3 Gaussian filter on the particle image has been applied before correlation to ensure a Gaussian particle shape. The effect of this filter does not affect significantly the signal-to-noise ratio of the correlation peaks. The histogram of the decimals of the particle pixel displacement has been derived (fig. 2.6 left) to evaluate the level of peak-locking. The cumulative distribution of such histogram (fig. 2.6 right) has a 0.05 px maximum deviation from a perfectly sampled distribution (dashed line on figure) ensuring a low level of peak-locking.

In order to give an estimation of the error due to lack of resolution two characteristic lengths have been considered: half of the blade thickness and the blade chord. They are representative of the structures scales respectively in the wake of the blades and in the developing wake of the rotor. With the adopted multi-pass correlation algorithm with window deformation (Scarano & Riethmuller, 2000), having a final window size of 32 px × 32 px and 50% overlap, a resulting vector resolution of 1.5 mm is obtained. According to Schrijer & Scarano (2008) the present resolution and reference lengths assess the uncertainty due to lack of resolution respectively to 10% and 1% for the two cases. It has to be taken into account that this uncertainty is a function of the measurement location in the PIV velocity fields.

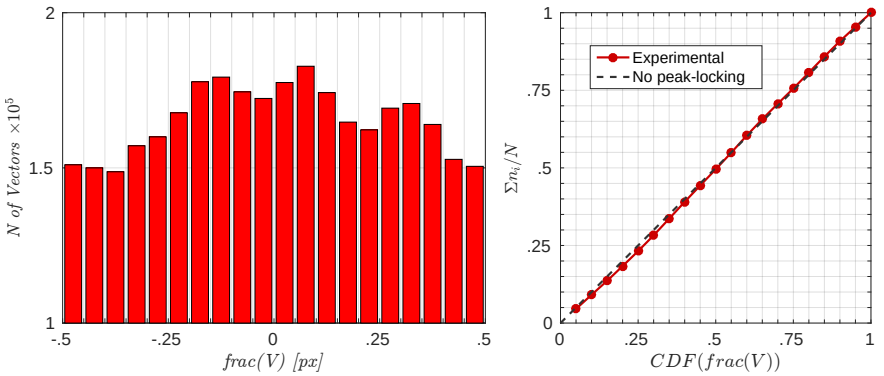

Figure 2.6: Particle pixel displacement decimal histogram (left) and its cumulative distribution function (right) showing the low level of peak-locking.

Other systematic sources of uncertainty include the calibration effects and the lens distortion, particularly relevant for the stereoscopic measurements. These are alleviated by a self-calibration procedure and quantified as fit RMS of the mapping algorithm by the Davis software itself. Obtained values of the residual of 0.27 px (average) and 0.53 px (maximum) ensure good calibrations (Raffel *et al.*, 2013).

The main random component of uncertainty in the instantaneous velocity fields is the cross-correlation uncertainty. Typical values have been reported between 0.05 px to 0.15 px for a range of window-sizes down to 32 px × 32 px (Westerweel, 1997).

Another source of uncertainty when dealing with statistical properties of the phase-locked flow fields is the phase unsteadiness due to the jitter of the system and to flow turbulence. With an engine rpm jitter of ±0.01 Hz, considering that the reference time adopted for the phase locking is fixed during the measurement acquisition, an expected variation of ±60 µs corresponds to 0.04° in rotation. Translating this uncertainty in the acquired phase into an uncertainty in the averaged velocity is not straightforward. Its quantification implies the use of the temporal gradients of the velocity fields and the effect is highly local. In most parts of the wake, where the flow velocities and the gradients are low, this unsteadiness does not have a significant effect in the averaged values. In the presence of high velocities (blade flow) or high gradients (vortex structures) the discussion is limited to a qualitative analysis. The statistical convergence scales these effects with $1/\sqrt{N}$ (with $N = 150$ the number of samples in the ensembles). Figure 2.7 shows an example of the convergence analysis of the phase-locked mean components at evaluation points in the H-plane and S-plane. The plot highlights the high coherence of the flow and how the chosen sample size leads to converged mean values with incremental variations below 0.1% of V_∞. Similar analysis have been performed for different data sets of both the orthogonal and stereoscopic PIV measurements in multiple regions of the domain to assure converged statistical sets.

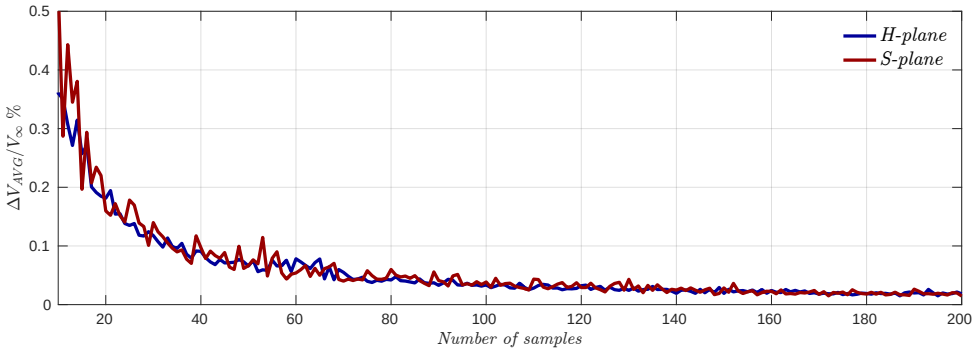

Figure 2.7: Statistical convergence of the phase-locked mean components.

2.2. RESULTS

H-PLANE

The measurements at the equatorial plane aim at analyzing the evolution of the wake in the horizontal symmetry plane, from the mechanism of shedding of vorticity by the blade trailing edge to the transition into the full rotor wake. The present paragraph presents contour plots of the stream-wise velocity component (fig. 2.8 on page 28), cross-stream velocity component (fig. 2.9 on page 28), absolute velocity fluctuations (fig. 2.10 on page 29), and out-of-plane vorticity (fig. 2.11 on page 29).

The plots are obtained as ensemble averages over 150 instantaneous velocity fields phased-locked with the blade revolution at $\theta = 90°$ (blades at the most upwind/downwind positions). In the plots the wind is coming left to right and the turbine rotates counter clockwise. The blade trajectory is indicated as a dashed line, while the non measured areas are blanked. The velocities are normalized with the free stream velocity, V_∞, while the vorticity (obtained from the velocity fields with a central difference scheme) is normalized with the chord and the free stream velocity. Both abscissa and ordinate are normalized with the rotor radius. The presented results are discussed in section 2.3 on page 36.

S-PLANES

The measurements of the flow at the vertical planes aligned with the free stream (S-planes) aim at extending the analysis of the wake dynamics from the symmetry plane to the 3D volume, with a focus on the evolution and the role of the tip vortices. Figures 2.12 to 2.16 present the stereoscopic phase-locked experimental results at 7 cross-stream positions: y/R = +1.0, +0.8, +0.4, 0, -0.4, -0.8 and -1.0 (from the most windward on the top to the most leeward on the bottom).

As for the H-plane results, the plots are obtained as ensemble average over 150 phase-locked instantaneous velocity fields. To minimize blade and laser shadows on the PIV data, the velocity fields are acquired with the blades at the most windward/leeward positions ($\theta = 0°$). The measurements have been taken at the only top half of the domain considering the symmetry of the flow. The wind is coming left to right and the intersection between the rotor volume and the measurement plane is indicated by a dashed line. Contour plots of normalized stream-wise velocity component (fig. 2.12 on

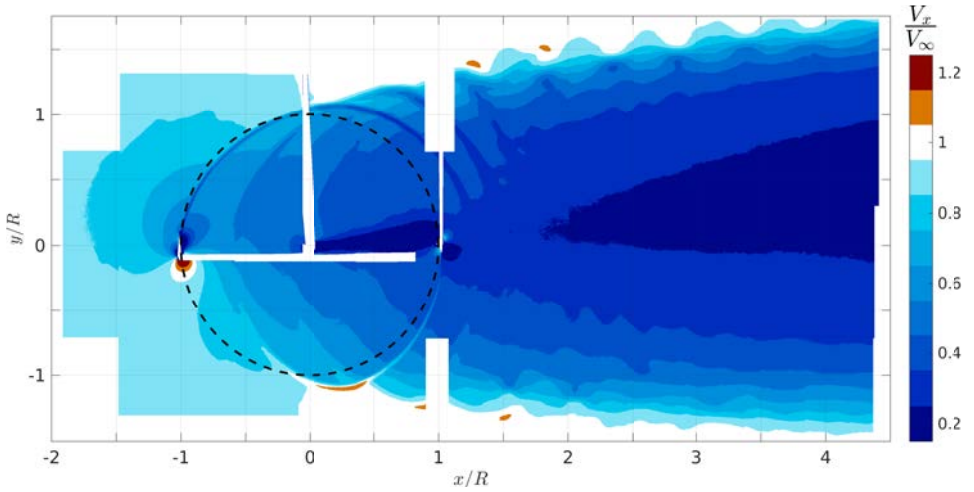

Figure 2.8: Contours of normalized stream-wise velocity for the equatorial H-plane.

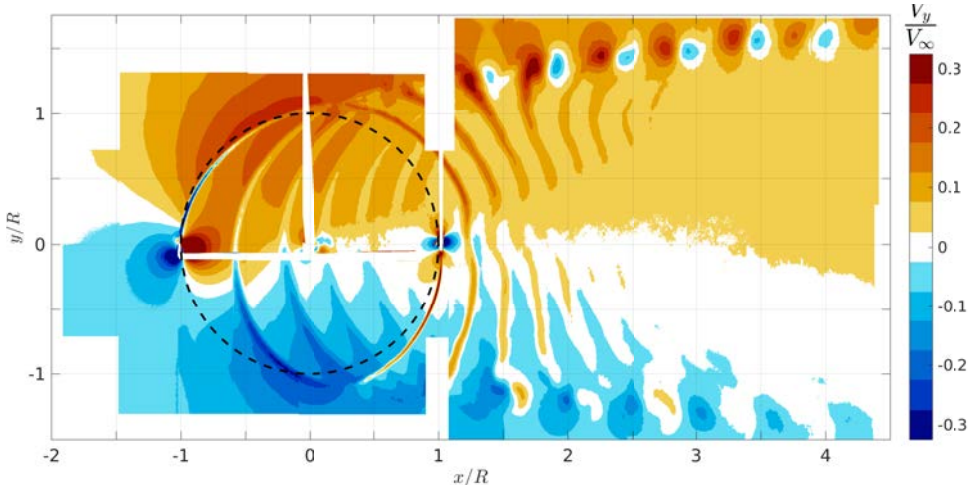

Figure 2.9: Contours of normalized cross-stream velocity for the equatorial H-plane.

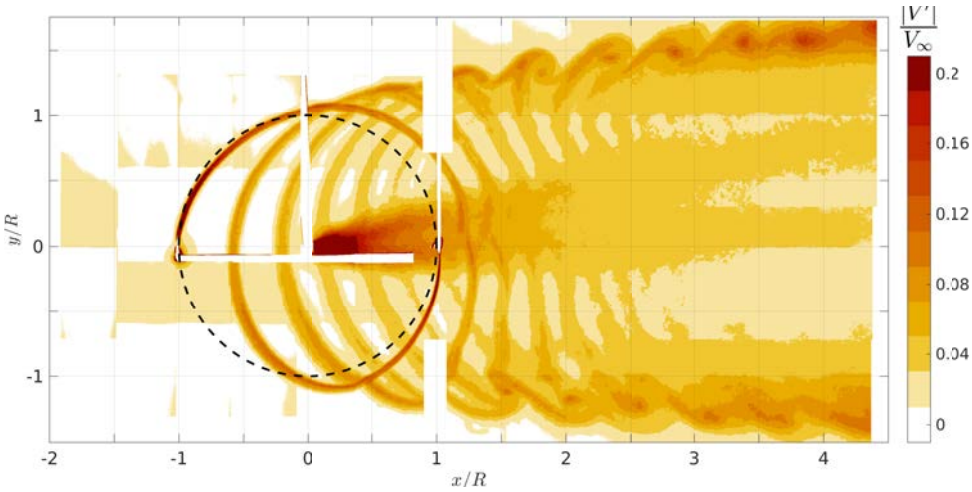

Figure 2.10: Contours of normalized absolute velocity fluctuations for the equatorial H-plane.

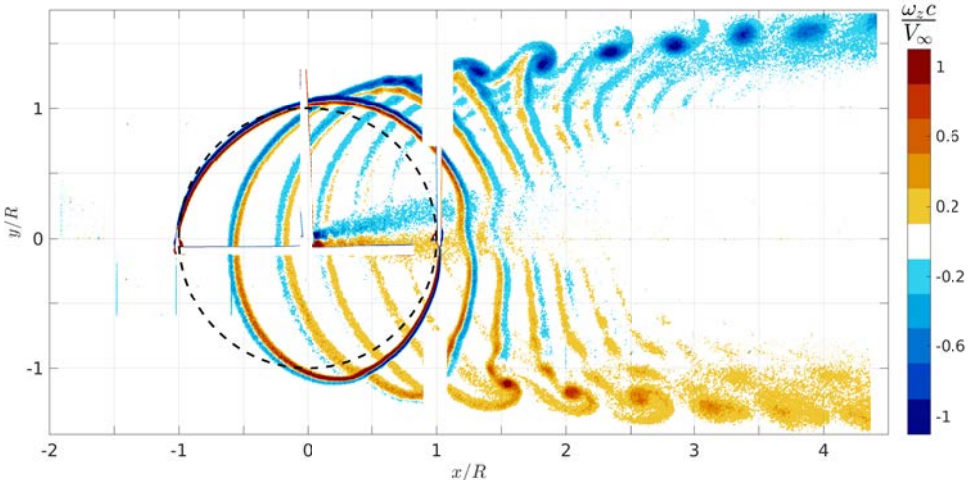

Figure 2.11: Contours of normalized out of plane vorticity for the equatorial H-plane.

page 31), cross-stream velocity component (fig. 2.13 on page 32), vertical velocity component (fig. 2.14 on page 33), absolute velocity fluctuations (fig. 2.15 on page 34), and cross-stream vorticity (fig. 2.16 on page 35) are presented. The velocities and vorticity normalizations are consistent with the previous results. The abscissa is normalized with the rotor radius while the ordinate is normalized with the turbine height. The presented results are discussed in section 2.3 on page 39.

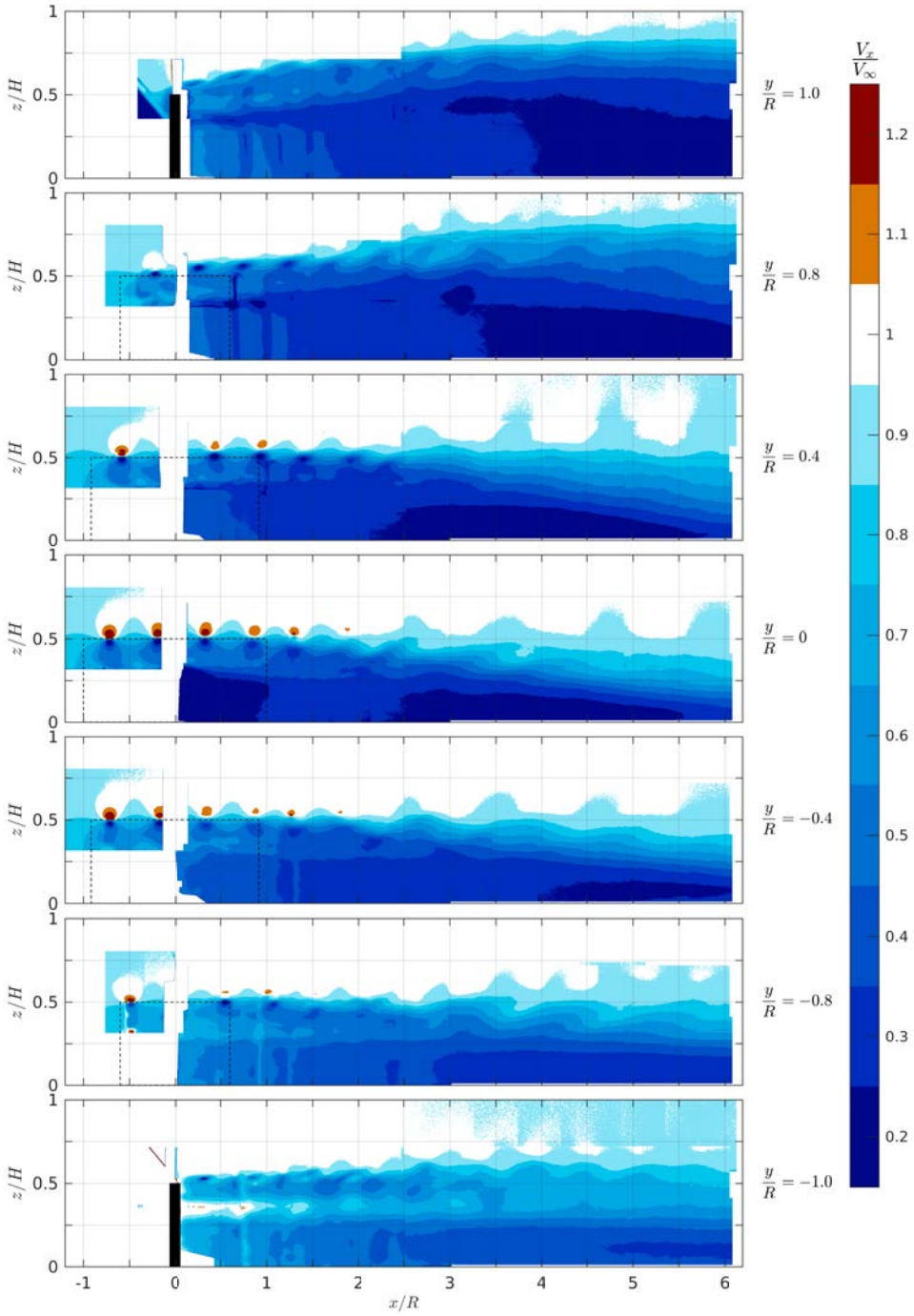

Figure 2.12: Contours of normalized stream-wise velocity for S-planes at different y/R locations.

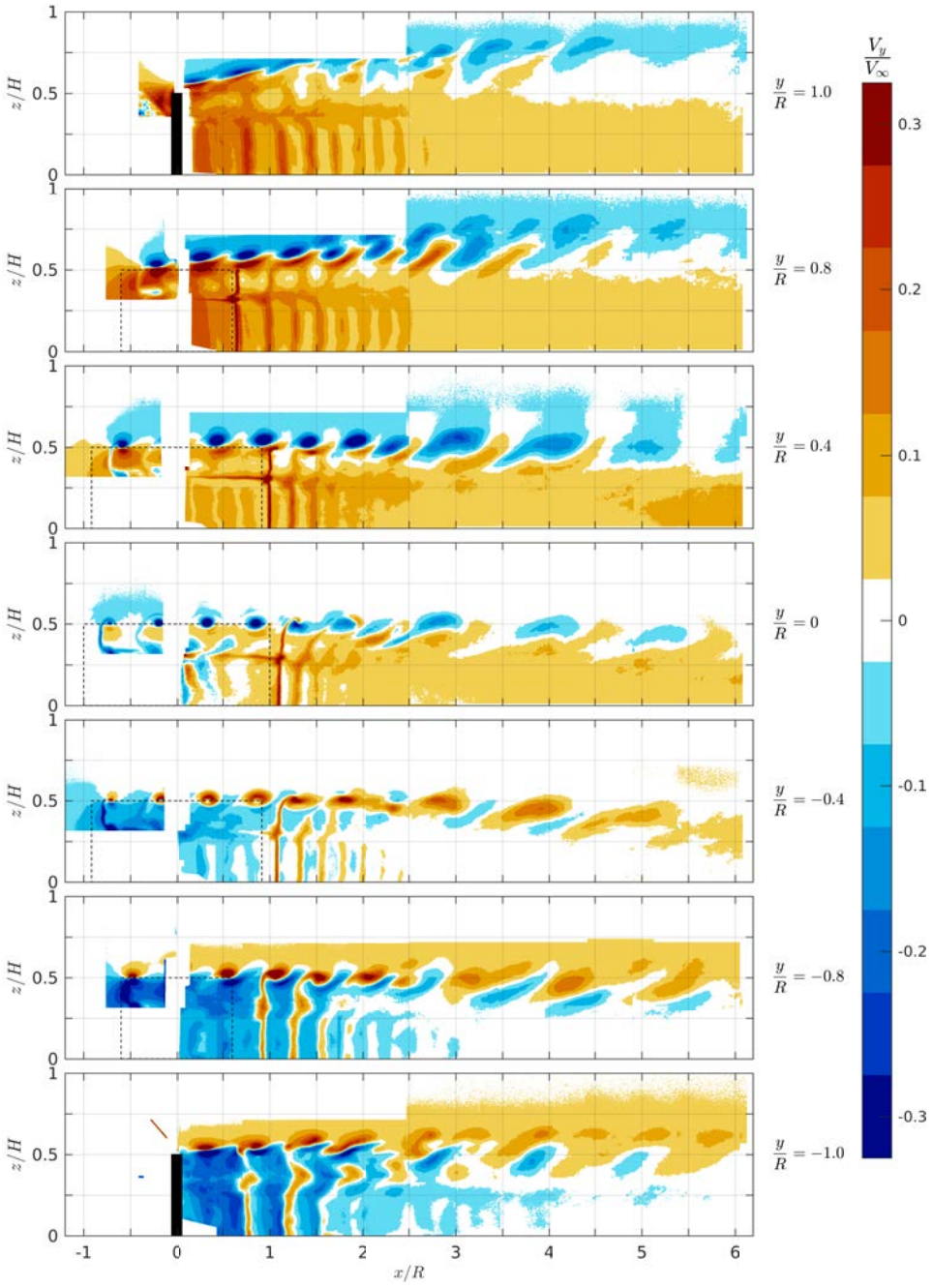

Figure 2.13: Contours of normalized cross-stream velocity for S-planes at different y/R locations.

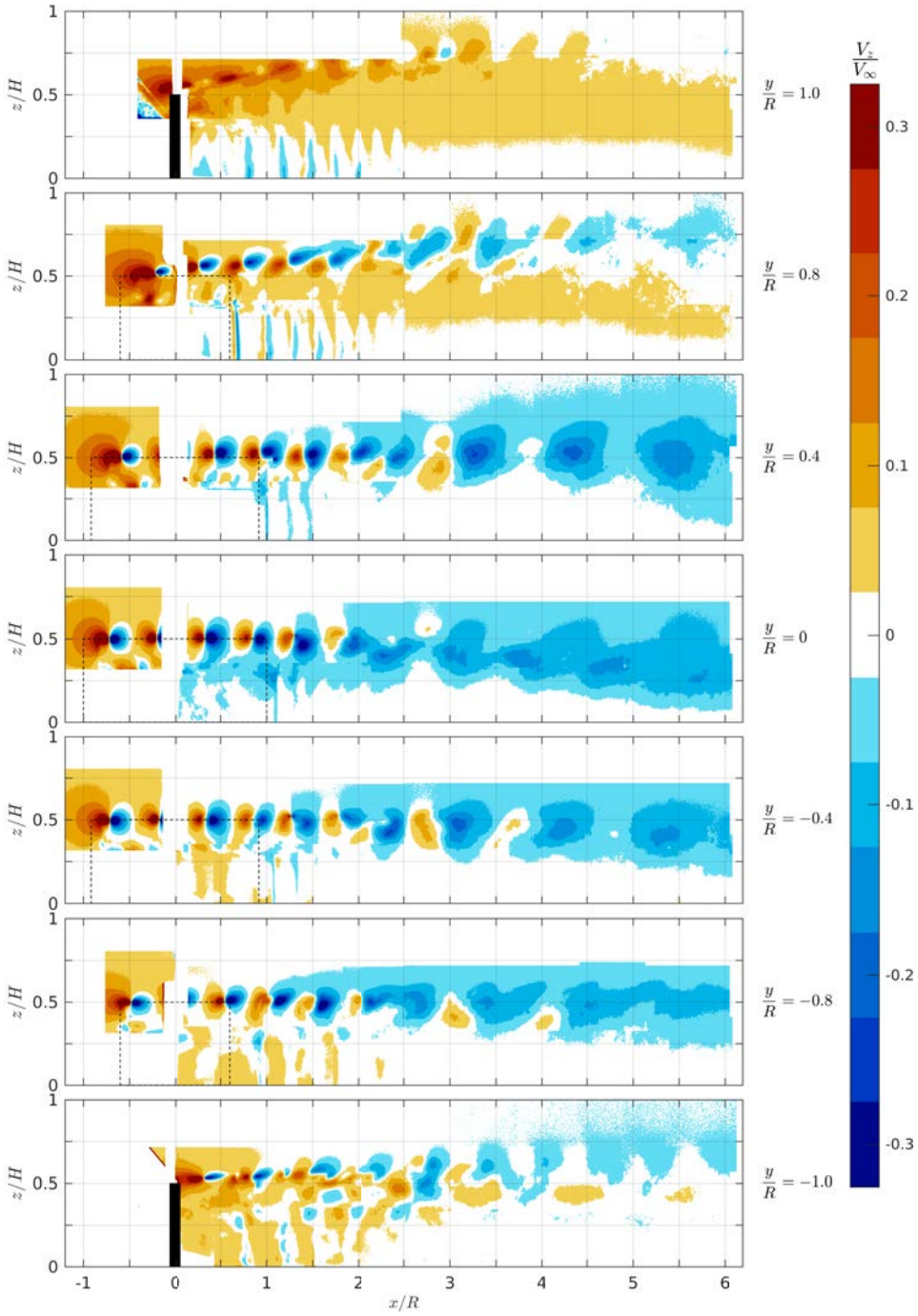

Figure 2.14: Contours of normalized vertical velocity for S-planes at different y/R locations.

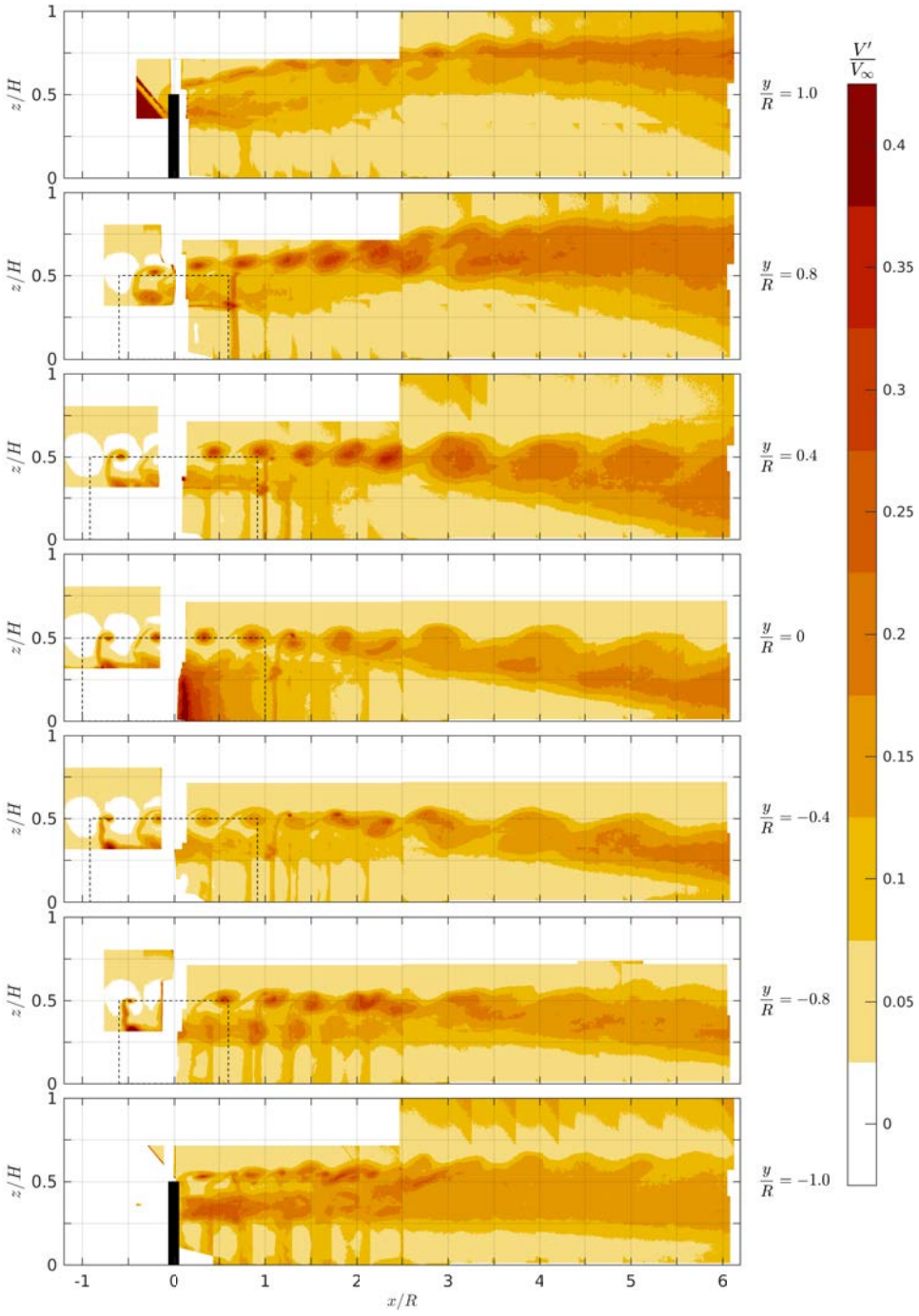

Figure 2.15: Contours of normalized absolute velocity fluctuations for S-planes at different y/R locations.

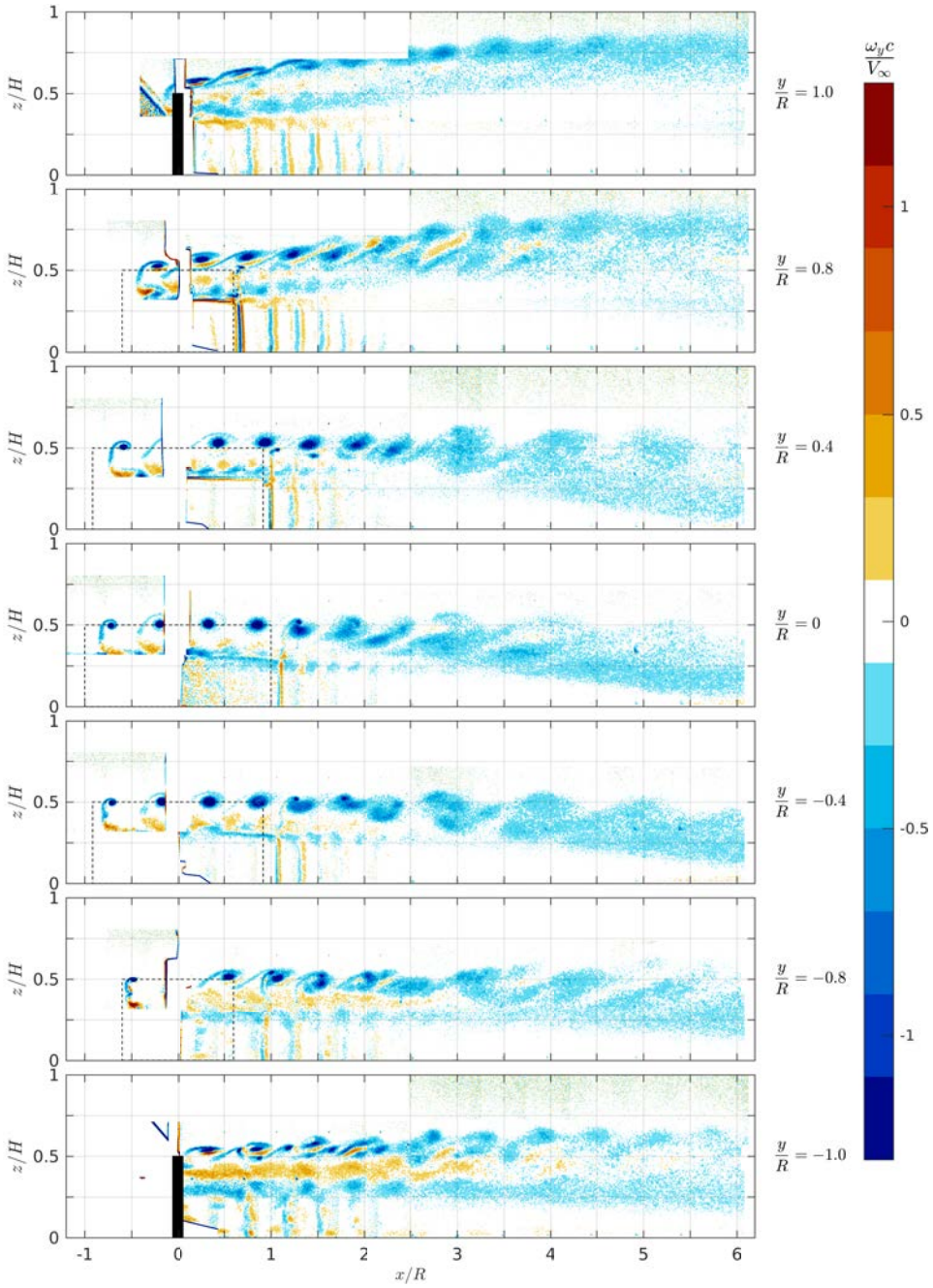

Figure 2.16: Contours of normalized cross-stream vorticity for S-planes at different y/R locations.

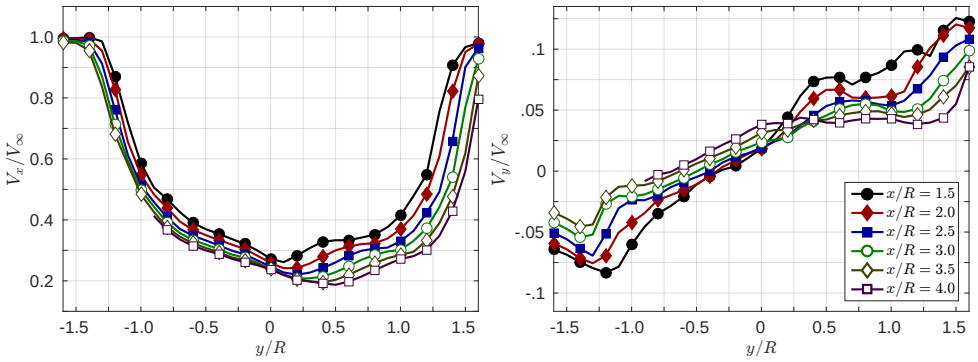

Figure 2.17: Asymmetric wake velocity profiles, stream-wise component (top) and cross-stream component (bottom). Variation in x/R.

2.3. DISCUSSIONS

H-PLANE

The stream-wise velocity plot (fig. 2.8, on page 28) shows the velocity deficit in the equatorial section of the wake as an effect of the energy extraction and the consequent wake expansion. From this point of view, the horizontal section of the wake of a Vertical Axis Wind Turbine (VAWT) is not very dissimilar to any radial section of the wake of a Horizontal Axis Wind Turbine (HAWT), except that a certain degree of asymmetry can be observed.

The asymmetry is evident in fig. 2.17 (left) showing a series of stream-wise velocity profiles extracted at different downstream locations. The wake profile at the most upstream location shows a little degree of skewness with a de-centered velocity minimum ($y|_{min(V_x)} = +0.1R$, for $x/R = 1.5$), a steeper gradient and a more pronounced expansion toward the windward side (right side of the plot). The asymmetry is enhanced as the wake develops downstream with a migration of the location of maximum velocity deficit toward the windward side ($y|_{min(V_x)} = +0.5R$, for $x/R = 4$) and an increase in the profile skewness.

The increasing wake asymmetry can be observed also in fig. 2.17 (right) showing the downstream series of wake cross-stream velocity profiles. While the slope of the profiles decreases as the wake develops, indicating a decreasing cross-stream velocity magnitude and rate of wake expansion, the location of the zero cross-stream velocity tends to migrate toward the leeward side (from $y|_{V_y=0} = -0.3R$ for $x/R = 1.5$ to $y|_{V_y=0} = -0.7R$ for $x/R = 4$).

This is in contrast with the natural tendency of an asymmetric wake to develop a more symmetric velocity profile as it spreads (Thomas & Liu, 2004), suggesting that the mechanism causing this asymmetry is not localized entirely at the rotor but transported in the wake. While the asymmetric blade incidence envelope at the windward and leeward part of the blade trajectory and the tower rotation (Magnus effect) can be addressed as localized asymmetry sources, the increasing asymmetry of the wake is an effect of the self-induction as well.

The presence of the rotating tower can be clearly seen not only on the stream-wise velocity contours but also, and more clearly, in the contour plots of the velocity fluctuations and of the out of plane vorticity (figs. 2.10 and 2.11 on page 29). The tower wake is here a region with a local velocity deficit, a high level of fluctuations and two parts of counter-rotating vorticity. It presents a lateral motion towards the windward side (concordant with its rotation) and extends approximately until $x/R = 3$.

The contour plots of the cross-stream velocity component, the RMS of the 150 phase-locked velocity fields and the out-of-plane vorticity (figs. 2.9 to 2.11 on pages 28 and 29) show two important features of VAWT wake: the cycloidal patterns and the *edge vortices*.

The cycloidal patterns are a result of the viscous wakes released by a blade which is moving in a circular motion and transported downstream[2]. Here the flow is dragged by the blade motion and appears as a thin region of negative (or less positive) V_y for the upwind blade passage, and as a thin region of positive (or less negative) V_y for the downwind blade passage. They are also characterized by a higher level of velocity fluctuations and out-of-plane vorticity.

As a consequence of the wind being directed perpendicular to the axis of rotation, VAWT blades undergo a periodic change in the relative velocity vector during their orbit which translates in a change of the circulation bound to the airfoil. For Kelvin's circulation theorem when the airfoil undergoes a change in its bound circulation an equal and opposite amount of circulation is released in its wake. The wake of a VAWT blade is then characterized by a continuous release of shed vorticity. The shed vorticity assumes the form of two vorticity sheets of opposite signs as result of the non sharp trailing edge. Since the azimuthal derivative of the airfoil circulation is not constant and it changes sign in the most upwind and downwind positions ($\theta = 0°$ and $180°$), the net sum of the two vorticity sheets is not constant and changes sign as well.

The turbulence of the tower wake and the interaction between convex and concave segments of the cycloid at the wake center, where the vorticity of the segments is lower, result in a quick diffusion and disappearance of the cycloidal patterns which are no longer detectable for $x/R > 3$.

The second feature is the presence of regions of concentrated vortical structures at the windward and leeward edges of the wake. These structures, referred to as *edge vortices*[3], are clearly visible in the vorticity contour plot (fig. 2.11), and as coupled regions of high positive and negative cross-stream velocity in fig. 2.9. Strong fluctuations are also detected at the location of the vortices in fig. 2.10. Here the high values of the velocity fluctuations are associated to both the increased turbulence level of the flow and to the effect that the vortex meandering has on the average operation.

The mechanism leading to the formation of such structures is identified in the inherent unsteadiness of the blade's aerodynamics. As mentioned before, the unsteady blade operation translates in a cycloidal blade wake with varying vorticity: positive (counter-

[2] They are indeed a pseudo-form of non-ordinary cycloids, or trochoids, one for each blade and depending on the turbine tip speed ratio λ. The original cycloid form is soon deformed by multiple interactions and the induction field.

[3] The term is introduced here for the first time, by the need to differentiate these structures from the tip vortices for their different origin and evolution.

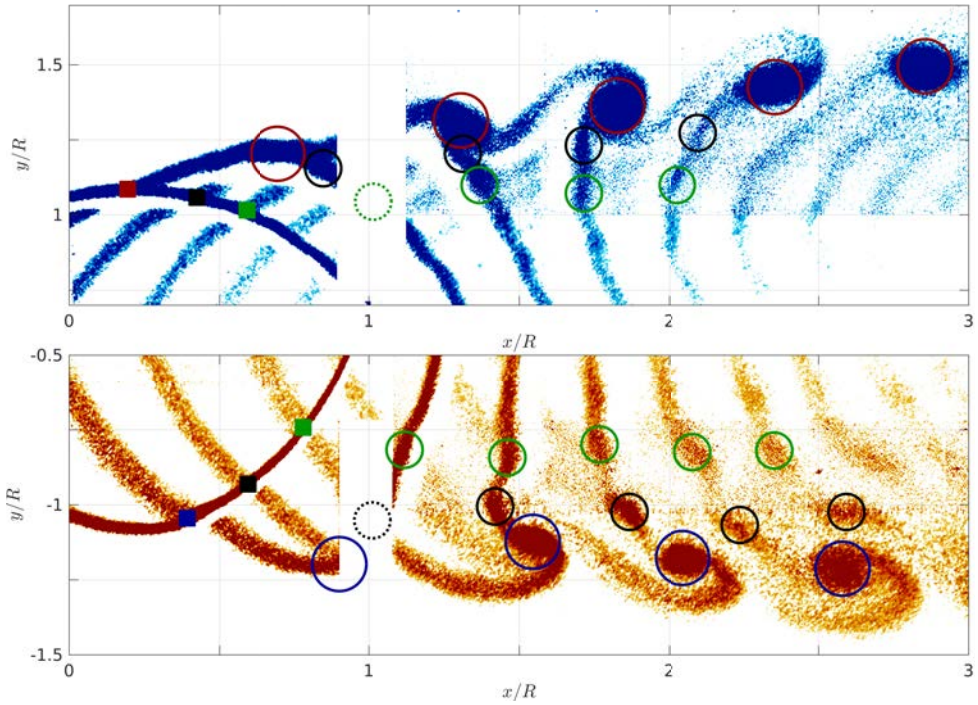

Figure 2.18: Blade-wake interactions (squares) and roll-up of the edge vortices (circles) in the windward (top) and leeward (bottom) edges of the wake. Background of out-of-plane vorticity.

clockwise) on the leeward side with a maximum around $\theta = 180°$, and negative (clockwise) on the windward side with a minimum around $\theta = 0°$. These regions of positive and negative vorticity tend to organize in concentrated vortical structures. Such tendency is triggered as a consequence of the blades operating inside their wakes.

The effect of the blade rotating in the same plane as the wake develops is that the blade will pass during its revolution in its own, and other blades, previously generated wakes leading to multiple Blade-Wake Interactions (BWIs). The passage of the blade inside the wake vorticity sheet locally deforms the wake geometry. In addition the new released wake will overlap to the previous wake resulting in a concentration of vorticity. The local peak in vorticity and the deformation trigger the roll-up of the wake in large scale vortical structures.

Figure 2.18 shows the onset of these peaks of vorticity at the intersection of multiple blade wakes and the formation of the edge vortices rolling around these pivots, for the windward (top) and leeward (bottom) regions. The roll-up begins approximately around $x/R = 1.5$. A main set of vortices with the higher level of vorticity at the most windward and leeward locations is visible through all the measured volume. A second and third set of vorticity concentrations are partially visible until either roll-up and merge into the main set or quickly diffuse around $x/R = 2.5$. For $x/R > 3$ the main vortices at the edges of the wake are the only dominant structures detectable.

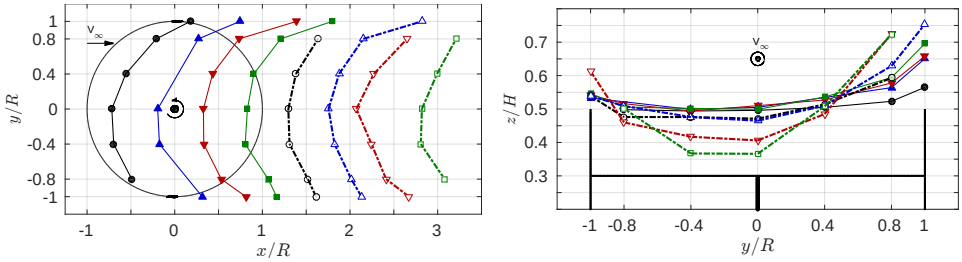

Figure 2.19: Projection of tip vortex tubes location (only convex segments) in the horizontal planes (left) and vertical/cross-stream planes (right).

S-PLANES

The cross-stream vorticity contours (fig. 2.16, on page 35) allow a first analysis of the 3D dynamics in the H-VAWT wake and the identification of an initial region of the wake in a similar way as was done for the H-plane. The first region, which extends inside the rotor volume and until around $x/R = 3$, it is characterized by the presence of the viscous blade wakes as regions of high velocity gradients and fluctuations. Also the tower wake and the struts and strut-blade connections wakes are visible. The latter create a turbulent region extending even further downstream especially at the most windward and leeward positions.

The second visible feature of such initial wake region is the formation and evolution of the tip vortices. Trailing vorticity is released along the whole blade span for Helmholtz's second theorem, as a result of a span-wise distribution of bound vorticity. It rapidly rolls-up into strong vortical structures at the tips of each blade, with the axis originally lying on the horizontal planes directed as the blade chord.

The vorticity and the velocity fluctuation contours (figs. 2.15 and 2.16, on pages 34 and 35) clearly show the release and the roll-up of the series of the two upper tip-vortices (of the upwind and downwind passage of the blade through the measurement planes). The vortical structures released by the blade tips form a continuous curve retaining a similar cycloidal shape observed in the H-plane results, as can be seen in fig. 2.19 (left), displaying the projection of the tip vortices position in the horizontal planes (only showing the stronger, upwind-released vortices). The curvature of the tip vortex axis is also observed in fig. 2.16 as a stretching of the vorticity regions at the windward and leeward sides of the wake, where the measurement planes cut the vortices not normal to their axis.

These structures undergo a substantial deformation during their downstream transport, just downwind of the rotor volume because of the interaction and mutual induction between the vortex released during the upwind blade passage (convex part of the tip vortex curve) and that released during the downwind passage (concave part). Figure 2.20 shows a close-up view of such interaction for the meridian S-plane. Although the vortex axis has rotated 180°, both sections of the tip vortex curve have a negative (clockwise) vorticity forming a co-rotating system. Indeed, as the blade changes angle of attack during its revolution the pressure and suction parts flip sides at the most leeward and windward

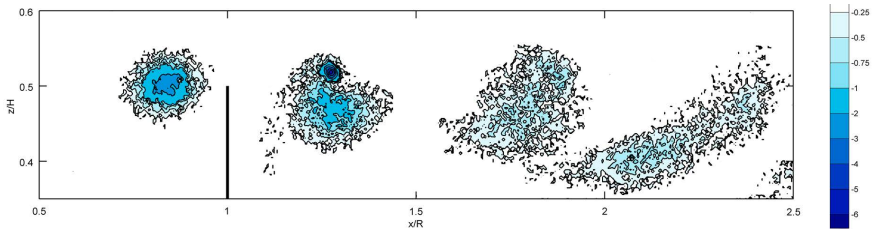

Figure 2.20: Interaction of upwind and downwind generated tip vortices for the meridian S-plane, $y/R = 0$ (normalized vorticity isocontours).

positions ($\theta = 0°$ and 180°), leading to a change of sign in the bound circulation and in the vorticity vector. For the same reason the vorticity magnitude along the vortex curve is not constant with a local maximum at the most upwind and downwind positions ($\theta = 90°$ and 270°)[4].

Once released from the blade tip, the downwind vortex starts to interact with the upwind vortex in a co-rotation of the vortex pair. The positions of the tip vortex pairs are shown in fig. 2.21 in the different measured S-planes. This rolling motion locally enhances the vortex deformation and the turbulent diffusion, contributing to the breakdown of the structures. Around $x/R > 4$ the concentrated structures are hardly detectable, merged and diffused in spread vorticity regions. The local peaks of velocity signaling the presence of the tip vortices (observable in the cross-stream and vertical velocity contours figs. 2.13 and 2.14, on pages 32 and 33) show a sensible reduction in magnitude after $x/R = 2$ identifying the vortex diffusion, but can be still detected for the central part of the wake ($-0.4 < y/R < 0.4$) until $x/R = 6$, suggesting that the breakdown process is still not fully completed. Similar results have been observed for the wake of a HAWT experimentally by Lignarolo *et al.* (2014), where the mutual induction starts approximately one diameter after the vortices are released and is linked to the wake recovery and a wake contraction. In the case of HAWTs the tip vortices create a quite stable helical system with constant spacing and magnitude, to the point that in the aforementioned research the instability was triggered by altering the vorticity of one tip vortex tube. In the case of VAWT the spacing between the upwind-released and downwind-released vortex is not constant as well as their strength, and the instability is inherent to the system, leading to an earlier breakdown.

The wake asymmetry observed in the equatorial H-plane extends and increases into the whole 3D volume of the wake, both in terms of wake geometry and of induction field. While in the H-plane the wake experiences a continuous lateral expansion, in the S-planes the geometry of the H-VAWT wake is characterized by a more complex evolution.

[4] For this reason the term *tip vortex curve* has been used instead of *tip vortex tube* commonly used in HAWT terminology, since a vortex tube has a constant strength. There is a continuous vertical flux of vorticity between the trailing vorticity of the tip vortices (which have maximum strength at the most upwind and downwind positions) and the shed vorticity of the edge vortices (which have maximum vorticity at the most leeward and windward positions).

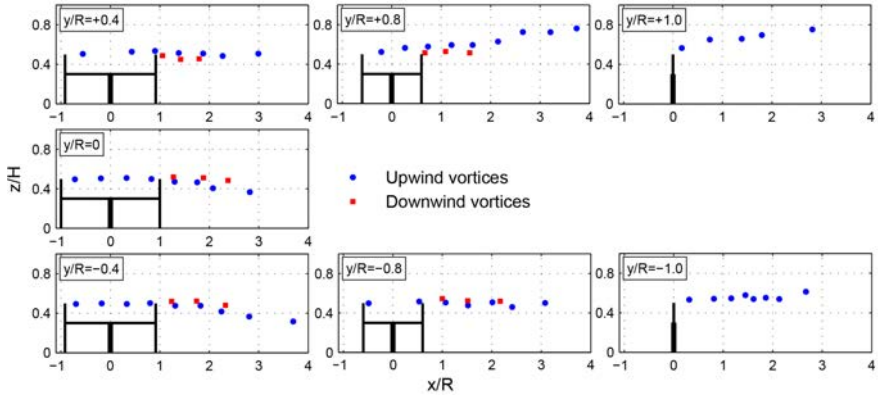

Figure 2.21: Location of tip vortex pairs at different y/R locations.

The stream-wise and cross-stream velocity contours (figs. 2.12 and 2.13, on pages 31 and 32) show larger regions of higher velocity deficit and diverging velocities in the windward S-planes (top plots), and a zero cross-stream velocity located in the leeward side, moving from $y/R = -0.4$ to $y/R = -0.8$. While the flow diverges in the cross-stream direction for $z/H < 0.5$ (leading to the lateral wake expansion), the flow above the wake converges for $z/H > 0.5$. The windward side is also characterized by a higher level of velocity fluctuations (fig. 2.15, on page 34).

The most notable feature in the 3D wake geometry is the behavior in the vertical direction. While the two most windward planes ($y/R = 1, y/R = 0.8$) show a positive vertical velocity and a wake outward motion, the other planes show a negative vertical velocity and a wake inward motion, with the exclusion of the most leeward ($y/R = -1$) where only an initial slight outward motion is present. Such vertical kinematics can be found also by observing the tip vortices positions as shown in fig. 2.19 (right) and fig. 2.21 displaying the projection of the tip vortices position in the vertical planes.

An inward motion of the tip vortex can be observed in the region between $y/R = 0.4$ and $y/R = -0.8$, while an outward motion is noticed for the most leeward ($y/R = -1$) and windward ($y/R > 0.8$) positions. The beginning of the inward motion coincides with the interaction between the upwind-released and downwind-released vortices (the concave and convex parts of the vortex curve), downwind of the rotor area. Within the rotor swept area, the vortex path remains almost horizontal, with the only exception of the most windward region ($y/R > 0.8$). The variation of this vertical motion in the cross-stream direction is not symmetrical with respect to $y/R = 0$: the maximum inward motion is achieved for $-0.4 < y/R < 0$, while the outward motion is much more pronounced in the windward side.

Hofemann *et al.* (2008) have previously shown experimentally an inward motion of the tip vortices, while numerical studies (Ferreira, 2009; Scheurich *et al.*, 2011) have also obtained similar results. Tip vortex inboard motion has also been observed in the near wake of a HAWT (Micallef *et al.*, 2013), although only in a small proximity of the blade.

Figure 2.22, displays vertical profiles of the stream-wise velocity component at sev-

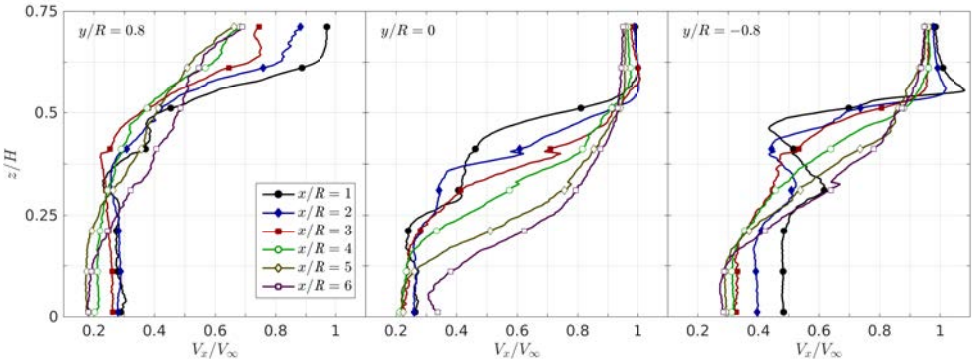

Figure 2.22: Vertical V_x/V_∞ profiles at 6 downwind wake positions for the windward ($y/R = 0.8$, left), meridian ($y/R = 0$, center) and leeward ($y/R = -0.8$,right) S-planes.

eral downstream wake positions in three S-planes ($y/R = 0.8$, $y/R = 0$, and $y/R = -0.8$) and z/H=shows the asymmetric behavior in the induction field. The windward side (left plot) is characterized by a higher region of velocity deficit (extending above $z/H = 0.75$) a stronger and more consistent induction in the lower part and a steeper gradient in the higher part. While the central and leeward sides have less extended velocity deficits and profiles which tends to smooth their gradients.

While in the H-plane measurements, extending until $x/R = 4.5$, the wake undergoes a continuous induction with an increasing stream-wise velocity deficit, the S-plane measurements show signs of wake recovery, already partially visible in fig. 2.22.

Figure 2.23 shows the evolution of the stream-wise velocity component at several vertical positions traveling downwind the wake for the meridian S-plane ($y/R = 0$). The oscillations present in the lines indicates the presence of the vortical structures and their magnitude increases with the proximity to the vortex core. The lower three lines ($z/H = 0.1, 0.2, 0.3$) show a point of minimum velocity (maximum velocity deficit) marking the start of the wake recovery which travels upwind moving upward from the wake center (from $x_{min(V_x)} = 4.5R$ for $z/H = 0.1$ to $x_{min(V_x)} = 2R$ for $z/H = 0.3$).

The locus of all the maximum velocity deficit for several S-planes is presented in fig. 2.24, for $0 < z/H < 0.3$ where the influence of the vortical structures is limited. This wake recovery map shows how the central region of the wake, close to the meridian S-plane, experiences a faster recovery, starting around $1.5 < x/R < 2.5$ at $z/H = 0.3$ and moving to $4.0 < x/R < 4.5$ at $z/H = 0$. The fastest recovery is achieved in the first leeward S-plane for $y/R = -0.4$. Moving to the horizontal edges of the wake, the recovery is later achieved and for the most windward and leeward planes it falls outside the measured domain.

The results represented in fig. 2.24, suggest that the wake recovery happens due to a mechanical transport of the outer flow in the vertical direction following the tip vortices pair-wise instability, while in the horizontal direction the edge vortices, characterized by a longer persistence, act as a shield delaying the mixing.

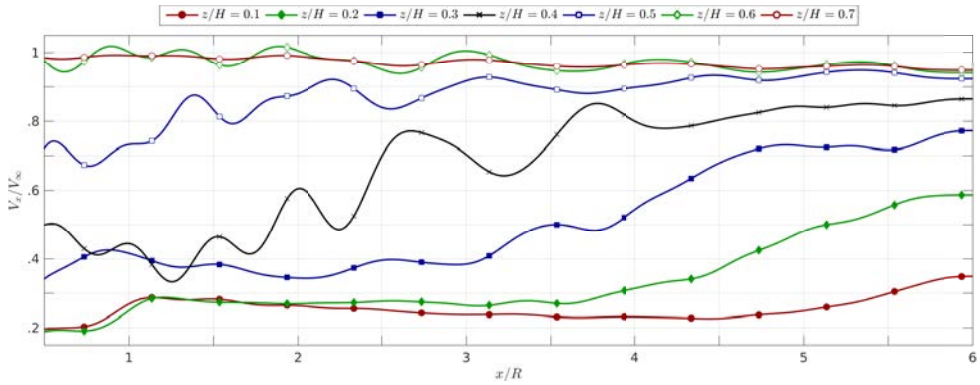

Figure 2.23: Horizontal V_x/V_∞ profiles at 7 vertical positions for the meridian S-plane ($y/R = 0$).

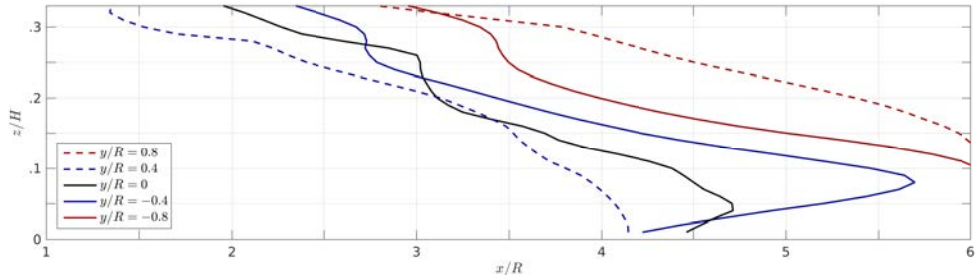

Figure 2.24: Wake recovery map (loci of maximum velocity deficit) for different S-planes.

2.4. CONCLUSIONS

The results of the detailed experimental investigation presented in this chapter helped characterizing the VAWT wake and offered a considerable insight into the physics involved. The use of the PIV technique with the ability to record an extended 2D domain of velocity and vorticity components proved to be extremely helpful in identifying the relevant dynamics.

The first conclusions concern the 3D wake geometry. The wake of a H-VAWT shows an horizontal expansion, a vertical contraction for the inner part and a vertical expansion at the most windward and leeward sides. It is also characterized by a high degree of asymmetry, with the highest velocity deficit, the largest wake expansion and the steeper velocity gradients at the windward side. Moreover this asymmetry increases while the wake travels downstream, suggesting that its origin is not confined to the rotor volume (the asymmetric blade flow from the windward and leeward sides and the rotating tower) but transported in the wake itself by the vortical structures.

The second consideration regards the vorticity dynamics. Two main mechanisms are identified: the formation of the edge vortices at the horizontal boundaries of the wake and the evolution of the tip vortices. The first are caused by the azimuth variation in blade circulation and the consequent release of shed vorticity from the blade trailing edge which then rolls-up in concentrated structures around the location of the multiple BWIs, forming a system of contra-rotating vortices with a vertical axis at the windward and leeward wake edges.

The tip vortices create a cycloidal system with convex and concave parts released by the upwind and downwind blade passages. Since the suction/pressure sides of the blade flip side at the most leeward and windward blade positions the cycloidal system is characterized by co-rotating varying vorticity. The upwind and downwind segment undergo a pair-wise mutual induction which enhance vortex deformation and diffusion finally leading to the vortex break-down. The mutual induction marks also the vertical motion of the structures directed inward in the central part of the wake. Associated with such dynamics there is an early velocity recovery which moving from the upper wake boundary reaches the equatorial plane around 4 radii downstream the turbine tower for the central part of the wake.

The wake can be thus divided into two regions: a first near wake where the geometry of the turbine is clearly visible with cycloidal blade wakes, strong and distinct tip vortices, and a central tower wake. Such region is characterized by strong velocity gradients, a non-uniform induction field and extends until around 3 radii downstream from the tower for the tested VAWT. The transition to the second region is identified with the disappearance of the blades and tower wakes, the mutual induction of the tip vortices, their consequent vertical inward motion and break-down, and the formation of the edge vortices which in the last part of the measured domain are the only visible structures in a wake characterized by a smooth induction field, a high degree of asymmetry and a velocity recovery.

CHAPTER REFERENCES

Chen, T.Y., & Liou, L.R. 2011. Blockage corrections in wind tunnel tests of small horizontal-axis wind turbines. *Experimental Thermal and Fluid Science*, **35**, 565 – 569.

Ferreira, C. 2009. *The Near Wake of the VAWT, 2D and 3D Views of the VAWT Aerodynamics*. Ph.D. thesis, Delft University of Technology.

Garner, H.C., Rogers, E.W.E., Acum, W.E.A., & Maskell, E.C. 1966. *Subsonic Wind Tunnel Wall Corrections*. Tech. rept. AD657092. Advisory Group for Aerospace Research & Development (AGARD).

Gerakopulos, R., Boutilier, M.S.H., & Yarusevych, S. 2010. Aerodynamic Characterization of a NACA 0018 Airfoil at Low Reynolds Numbers. *In: 40th Fluid Dynamics Conference and Exhibit, Chicago*.

Hofemann, C., Ferreira, C., Dixon, K., van Bussel, G.J., van Kuik, G., & Scarano, F. 2008. 3D Stereo PIV Study of Tip Vortex Evolution on a VAWT. *In: Proceeding of European Wind Energy Conference EWEC, Brussels*.

Lignarolo, L.E.M., Ragni, D., Krishnaswami, C., Ferreira, C., Chen, Q., & van Bussel, G.J.W. 2014. Experimental analysis of the wake of a horizontal-axis wind-turbine model. *Renewable Energy*, **70**, 31 – 46.

Micallef, D., van Bussel, G., Ferreira, C., & Sant, T. 2013. An investigation of radial velocities for a horizontal axis wind turbine in axial and yawed flows. *Wind Energy*, **16**(4), 529–544.

Nakano, T., Fujisawa, N., Oguma, Y., Takagi, Y., & Lee, S. 2007. Experimental study on flow and noise characteristics of {NACA0018} airfoil. *Journal of Wind Engineering and Industrial Aerodynamics*, **95**(7), 511 – 531.

Raffel, M., Willert, C.E., Wereley, S., & Kompenhans, J. 2013. *Particle Image Velocimetry: A Practical Guide*. Experimental Fluid Mechanics. Springer Berlin Heidelberg.

Scarano, F., & Riethmuller, M. 2000. Advances in iterative multigrid piv image processing. *Experiments in Fluids*, **29**(2), S51–S60.

Scheurich, F., Fletcher, T.M., & Brown, R.E. 2011. Simulating the Aerodynamic Performance and Wake Dynamics of a Vertical-Axis Wind Turbine. *Wind Energy*, **14**(2), 159–177.

Schrijer, F.F.J., & Scarano, F. 2008. Effect of predictor-corrector filtering on the stability and spatial resolution of iterative PIV interrogation. *Experiments in Fluids*, **45**(5), 927–941.

Selle, J. 1997. *Study on the effectiveness of turbulator tape on boundary-layer transition*. M.Phil. thesis, University of California at Davis.

Stern, F., Muste, M., Beninati, M-L., & Eichinger, W.E. 1999. *Summary of experimental uncertainty assessment methodology with example*. Tech. rept. IIHR Technical Report No. 406. Iowa Institute of Hydraulic Research.

Thomas, F.O., & Liu, X. 2004. An experimental investigation of symmetric and asymmetric turbulent wake development in pressure gradient. *Physics of Fluids*, **16**(5), 1724–1745.

Timmer, W.A. 2008. Two-dimensional low-Reynolds number wind tunnel results for airfoil NACA 0018. *Wind Engineering*, **32**(6), 525–537.

Westerweel, J. 1997. Fundamentals of digital particle image velocimetry. *Measurement Science and Technology*, **8**(12), 1379.

3

THE USE OF A VORTEX ELEMENT METHOD FOR VAWT WAKE AERODYNAMICS

IN the previous chapter the experimental data have been used to gain insight on the physics of Vertical Axis Wind Turbine (VAWT) wake. They have also a critical role in the development of proper numerical models, since their validation relies on detailed experimental data.

The following chapter presents the investigation of a panel code with a free vortex wake as a tool to analyze the aerodynamics of VAWTs, with the ability to represent local flow quantities and a focus on the vorticity dynamics. The model is first presented in its mathematical formulation and numerical implementation, then it is verified against discretization sensitivity, convergence and numerical stability. Finally the data from the simulation are compared with the experimental data from the previous chapter and the accuracy of the model is evaluated.

This chapter is a revised and extended version of the paper *Analysis of a Free Vortex Wake Model for the Study of the Rotor and Near Wake Flow of a Vertical Axis Wind Turbine*, by G. Tescione, C. Ferreira, G.J.W. van Bussel, published on *Renewable Energy* 87 (2016) 552-563, on March 2016.

3.1. APPROACH

The present chapter investigates the use of an unsteady free vortex-wake model developed at TUDelft (Dixon, 2008) for the analysis of the aerodynamics of the wake of a VAWT. First, the model is introduced by the mathematical formulation, the numerical implementation used and the simulated VAWT operation. Then, a verification of the model is performed addressing convergence and stability of the solution. Geometrical discretization of the paneled body and of the vortex wake and temporal discretization are related to the perceived angle of attack of the blade section at the equatorial plane, to assess sensitivity of the results inside the rotor volume. The effect of the initial transient solution originated by the impulsive start of the simulation is also determined and guidelines on the duration of such transient are given. A similar analysis is further performed evaluating the effect on the induction field at different downwind position in the wake to assess the extent of the applicability of the model. Finally, the results of the verified model are validated against the experimental measurements presented and discussed in chapter 2.

3.2. NUMERICAL MODEL

3.2.1. MATHEMATICAL FORMULATION

The model used for this numerical investigation is 3D, unsteady and based on a panel method coupled with a free vortex wake. Aerodynamic panel methods have been known since the 1960s and extensively used in the aeronautic field as analysis and design tools[1].

The model is based on the assumption of an incompressible and potential (inviscid, irrotational) flow, with the exception of vorticity singularities introduced in the wake elements and on the body. Given the relative low Mach number ($M < 0.3$) and high Reynolds numbers ($O(Re_c) \geq 10^5$) experienced by VAWTs such assumptions are considered to be reasonable everywhere in the flow outside the boundary layer.

The potential flow assumption allows for the use of a Boundary Integral Equation for the velocity potential (ϕ, the velocity being $\vec{u} = \nabla\phi$) expressed in one of its general forms as:

$$\phi = \frac{1}{4\pi}\int_{body}\left[\frac{1}{r}\sigma + \frac{\partial}{\partial n}\left(\frac{1}{r}\right)\mu\right]dS + \frac{1}{4\pi}\int_{wake}\frac{\partial}{\partial n}\left(\frac{1}{r}\right)\mu dS + \phi_\infty \tag{3.1}$$

where σ and μ are the singularities on the body and wake surface (S) and r is the distance between the singularity and the location of the potential evaluation. The present model uses a coupled formulation of sources (σ) and doublets (μ) on the actual body geometry for the singularity mix (Morino & Kuo, 1974). Here the doublet strength is taken as independent on each panel and equals the exterior surface value of perturbation potential while the source strength equals its normal derivative ($\vec{n}\cdot\nabla\phi = -\vec{n}\cdot\vec{u}$) to fulfill the zero-normal-velocity boundary condition. To solve for the non-uniqueness of the solution, the Kutta condition, that the pressure difference vanishes at the trailing edge, is used, which drives the entire solution by determining the circulation distribution.

[1] For a review on the history of the methods and overview of the different formulations the reader is referred to Hess (1990), Willis (2006) and the book from Katz & Plotkin (1991).

The wake is modeled as a curved lattice of straight vortex filaments. The wake contribution to the velocity potential in eq. (3.1) (the second integral) is shown as a doublets influence; the actual model shifts from doublets to vortex filaments (of vorticity γ) after few time steps. This is done as the use of a vortex lattice allows for a better handling of deformations of the wake geometry. The equivalence of the doublets and vortex distribution is well known (Hess & Smith, 1967).

Given the incompressibility assumption the time dependency of the solution follows straightforwardly from the time-dependent boundary conditions, hence the unsteady nature of the model. This is of primary importance given the inherent unsteadiness of VAWT aerodynamics.

The use of vorticity to describe the flow brings important advantages when associated to a Lagrangian approach and modifies the governing equation to a simplified form. The further hypothesis of no viscous diffusion and incompressible flow lead to the following formulation for the transport equation of the vorticity:

$$\frac{D\vec{\omega}}{Dt} - (\vec{\omega} \cdot \nabla)\,\vec{u} = 0 \tag{3.2}$$

However the non-linearity of the original Navier-Stokes equations is maintained in the vorticity formulation as the resulting equation describes a non-linear transport phenomenon, since the transport velocity ($\vec{u}$) depends itself on the transport quantity (the vorticity $\vec{\omega}$). The vorticity field induces a velocity field which is responsible for the evolution of the Lagrangian particles.

The recovery of the velocity from the vorticity field is obtained with the integral approach. The Poisson equation for the velocity ($\nabla^2 \vec{u} = -\nabla \times \vec{\omega}$) is solved by means of the Green's function for the Laplacian. This leads to the Biot-Savart law for the velocity induction ($\vec{u}_i$) by a vorticity field ($\vec{\omega}$):

$$\vec{u}_i(\vec{x}, t) = \frac{1}{4\pi} \int_{\mathscr{D}} \frac{\vec{\omega}(\vec{y}, t) \times (\vec{x} - \vec{y})}{|\vec{x} - \vec{y}|^3} d\vec{y} \tag{3.3}$$

which is the basis for the wake-to-wake and wake-to-body induction calculation. The advantage of a vorticity formulation rather than a velocity formulation is that vorticity has a compact support, so the integration is limited to the domain $\mathscr{D}$ where vorticity is non-zero while the velocity field can be evaluated on a larger domain.

3.2.2. NUMERICAL IMPLEMENTATION

The numerical model is implemented in hybrid MATLAB®/CUDA®-C code for an easier use with an Object Oriented Programming (OOP) approach to increase flexibility. The code is, indeed, capable of handling multi-body objects in 2D or 3D of generic geometries and different arbitrary (and time-dependent) motions (Dixon, 2008).

The blades are discretized with flat panels of constant source and doublet strengths. The geometric discretization is refined towards the leading and trailing edges and towards the tips of the blades to account for curvature and higher pressure (velocity) gradients. No deformation of the body is accounted for, so the blades are subject to a rigid

rotation around the vertical axis. This allows to build in a pre-processing phase the aerodynamic influence coefficients of each blade panel to each other, and to use matrix multiplication during the simulation to compute the body-to-body induction.

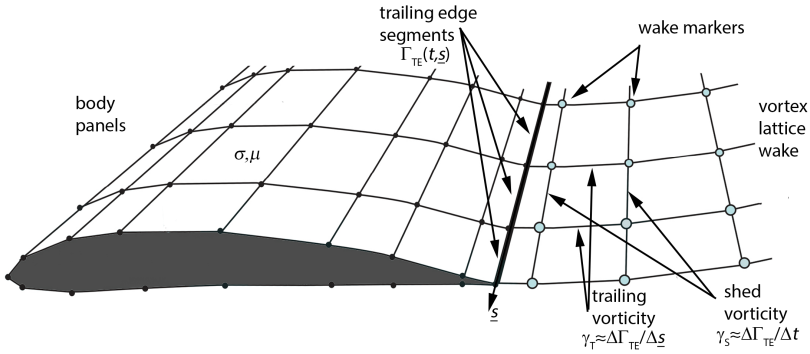

Figure 3.1: Schematics of the vortex lattice wake discretization and the different contributions to the wake vorticity

The wake is modeled as a curved lattice of straight vortex filaments (see fig. 3.1). The strength of the wake elements released each time step is derived by the linearized Kutta condition at the blade trailing edge segments (along the coordinate $\vec{s}$). Spatial derivatives of the circulation between adjacent trailing edge segments ($\frac{\Delta\Gamma_{TE}}{\Delta\vec{s}}$) determine the trailing vorticity (γ_T) of the wake filaments perpendicular to the trailing edge. Temporal derivatives ($\frac{\Delta\Gamma_{TE}}{\Delta t}$) determine the shed vorticity (γ_S) of the wake filaments parallel to the trailing edge. Wake elements are emitted only by the trailing edges, no wake elements are emitted in the span-wise direction from the tip of the blades. The new wake marker position is defined by calculating the local kinematic velocity at the trailing edge.

A free-wake analysis is used where the new position of each wake marker is an integral part of the problem. This is essential in the cases of VAWT as the rotor operates partially in its own wake. For each time step the induction field of all the wake filaments and of the body panels is computed on the location of the wake markers (the filaments' endpoints) by a direct summation.

To ensure de-singularization of eq. (3.3) the filaments have a viscous core with a Rankine-type behavior. No viscous diffusion of the filament vorticity is currently included in the model. As the endpoints of the filaments are used as markers, vortex stretching and tilting is automatically considered (the $(\vec{\omega}\cdot\nabla)\,\vec{u}$ term in eq. (3.2)). Because of its completely Lagrangian formulation the model requires no grid creation and avoids numerical dissipation of vorticity. An explicit second order Adam-Bashforth method is used for the time marching scheme. No wake cut-off is used: all wake elements are retained for the whole simulation.

The resulting N-body problem (with an $O\left(N^2\right)$ computational cost and an $O(N)$ memory access) is very suitable for computational parallelization, especially with the use of Graphic Processing Unit (GPU) -based systems (Stock & Gharakhani, 2008). The most computational expensive functions, the wake-to-wake and wake-to-body induction calculations, have been implemented in CUDA®-C and run parallel on a NVIDIA® Quadro

4000 GPU (256 cores, 243 GFlops in double precision and 89.6 GB/s memory bandwidth). This brings to a speed up of the calculations up to 120× with respect to a pure MATLAB® execution for a mid-refined simulation. This allows for higher refined and/or long-time simulations.

The simulation output records the position of the filaments markers and associated vorticity strength for the desired time steps together with the position of the blade panels and their singularity strength. In a post-process phase the velocity can then be evaluated at the desired locations with the same functions used during the simulation for the velocity recovery of eq. (3.3).

A simplified geometry of the VAWT model used in the experimental analysis of chapter 2, consisting of the turbine's blades only has been used in the numerical analysis. No central shaft and no supporting struts are included in the computation. Moreover the incoming wind (V_∞) is supposed to be uniform without any turbulence added.

3.3. MODEL VERIFICATION

3.3.1. DISCRETIZATION AND SENSITIVITY ANALYSIS

A sensitivity analysis has been conducted to determine the influence of the temporal and spatial discretization of the model. Three independent parameters have been considered: the azimuth step ($\Delta\theta$), for the temporal discretization; the number of Span-wise Panels (SPAN) and Chord-wise Panels (CPAN), for the spatial discretization. A simplified one-factor-at-a-time approach is used, where for each study only one of the three parameters is varied while the others are kept at a baseline value. The perceived angle of attack of the section at the middle of the blade ($\alpha_{z0}(\theta)$) is used as the evaluation output. This is determined from the induced velocity at six locations distributed around the quarter chord point, and represents a more detailed choice than using an integral parameter such as the thrust or power coefficient.

In the following plots (figs. 3.2 to 3.5) two parts with different behavior can be identified: the upwind part of the blade rotation ($0° \leq \theta \leq 180°$), characterized by a smooth sinusoidal-like distribution of $\alpha_{z0}(\theta)$, and the downwind part of the rotation ($180° \leq \theta \leq 360°$), where multiple Blade-Wake Interactions (BWIs) cause a noisy, relatively flat, distribution of $\alpha_{z0}(\theta)$. This is the region where the lines show the largest deviations; it is, however, a region characterized by a lower level of coherence as the location of the BWIs can slightly differ for each realization.

Figure 3.2 shows the sensitivity analysis for the azimuth step, ranging from $\Delta\theta = 10°$ (blue line) to $\Delta\theta = 1°$ (black line), for a standard simulation (30 panels chord-wise, 30 panels span-wise, 15 simulated rotations).

The four lines in the figure show overall small deviations. Apart from some small regions, differences in $\alpha_{z0}(\theta)$ are bounded to $\pm 0.1°$ and $\pm 0.2°$ in the upwind and downwind parts. Since there is no sensible difference between the $\Delta\theta = 5°$ and the $\Delta\theta = 2°$, while the computational cost increases by almost ten times (it simultaneously affects the elements in the wake and the number of evaluations), $\Delta\theta = 5°$ is chosen for the following simulations.

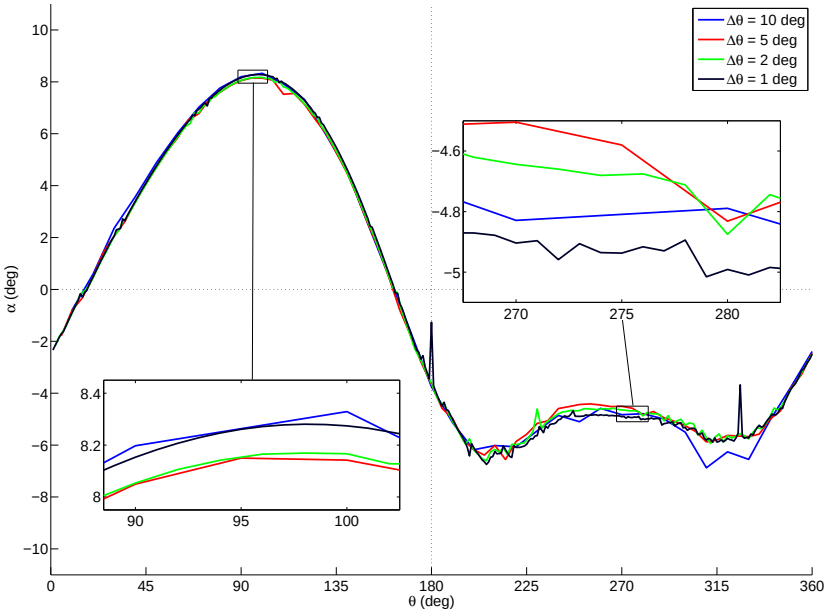

Figure 3.2: Effect of the azimuth step ($\Delta\theta$) on the angle of attack at the middle of the blade ($\alpha_{z0}(\theta)$) across the azimuth (θ)

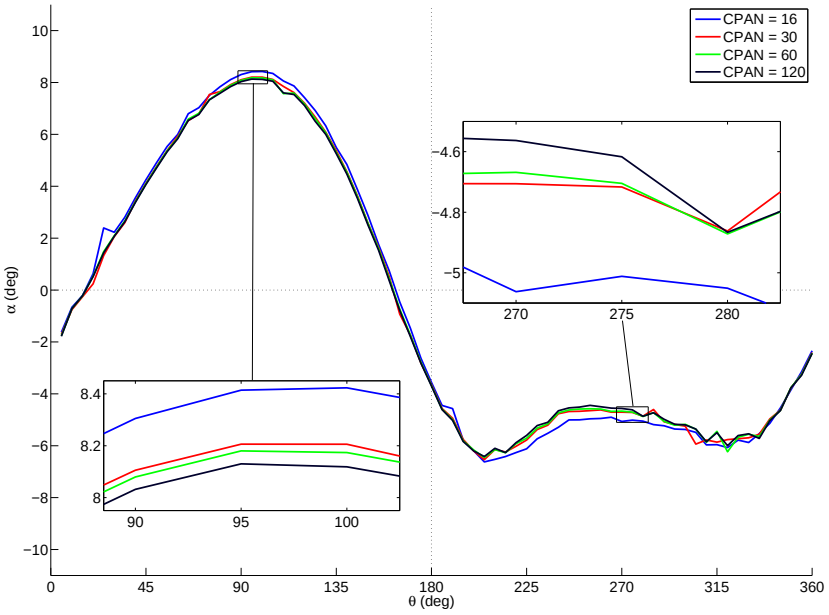

Figure 3.3: Effect of the number of chord-wise panel (CPAN) on the angle of attack at the middle of the blade ($\alpha_{z0}(\theta)$) across the azimuth (θ)

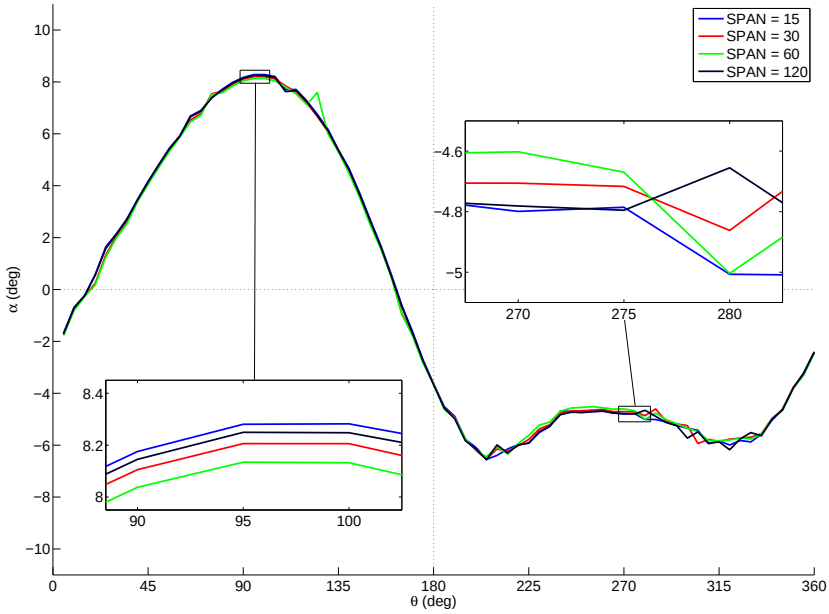

Figure 3.4: Effect of the number of span-wise panel (SPAN) on the angle of attack at the middle of the blade ($\alpha_{z0}(\theta)$) across the azimuth (θ)

The influence of the spatial discretization is investigated by refining the number of panels on the blade, both in chord-wise and span-wise direction. Increasing the number of span-wise panels increases also the number of elements in the wake resulting in a significant increase in computational time; while increasing the number of chord-wise panels has a smaller effect. Figure 3.3 shows the sensitivity of the output to the chord-wise panels. The chord-wise discretization seems to be of relative influence, with the first refinement (from 16 to 30 CPAN) being of higher impact than the following. A 30 chord-wise panels is chosen for the following simulations, since the incremental value of a grid refinement is minimal.

Figure 3.4 shows the effect of a refinement in the number of span-wise panels. The parameter does not have a significant effect on the flow perceived by the blade at the equatorial plane, with variations of angle of attack in the range of values considered (15 to 120 span-wise panels) of $\pm 0.1^\circ$ and $\pm 0.2^\circ$ in the upwind and downwind parts. It is important, however, to consider that the parameter has an effect on the ability of the wake lattice to correctly follow deformations in its vertical extension. Since the maximum deformations are expected to happen at the vertical boundaries for the roll-up of the tip vortices, a value of 60 span-wise panels with a refined discretization at the blade tips is chosen for the following simulations. A reduction to 30 panels will lower the accuracy of the tip vortex evolution in the wake, but will be of minimal impact on the rotor flow while decreasing the computational time of 8.5×.

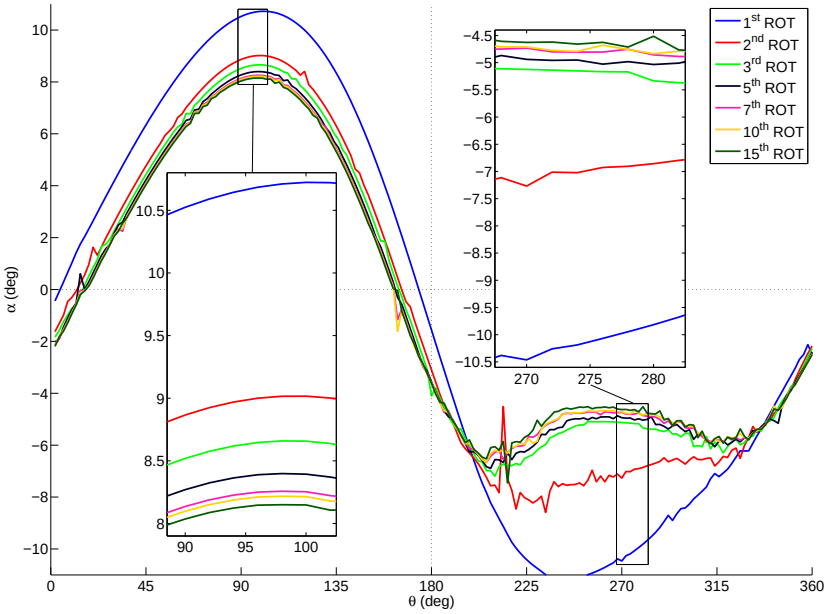

Figure 3.5: Effect of the simulated number of rotations (SROT) on the angle of attack at the middle of the blade ($\alpha_{z0}(\theta)$) across the azimuth (θ)

3.3.2. CONVERGENCE ANALYSIS AND NUMERICAL UNCERTAINTY

Since the model is unsteady and the simulation starts with an impulsive start of the rotor with no wake, an initial transient develops before the flow field reaches a converged periodic solution. An effect similar to the starting vortex of an airfoil is observed with the initial wake rolling up behind the rotor and the induction field at the rotor level gradually building up as more wake is released. The required minimum wake length for a converged periodic solution is evaluated here, as well as the periodicity of the solution for both the rotor flow and the wake flow.

Figure 3.5 shows the convergence analysis for the rotor flow. The number of Simulated Rotations (SROT) is varied for a standard simulation (30 panels chord-wise, 60 panels span-wise, $\Delta\theta = 5°$). The perceived angle of attack of the section at the middle of the blade ($\alpha_{z0}(\theta)$) is used as in the previous section as a local value representative of the rotor flow. A converged solution is reached after 7 rotations with incremental values bounded at 0.1° and 0.2° in the upwind and downwind parts. These values, comparable to the one found for the sensitivity analysis, correspond to variations of 1.5% of V_∞ and are considered the numerical uncertainty of the solution in the rotor volume (ϵ_R).

An analysis of the instantaneous flow field at different time steps of the converged simulation showed a highly coherent periodical flow with a frequency of N/Ω, with the region of the BWIs showing the higher degree of fluctuations.

Since the wake induction scales with $1/r^2$ (eq. (3.3)), further downstream locations reach convergence at a later stage. An extended simulation (45 full rotations) has been

x/R	SROT	$\epsilon_W(x)$	x/R	SROT	$\epsilon_W(x)$	x/R	SROT	$\epsilon_W(x)$
1	7	1.4%	4	11	4.7%	8	21	6.2%
2	9	1.5%	5	17	5.5%	10	23	6.5%
3	10	4.0%	6	18	6.1%	12	27	7.3%

Table 3.1: Number of rotations for convergence (SROT) and numerical uncertainty for the wake flow ($\epsilon_W(x)$).

performed to evaluate convergence and periodicity of the solution in the wake flow until 6 diameters downwind the shaft. Averaged values of the stream-wise velocity component have been analyzed inside and outside the wake.

The coherence of the solution with the frequency of the blade rotation gradually decreases as the wake moves downstream. A series of averages over one rotation show periodic deviations which become more random when the average is done over a longer period. There is a sensible decrease in the spread between consecutive averages as the starting wake influence decreases; when convergence is reached the deviations between the different profiles oscillate between fixed limits. Table 3.1 shows an extract of the analysis with the simulated rotations needed to reach convergence at different downstream positions and the maximum velocity oscillations (as % of V_∞) found after convergence at the wake center line, which are representative of the numerical uncertainty for the wake flow ($\epsilon_W(x)$).

3.4. MODEL VALIDATION

The model validation is performed by comparing the velocity fields from the simulation with those obtained in the experimental campaign described in chapter 2. The simulation parameters used for the model validation are a 5° azimuth step, 30 panels chord-wise, 60 panels span-wise and a 20 rotations transient, in order to reach a converged solution in the whole domain interested by the experimental measurements.

The experiments provided averaged phase-locked velocity fields at the equatorial plane (H-plane) and at seven vertical planes (S-planes) spanning in the cross-stream direction ($y/D = -0.5, -0.4, -0.2, 0, 0.2, 0.4, 0.5$) in the rotor area and until 3 diameters downstream the shaft. In order to account for the oscillations observed in the solution in section 3.3.2 the numerical data are also a phase-locked averaged. They are obtained by considering the instantaneous solutions every 180°[2] for the next 25 rotations after reaching the convergence, and performing the average of the 50-samples set.

With this parameters, 785'000 vortex filaments are computed in the last step of the simulation. On the workstation used for the calculations[3] the computational time is of circa four hours.

H-PLANE

The first comparison between the simulations and the experimental data is on the velocity fields in the equatorial H-plane. Figures 3.6 and 3.7 show the contour plots for the

[2] taking into account the symmetry of the two-blades rotor

[3] intel i7-950 with 8 cores @ 3 GHz, 12 GB RAM, and NVIDIA® Quadro 4000 GPU with 256 cores, 243 GFlops in double precision and 89.6 GB/s memory bandwidth

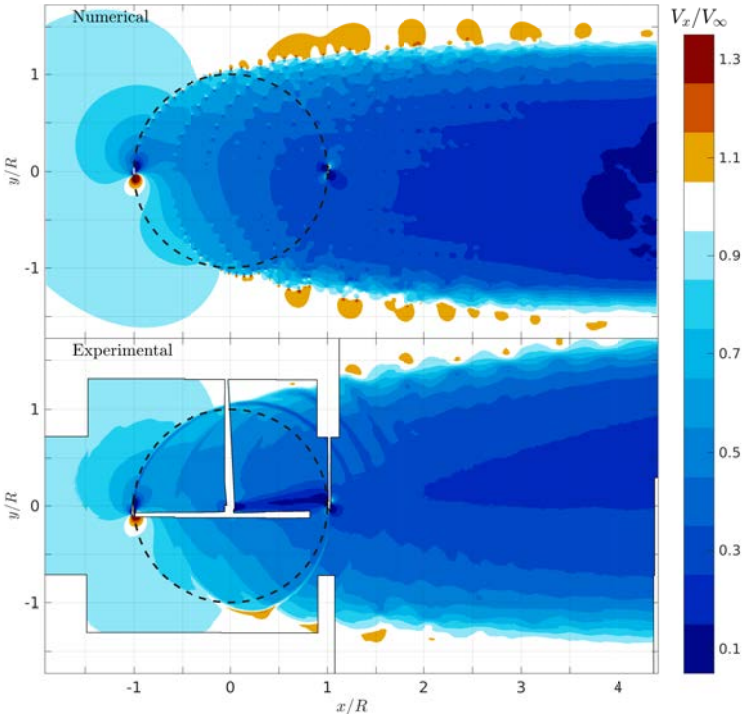

Figure 3.6: Contour levels of the stream-wise velocity component (V_x/V_∞) in the equatorial H-plane ($z = 0$) for the numerical (top) and experimental (bottom) results.

stream-wise and cross-stream velocity components (V_x and V_y respectively) for $z = 0$. The numerical data are shown on the top and the experimental data on the bottom. The velocities are made non-dimensional by the free stream V_∞ and the experimental and numerical contour plots share the same contour levels for an easy comparison.

The stream-wise velocities (fig. 3.6) are very well predicted for the upwind ($\frac{x}{D} \leq -0.5$) and in-rotor ($-0.5 \leq \frac{x}{D} \leq 0.5$) area with the exclusion of the region just downstream of the turbine shaft ($\frac{x}{D} \geq 0$, $\frac{y}{R} \approx 0$). Here, the experimental results show a dominant viscous wake of the rotating cylinder while in the numerical results this is absent since the shaft is not simulated.

The wake flow in the numerical solution presents some differences with the experimental data which affect the asymmetry of the wake. The wake of the numerical simulation in the equatorial H-plane lacks the high level of asymmetry observed in the experiments. While the wake extension is well predicted for the leeward side ($\frac{y}{R} \leq 0$), in the windward side ($\frac{y}{R} \geq 0$) the numerical results underestimate the wake expansion by roughly 20% at $x/R = 4$. The cross-stream velocity contour plot shows indeed an outward velocity component in the windward part of the wake (the orange area in fig. 3.7) for the experimental data which is absent in the numerical results. The lack of the rotating shaft in the numerical simulation can be addressed as a source of such discrepancy, but its contribution has not been quantified.

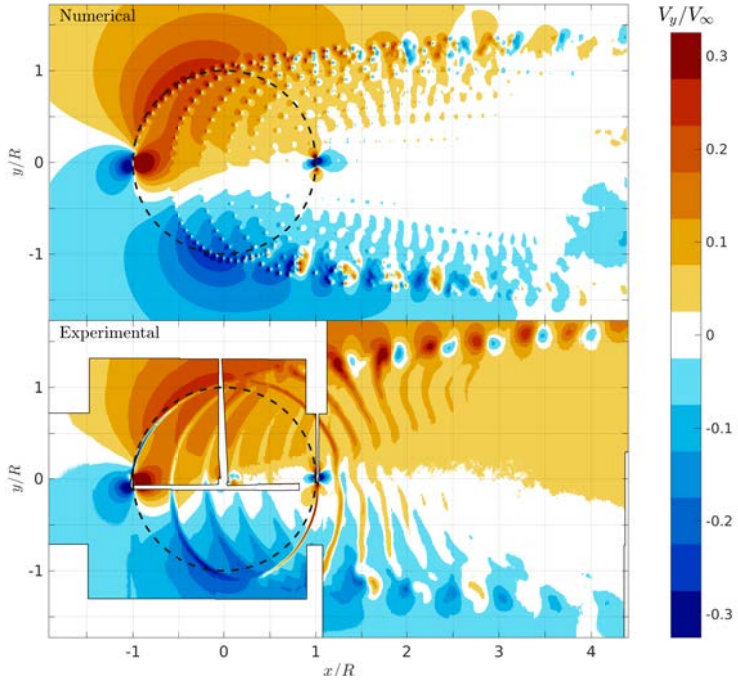

Figure 3.7: Contour levels of the cross-stream velocity component (V_y/V_∞) in the equatorial H-plane ($z = 0$) for the numerical (top) and experimental (bottom) results.

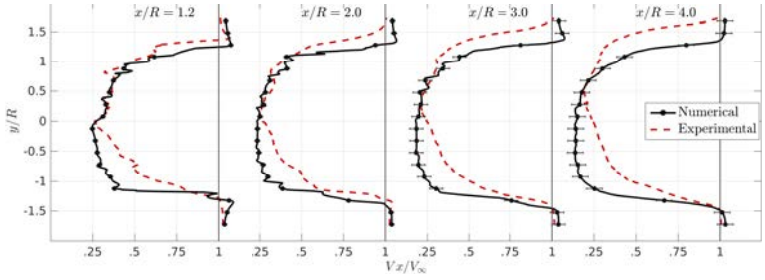

Figure 3.8: Stream-wise velocity profiles (V_x/V_∞) at different downstream positions in the equatorial H-plane ($z = 0$) for the numerical (black line) and experimental (red line) results.

The comparison of the induction levels can be observed on fig. 3.8 which shows the stream-wise velocity profiles at different downstream locations in the wake. Although the leeward wake expansion is well predicted, the induction level at the leeward side and part of the windward side ($\frac{y}{R} \leq 0.5$) is higher for the numerical simulation than for the experimental data. The deviations supersede the numerical uncertainty reaching an RMS value of 14% at $x/R = 1$ and 17% at $x/R = 4$. This results also in a steeper shear layer in the leeward boundary of the wake.

On the other side the induction of the most windward part of the wake ($\frac{y}{R} \geq 0.5$) is lower in the numerical simulation with an RMS error value of 15% at $x/R = 1$ and 34% at $x/R = 4$. The two effects counteract each other and integral values of the stream-wise velocity in the two wakes have differences of around 4.5% with the numerical results showing the higher velocity deficit.

S-PLANES

Figures 3.9 to 3.13 show the comparison of the contour plots of the stream-wise, cross-stream and vertical velocity components (V_x, V_y, and V_z, respectively top, middle, and bottom parts of the figures) for the S-planes in the windward side (fig. 3.9:$y/R = 0.8$, and fig. 3.10:$y/R = 0.4$), for the meridian S-plane (fig. 3.11:$y/R = 0$) and in the leeward side (fig. 3.12:$y/R = -0.4$, and fig. 3.13:$y/R = -0.8$). As for the previous case, the velocities are made non-dimensional by the free stream V_∞ and the same contour levels are used for the numerical (upper plots) and experimental (lower plots) results.

Observing the contour plots an overall good agreement can be seen between experimental and numerical results. Contour levels are well predicted for the stream-wise velocity and especially for the cross-stream and vertical velocity, with some local discrepancies. Also the dynamics of the tip vortices is correctly captured with their inboard motion in the middle part of the wake, already observed in other experiments and simulations (Ferreira, 2009; Hofemann *et al.*, 2008; Scheurich *et al.*, 2011).

The most noticeable difference is in the vertical expansion of the windward side of the wake ($y/R \geq 0$) where the experiments showed a pronounced vertical expansion, higher than the one in the leeward side($y/R \leq 0$), while the numerical solution shows a reduced expansion comparable to the one on the leeward side. A similar result was observed in section 3.4. In this sense the results from the S-planes extend the findings of the comparison for the equatorial H-plane, with the wake of the numerical simulation showing a lower degree of asymmetry also in the vertical direction.

The cross-stream velocity fields give more insight in the wake dynamics not correctly predicted by the numerical model and explain some of the differences found in the previous section. The experimental results showed positive cross-stream velocities inside the wake in the windward side and in the meridian plane, leading to a migration of the wake to the windward side. The numerical results show a similar behavior only in the first 3 radii of the wake, where the blade wakes are still dominant. Further downstream, positive cross-stream velocities are localized only in the surroundings of the tip vortices for the windward side while negative values are found for the leeward side. This results

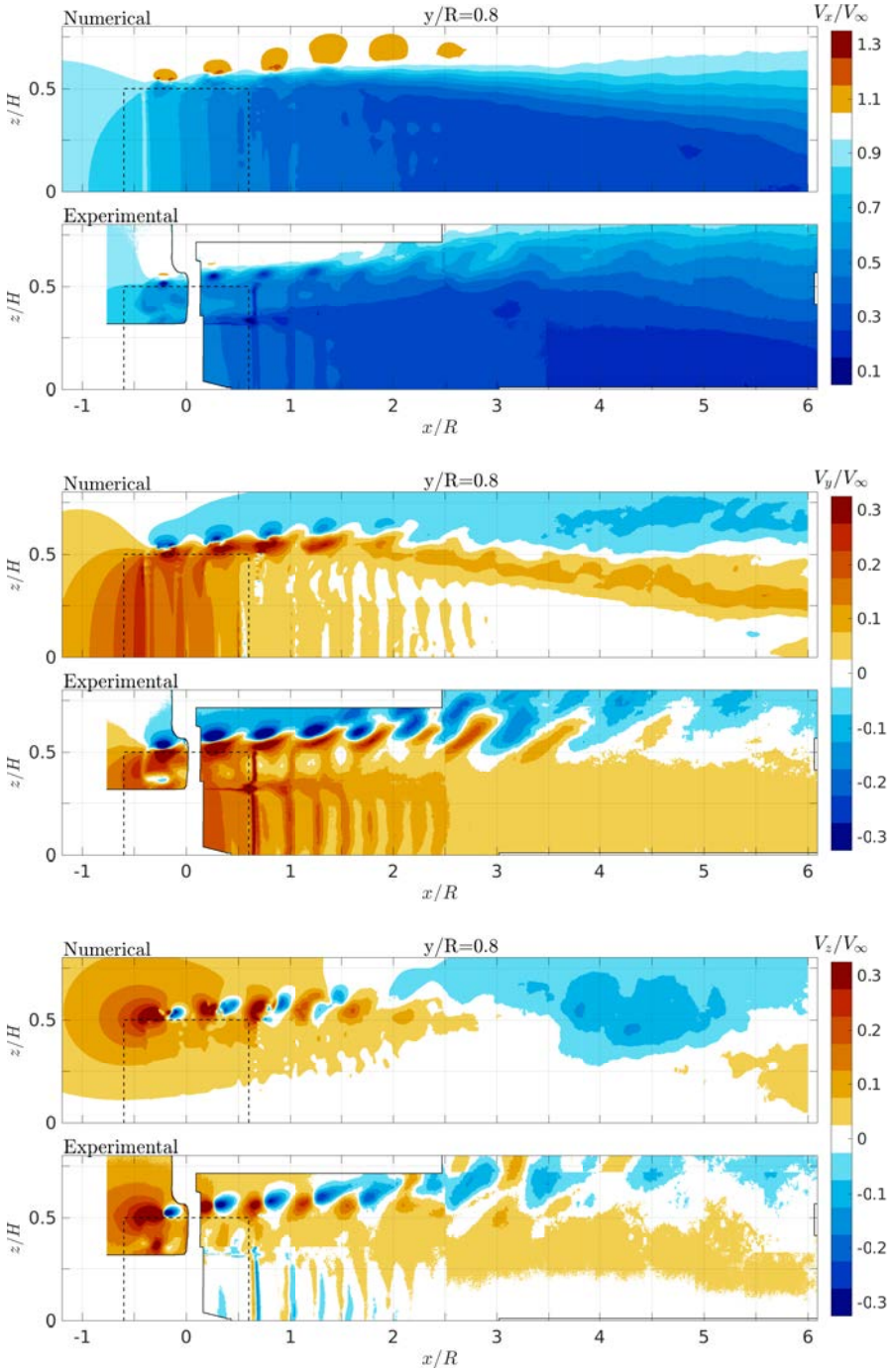

Figure 3.9: Contour levels of velocity components, V_x/V_∞ (top), V_y/V_∞ (middle), V_z/V_∞ (bottom), in the windward side ($y/R = 0.8$) for the numerical (upper plots) and experimental (lower plots) results.

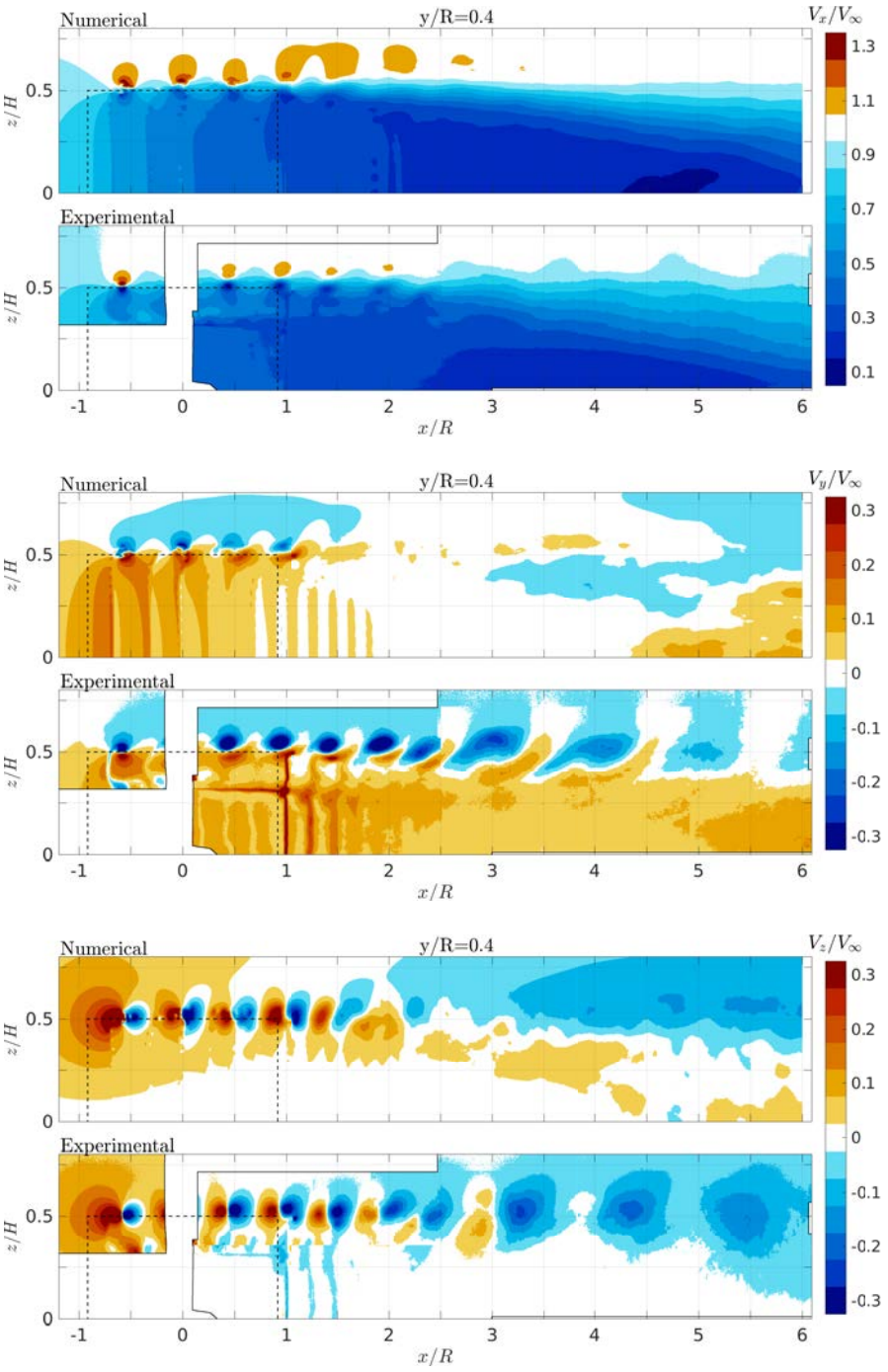

Figure 3.10: Contour levels of velocity components, V_x/V_∞ (top), V_y/V_∞ (middle), V_z/V_∞ (bottom), in the windward side ($y/R = 0.4$) for the numerical (upper plots) and experimental (lower plots) results.

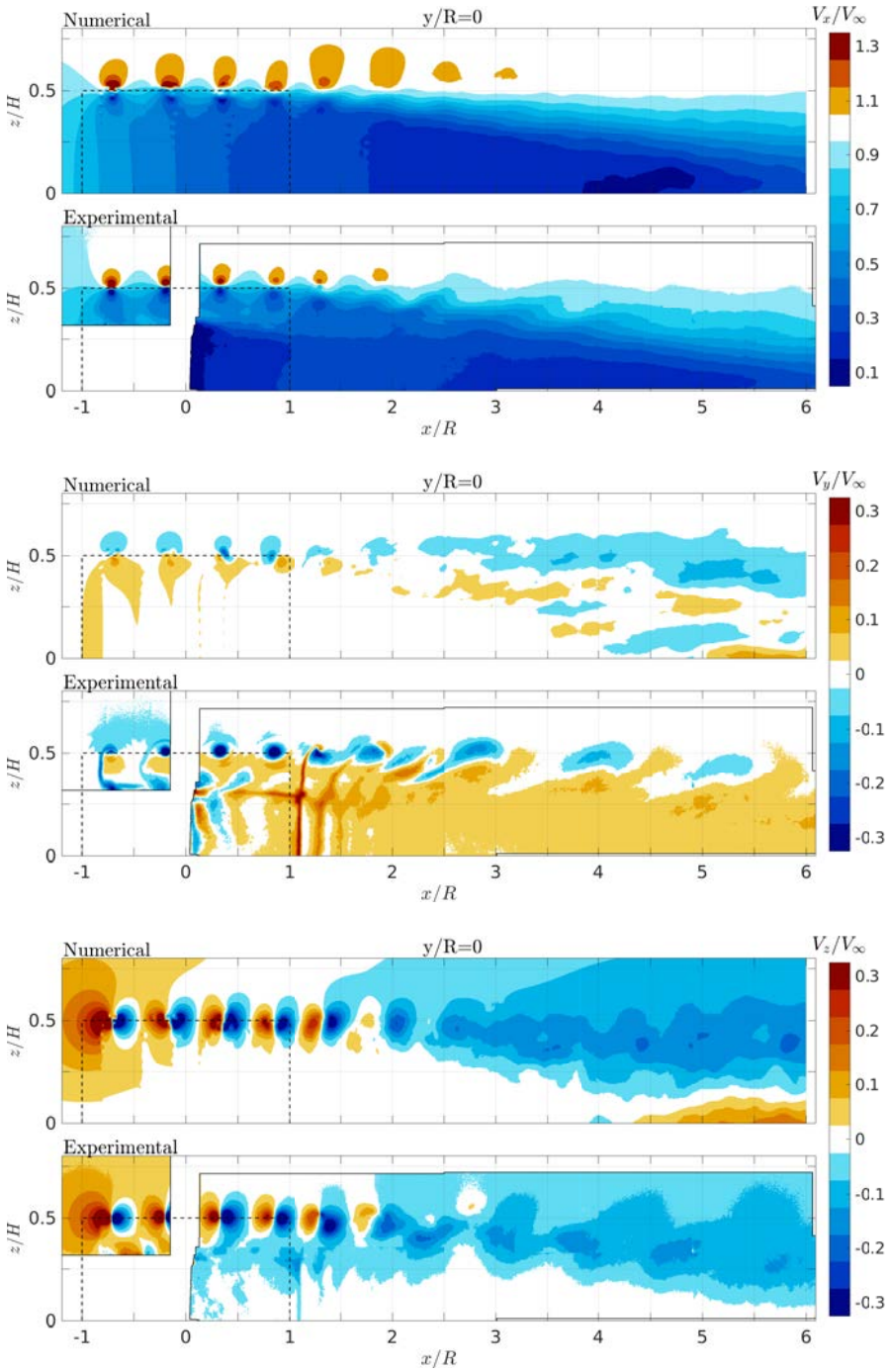

Figure 3.11: Contour levels of velocity components, V_x/V_∞ (top), V_y/V_∞ (middle), V_z/V_∞ (bottom), in the meridian plane ($y/R = 0$) for the numerical (upper plots) and experimental (lower plots) results.

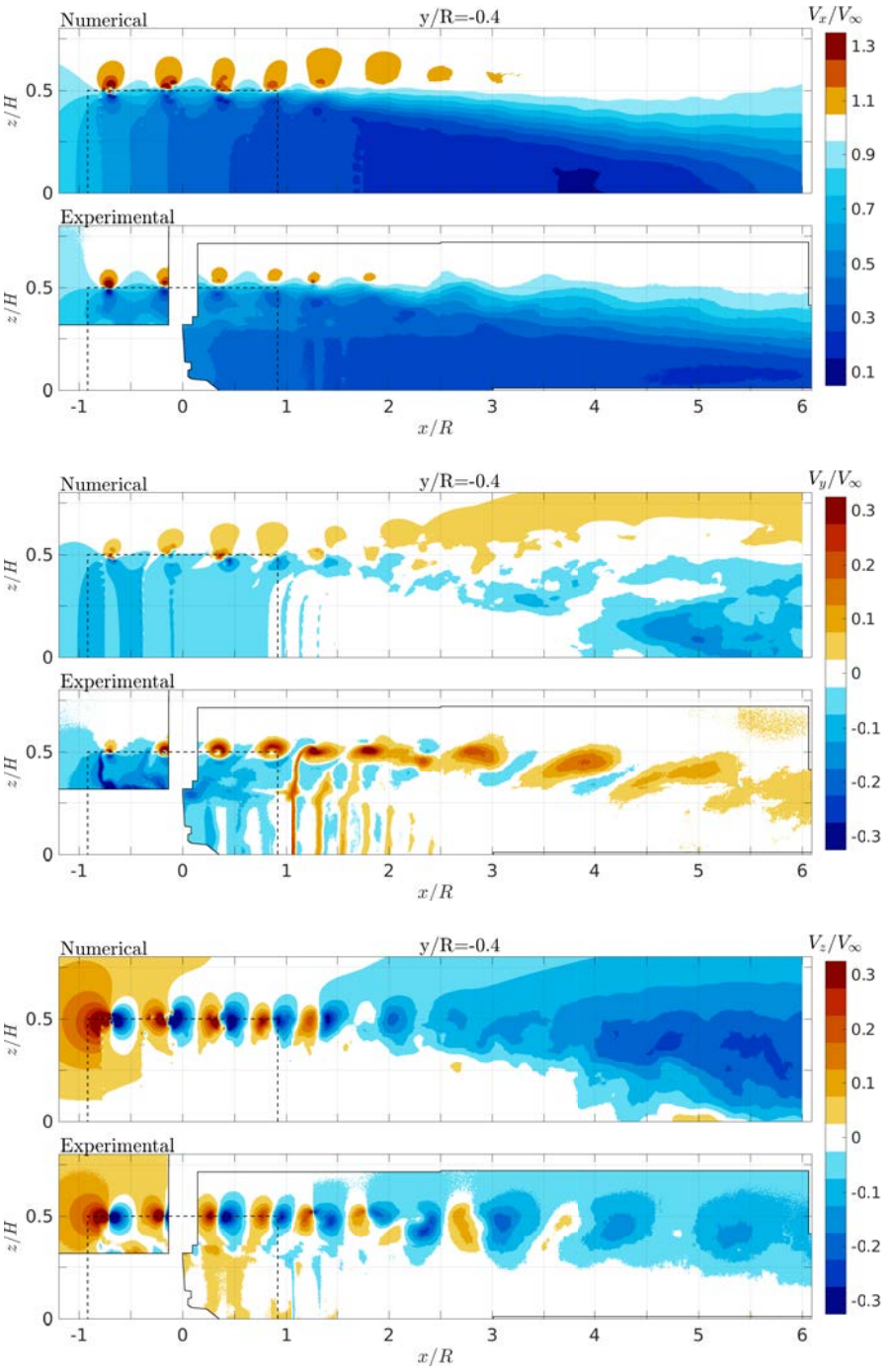

Figure 3.12: Contour levels of velocity components, V_x/V_∞ (top), V_y/V_∞ (middle), V_z/V_∞ (bottom), in the leeward side ($y/R = -0.4$) for the numerical (upper plots) and experimental (lower plots) results.

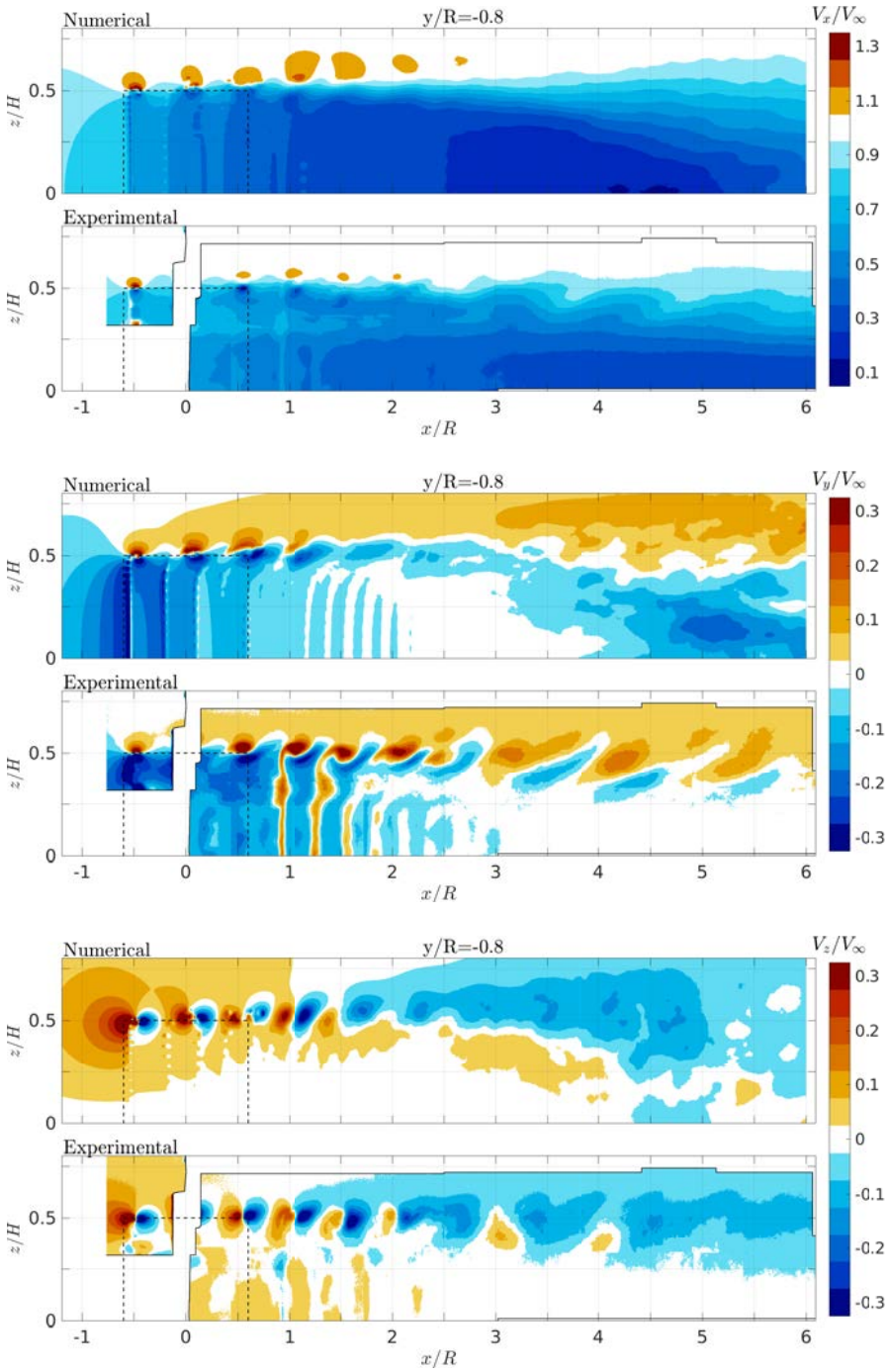

Figure 3.13: Contour levels of velocity components, V_x/V_∞ (top), V_y/V_∞ (middle), V_z/V_∞ (bottom), in the leeward side ($y/R = -0.8$) for the numerical (upper plots) and experimental (lower plots) results.

in an initial shift of the near wake to the windward side which is then counteracted by an opposite motion, partially restoring the initial asymmetry.

The comparison of the induction levels can be observed on fig. 3.14 which shows the stream-wise velocity profiles at different downstream locations in the wake, for the windward, meridian and leeward planes. There is an overall good agreement between numerical and experimental data, with better results for the central part of the wake and a lower level of confidence moving towards the wake boundaries. The wake expansion is well predicted with the exception of the underestimated vertical expansion of the most windward locations. Similarly to the H-plane case the leeward side shows higher induction factors in the numerical simulation while the windward side show a lower induction than the experimental data. The deviations are lower than the case of the H-plane, with average RMS values of 22.7%, 15.3%, 7.1%, 6.5%, 8.4%, 11.8%, 17.3% for $y/R = 1.0, 0.8, 0.4, 0, -0.4, -0.8, -1.0$.

3.5. CONCLUSIONS

A free vortex wake model has been verified and validated with experimental measurements of a VAWT wake. The model has been analyzed in terms of sensitivity of the output to the simulation parameters, and showed little sensitivity to the spatial and temporal discretizations.

Next, the convergence and coherence of the periodic solution has been investigated. For the flow inside the rotor (for loads evaluations of a single turbine), a medium discretization (30 chord-wise panels, 30 span-wise panels, 5° of azimuth step) gives a converged solution in terms of angles of attack experienced by the blade, after an initial transient of around 7 rotations. On a normal workstation equipped with a GPU such simulation leads to a computational time of 30 minutes. Any further grid refinement, by doubling the blade panels or halving the azimuth step, or any added simulated rotation leads to a marginal change in the angles of attack of maximum ±0.2°, corresponding to a velocity uncertainty of 1.5% of V_∞.

In the wake the flow reaches a converged periodic solution with an increasing transient moving further downstream. At the same time the coherence of the periodic solution decreases with the downstream distance and more energy is found at lower frequencies. At 3, 6 and 12 radii downwind the shaft a converged solution is reached after 10, 18 and 27 rotations with velocity uncertainties of 4.0%, 6.1% and 7.3% of V_∞.

The numerical results have been compared to the measurements of the previous experimental activity on wind tunnel model, running at a tip speed ratio of $\lambda = 4.5$ and a chord-based Reynolds number of 1.7×10^5. The model is capable of capturing all the dominant dynamics in the wake of VAWT and give also good quantitative evaluation of the flow field. Comparisons show very good prediction of the flow field upwind and inside the rotor area. The dynamics of the vortical structures in the horizontal plane is very well captured as well as the vertical motion of the tip vortices with the already observed central contraction and lateral expansion.

The results in the near wake show good prediction of the wake flow in the leeward side but tend to underestimate the wake horizontal and vertical expansion in the windward side by almost 20% compared to the experimental results, decreasing the high asymmetry observed in the experiments.

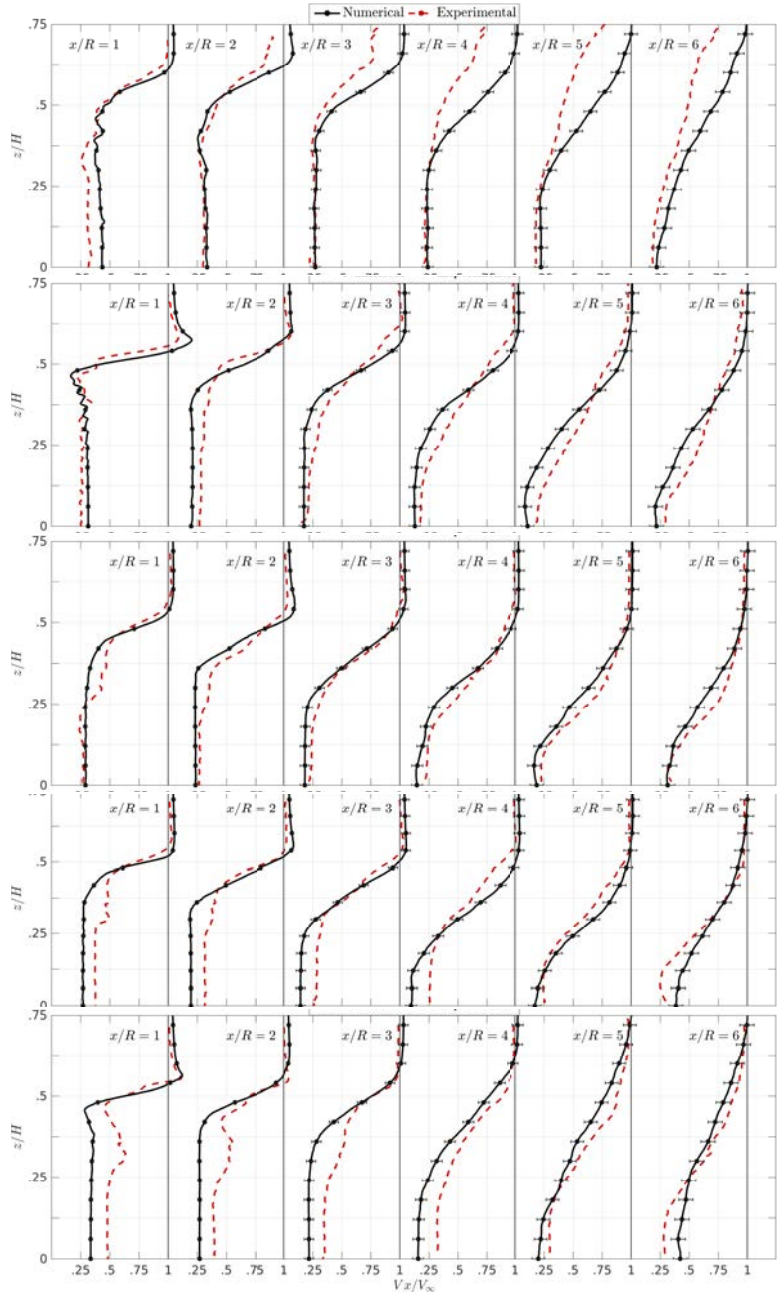

Figure 3.14: Stream-wise velocity profiles (V_x/V_∞) at different downstream positions in the equatorial H-plane ($z = 0$) for the numerical (black line) and experimental (red line) results.

The induction levels are predicted with a good accuracy which is higher for the central part of the wake. Considering the absence of the shift of the wake to the windward side, the integral values of induction are predicted within the numerical uncertainty, with the numerical model leading to higher velocity deficit of around 5%.

The reasons for such discrepancies are to be found in the comparison between a numerical model without diffusion scheme and an experimental model run at a low Reynolds number. Moreover the absence of the struts in the simulation may be responsible for an initial overshoot of the tip vortex strength and the absence of the turbine shaft for a part of the wake asymmetry.

It is believed that simulations of higher Reynolds number cases, comprising the struts and the turbine shaft will see their accuracy increased, making the model a valuable tool for the analysis of multi-MW VAWTs.

CHAPTER REFERENCES

Dixon, K.R. 2008. *The Near Wake Structure of a Vertical Axis Wind Turbine*. M.Phil. thesis, Delft University of Technology.

Ferreira, C. 2009. *The Near Wake of the VAWT, 2D and 3D Views of the VAWT Aerodynamics*. Ph.D. thesis, Delft University of Technology.

Hess, J.L. 1990. Panel Methods in Computational Fluid Dynamics. *Annu. Rev. of Fluid Mech.*, **22**, 255–74.

Hess, J.L., & Smith, A.M.O. 1967. Calculation of Potential Flow about Arbitrary Bodies. *Progress in Aeronautical Sciences*, **8**, 1–138.

Hofemann, C., Ferreira, C., Dixon, K., van Bussel, G.J., van Kuik, G., & Scarano, F. 2008. 3D Stereo PIV Study of Tip Vortex Evolution on a VAWT. *In: Proceeding of European Wind Energy Conference EWEC, Brussels*.

Katz, J., & Plotkin, A. 1991. *Low-Speed Aerodynamics: from Wing Theory to Panel Methods*. New York: McGraw-Hill.

Morino, L., & Kuo, C.C. 1974. Subsonic Potential Aerodynamics for Complex Configurations: A General Theory. *AAIA J*, **12**(2), 191–197.

Scheurich, F., Fletcher, T.M., & Brown, R.E. 2011. Simulating the Aerodynamic Performance and Wake Dynamics of a Vertical-Axis Wind Turbine. *Wind Energy*, **14**(2), 159–177.

Stock, M.J., & Gharakhani, A. 2008 (January). Toward Efficient GPU-Accelerated N-Body Simulations. *In: 46th AIAA Aerospace Sciences Meeting and Exhibit*.

Willis, D.J. 2006. *An Unsteady, Accelerated, High Order Panel Method with Vortex Particle Wakes*. Ph.D. thesis, Massachusetts Institute of Technology.

4

Numerical Analysis and Comparison of VAWT and HAWT Wakes

In chapter 2 the experimental approach proved to be useful for the understanding of the physical phenomena characterizing the dynamics of VAWT wake flow. Experiments, however, being rather expensive, can only be used in a limited number of test cases or with a limited spatial and temporal extent and resolution. The numerical approach is, on the contrary, much more sustainable and can, when properly validated, provide comparable and complementary information than those gained by experiments.

In this chapter the numerical model verified and validated in chapter 3 is used in order to extend the analysis performed experimentally in chapter 2. The model turbine is upscaled to a 5-MW machine and the three-dimensional topology of its wake is analyzed in more details and further downstream than the experiment setup allowed. Moreover, the results are compared to those of an equivalent horizontal axis wind turbine, and the energy available to a downwind turbine at different downstream distances is evaluated.

Results show how the peculiar geometry evolution of the wake of the vertical axis wind turbine leads to a decrease of the stream-wise turbine spacing in a wind farm and demonstrate the unsuitability of HAWT wake models for VAWT wind farm optimization and operation.

This chapter is a revised and extended version of the paper *A Comparison of the Wake Evolution for 5-MW Vertical and Horizontal Axis Wind Turbines*, by G. Tescione, G.J.W. van Bussel, C. Ferreira, submitted to *Journal of Wind Engineering and Industrial Aerodynamics* on February 2016 (Tescione *et al.*, 2016).

4.1. APPROACH

The present chapter follows up on the experimental analysis of chapter 2 and the verification and validation of the 3D unsteady free vortex-wake model for Vertical Axis Wind Turbine (VAWT) wake aerodynamics of chapter 3. The same numerical model is used to extend the experimental analysis from a model turbine to a full-scale 5-MW machine and in a more detailed and extended domain. While the experimental analysis was focused on phase-locked measurements at the horizontal equatorial plane and on 7 vertical stream-wise planes until 3 diameters downstream the turbine shaft, the numerical approach allows visualization of instantaneous flow quantities every 5 degrees, or averaged over one or more converged rotations, inside all the wake domain.

Details on the geometry and operation of the modeled VAWT and its numerical discretization are presented in section 4.2.1, while given the extension of the simulated domain in the stream-wise direction, the convergence of the numerical solution has been re-evaluated in section 4.2.2.

First the 3D topology of the wake of the VAWT is presented with contour plots of stream-wise velocity in planes perpendicular to the wind direction at different downstream locations (section 4.2.3). This sectional view of the evolution of the wake gives a combined idea of the horizontal expansion and vertical contraction, characteristic of the VAWT wake, and provides a phenomenological basis for the following analysis.

Then, the results of the analysis are compared to those of an equivalent Horizontal Axis Wind Turbine (HAWT): the National Renewable Energy Laboratory (NREL) 5-MW turbine (Jonkman *et al.*, 2009), as it represents a typical multi-MW offshore wind turbine and it comes with large availability of research data on it. Section 4.3.1 presents the HAWT and the source of the numerical data used. The equivalence has been obtained by varying the VAWT dimensions and operations in order to match the output power and the frontal area of the HAWT (section 4.3.2).

The comparison is made by considering both the wind field seen by a second wind turbine placed at different downwind position and with variations in horizontal offset, to simulate partial wake operation, and the wake expansion. In order to perform a meaningful, still straightforward, comparison, two new quantities, the Equivalent Velocity Profile (EVP) and the Equivalent Kinetic Energy (EKE) of the wake, have been introduced as opposed to the conventional axial momentum deficit, largely used for HAWT wake models. The results of the comparison are explained (in sections 4.3.3 and 4.3.4) in relation with the topological analysis in the first part of the current research.

4.2. TOPOLOGICAL ANALYSIS OF VAWT WAKE

4.2.1. VAWT MODEL

The VAWT used in this study is a two-bladed H-shaped turbine with straight, un-tapered blades equipped with National Advisory Committee for Aeronautics (NACA) 0018 airfoils. The rotor aspect ratio is $\mathcal{AR} = 1$, leading to a squared frontal area, and the turbine solidity is $\Sigma = 0.12$. The turbine is similar to the one used in the previous experimental study and for the code validation.

The model turbine used in this study is scaled up to match the frontal area and the power of the compared HAWT (see section 4.3.2). Its operation is kept at its optimal tip

speed ratio of $\lambda = 4.5$, as in the experimental campaign and the numerical validation. At this regime it has been shown (section 3.3.1) the blades experience a range of angles of attack below static stall, thus dynamic stall phenomena are avoided.

The tower and the struts are not modeled in order to limit the occurrence of mutual interactions between vortex filaments to increase the numerical stability of the simulation and hence extend the results to further downstream positions. The blades have 30 span-wise and 60 chord-wise panels, with a double cosine distribution, clustered at the tips of the blades and at the trailing and leading edges. An azimuthal step of $\Delta\theta = 5°$ is used for the simulation with an initial transient of 25 rotations, and 6 converged simulated rotations leading to a total of 3720 panels and 550000 vortex filaments at the end of the simulation. The choice of geometrical, temporal discretization and of the initial transient follow the previous validation and verification study of the model. There is no cut-off algorithm of the wake elements, all the vortex filaments are updated during the simulation and are considered for the calculation of the flow fields in the post-process phase.

4.2.2. IMPROVEMENT ON THE CONVERGENCE OF THE NUMERICAL MODEL

The numerical model used for the analysis of the VAWT is based on a panel method coupled with a free vortex wake. The model is capable of 3D, unsteady simulations of flows where vorticity plays an important role, as it lacks the numerical diffusion of grid-based models. For a description of the mathematical formulation and the numerical implementation of the model, as well as for an overview of the model validation the reader is referred to chapter 3.

In the previous validation, aspects as convergence and stability of the model were addressed and results showed a converged and coherent solution after 7 simulated rotations for the rotor flow. The length of the transient needed to reach convergence in the wake increases while the coherence of the periodic solution decreases with the downstream distance.

A spectral analysis on an extended simulation (65 full rotations) showed an expected periodicity of N/Ω (N being the number of blades and Ω the rotational speed of the rotor), for all the downwind positions considered. However, an increased amount of energy is found at lower frequencies as one moves downstream away from the rotor.

At this point it is not completely clear if such oscillations result from the numerical implementation or represent a physical phenomenon, such as an organization of the tip vortices in bigger structures. What is clear is that the average over one rotation is not able to represent the mean value of velocity deficit in the wake as it considers only partially such oscillations.

Figure 4.1 shows the convergence of the solution at different downwind locations. The average in the vertical direction at $y/R = 0$ and $-H/2 \leq z \leq H/2$ of the stream-wise velocity component (EVP) is selected as the evaluation parameter. To account for the lower frequency oscillations it is averaged over 6 continuous rotations. It is shown that further downstream locations reach convergence later with higher oscillations around the converged average value.

At a value of 25 rotations a very good convergence is seen for $x/R < 6$ and a good convergence until $x/R = 12$, with velocity oscillations of 0.8%, 2.5% and 4.2% for $x/R =$

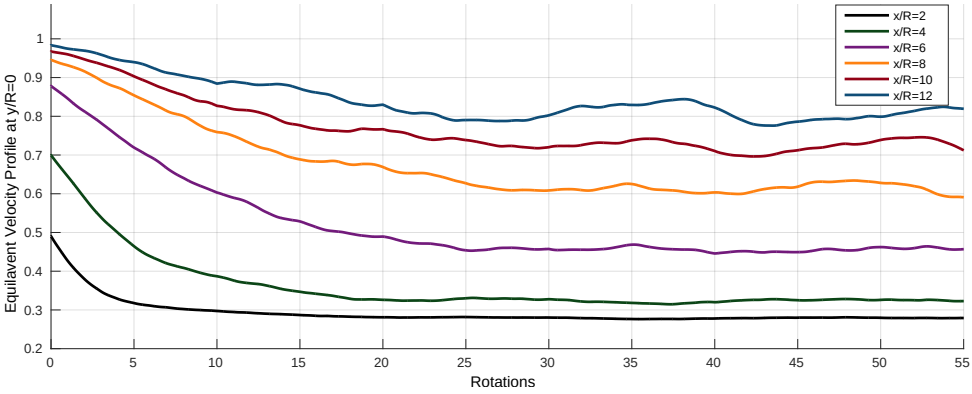

Figure 4.1: Convergence analysis for the EVP at $y/R = 0$ averaged over 6 continuous rotations for different downwind positions x/R

2, 6 and 12. These values represent the maximum oscillations present in the domain as different y/R positions imply only partial wake operation.

4.2.3. WAKE SECTIONS

The three-dimensional topology of the wake of the VAWT is presented in figs. 4.2a to 4.3f, with flow fields in planes perpendicular to the wind direction at different downstream locations. The vectors are in the yz plane and the contours show the stream-wise (out of plane) non-dimensional velocity component, V_x/V_∞. The vectors are scaled within each plot to allow for maximum readability, hence the scale factor is not kept across multiple plots.

This sectional view of the wake allows a simultaneous view of the horizontal expansion and vertical contraction. It also represents the incoming flow field that a second turbine placed a different downwind locations would encounter, giving a visual aid to the analysis of the energy content in the wake of VAWT (see section 4.3.3).

Figure 4.3b, taken at 3 radii downstream the turbine shaft, shows the presence of four vortical structures at the corners of the wake. These vortices extract flow from the wake lateral sides and inject undisturbed flow from the top and bottom sides into the wake. This leads to the characteristic ∞ shape of the wake of a H-shaped VAWT (H-VAWT). The position of these vortical structures, starting to appear immediately at $x/R = 0$, seems to be stable, at least until $x/R = 5$, after that the structures spread out and move without a distinct pattern.

The flow fields show a continuous expansion in the horizontal direction and an initial contraction in the vertical direction until $x/R = 5$ followed by a gradual expansion in both directions. At the same time the induction in the central part of the wake experiences an increase until $x/R = 5$, and a following decrease further downstream.

It is worth mentioning that since spatial oscillations of the wake have been observed for the instantaneous flow fields, the spread-out of the vortical structures, the vertical expansion and the decrease of the induction for the most downwind locations are partially a consequence of the time averaging process described in section 4.2.2. As in the

case of wake meandering (Ainslie, 1988) or vortex wandering (Oweis & Ceccio, 2005), the oscillations imply that any Eulerian time-average is actually a weighted average in both time and space, leading to a smoothing of the vortices and a lower velocity deficit. However, since our focus is to evaluate the effect of the wake on a downwind turbine (fixed in space), the Eulerian time-average is used without corrections as representative of the mean characteristics of the incoming flow.

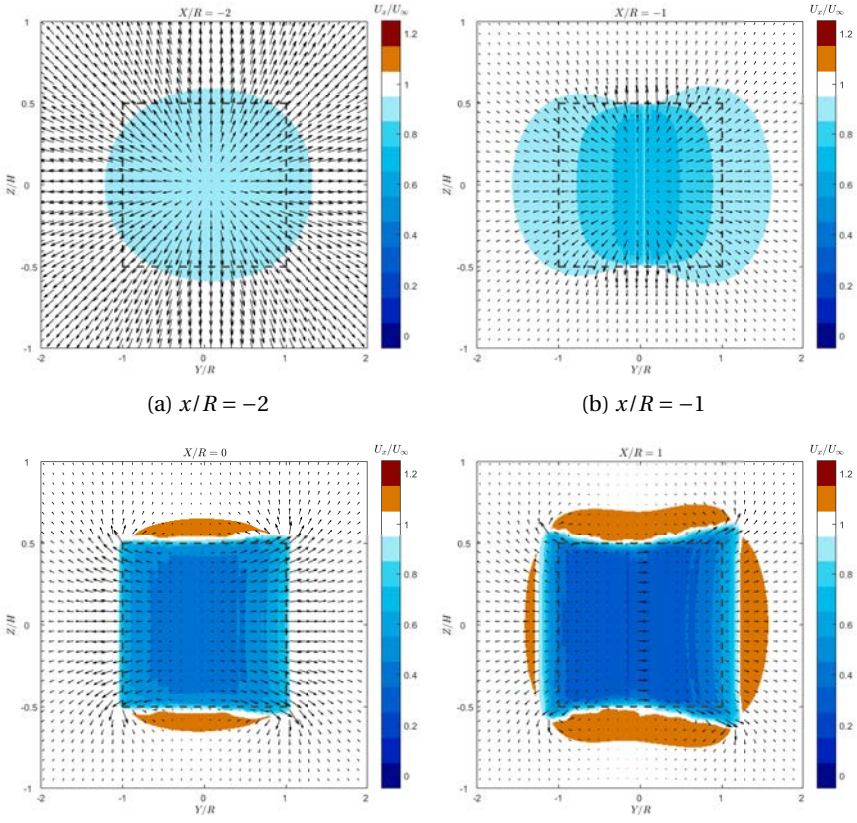

(a) $x/R = -2$ (b) $x/R = -1$

(c) $x/R = 0$ (d) $x/R = 1$

Figure 4.2: Flow field in the wake at different downstream locations

4.3. COMPARISON OF VAWT AND HAWT WAKES

4.3.1. HAWT MODEL

The HAWT chosen for this comparison is the NREL 5-MW reference wind turbine, as representative of multi-MW offshore conventional HAWT and because of the variety of existing studies and literature about it. For a detailed description of the turbine the reader is referred to Jonkman *et al.* (2009).

The data used in the present paper comes from Anderson *et al.* (2015) and the wake

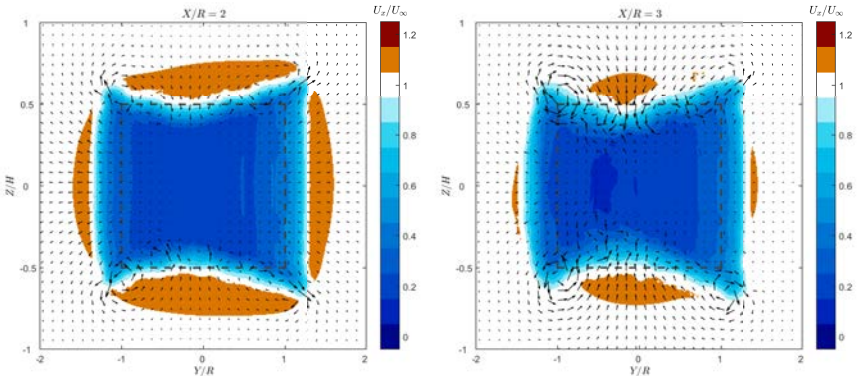

(a) $x/R = 2$ (b) $x/R = 3$

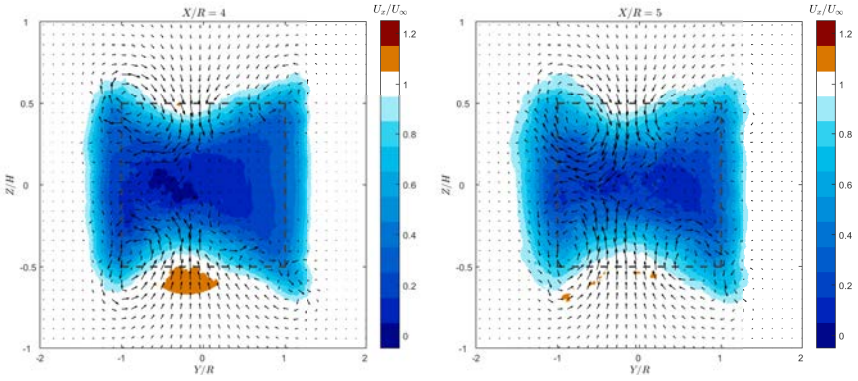

(c) $x/R = 4$ (d) $x/R = 5$

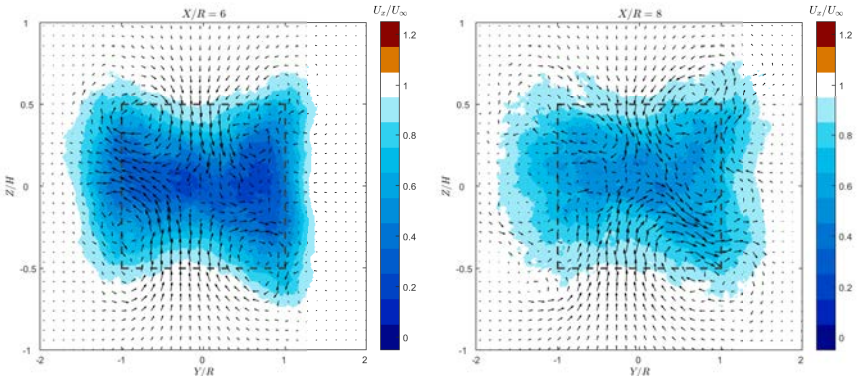

(e) $x/R = 6$ (f) $x/R = 8$

Figure 4.3: Flow field in the wake at different downstream locations (continued)

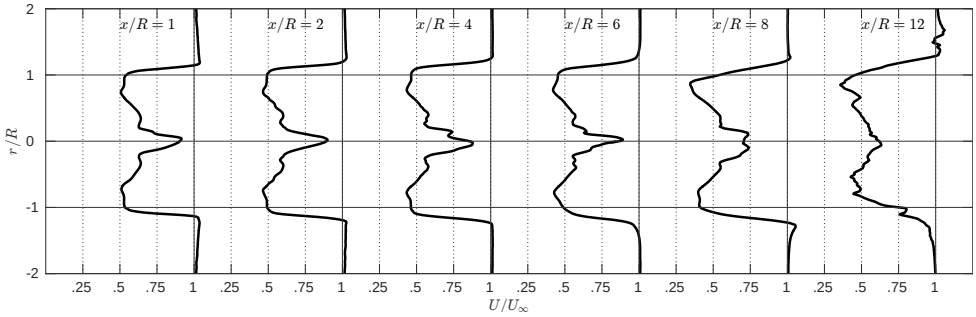

Figure 4.4: Axial velocity profile predicted by SOWFA for NREL 5-MW rotor at $V_\infty = 11 m/s$ and $\lambda = 7.13$, from Anderson *et al.* (2015)

characteristics are obtained with the NREL Simulator for Offshore Wind Farm Applications (SOWFA), which uses Large Eddy Simulation (LES) to model the flow field. For a detailed description of the numerical model the reader is referred to Churchfield & Lee (2015), while for the sensitivity analysis of the data used the reader is referred to Anderson *et al.* (2015).

The data obtained are the axial velocity profiles in radial direction at different wake sections ($x/R = 1, 2, 4, 6, 8$, and 12) for the NREL 5-MW operational point just below rated power ($V_\infty = 11 m/s, \lambda = 7.13$), on a grid with a 1 m grid size up to 6 diameters downstream as shown in fig. 4.4. The use of an LES model with a fine near wake grid is based on the need to limit the numerical dissipation of the bigger vortical structures in order to perform a valid comparison with the dissipation-free vortex model used for the VAWT simulation.

4.3.2. SIZING OF THE EQUIVALENT TURBINES

In order to establish a meaningful comparison of the development of the HAWT and VAWT wakes, the turbines have been equally scaled and their operation has to be set equivalent.

The geometry of the NREL 5-MW turbine is kept as it is and the simulated operational point is at a wind speed of 11 m/s and a tip speed ratio of $\lambda = 7.13$. This operation is below the rated power of the turbine, before the blades are pitched, and the wind speed represents a characteristic value for an offshore turbine.

The VAWT has been sized to match the frontal area of the HAWT, and the power output. At a tip speed ratio of $\lambda = 4.5$ the resulting VAWT has a blade span of 112 m. Table 4.1 summarizes the dimensions and the output of the turbines, while fig. 4.5 shows the frontal view of the two turbines together. The frontal and swept area of the HAWT are the same, while for the VAWT the swept area is the cylindrical surface covered by the blade in its rotation and is π times larger than the frontal area.

4.3.3. EQUIVALENT VELOCITY PROFILE AND KINETIC ENERGY

The time-averaged axial velocity profiles (V_x/V_∞) as presented in section 4.3.1, or the complementary velocity deficit ($1 - V_x/V_\infty$), are common representations for a wake of

	VAWT	HAWT
diameter (m)	112	126
number of blades	2	3
blade span (m)	112	63
tower height (m)	115	90
total height (m)	137	153
mean chord (m)	6.72	3.42
frontal area (m^2)	12544	12469
swept area (m^2)	39408	12469
wind speed (m/s)	11	11
rotor speed (rpm)	8.44	11.89
tip speed ratio	4.50	7.13
C_P	0.51	0.50
power (MW)	5.21	5.06
C_T	0.88	0.75
thrust (MN)	0.815	0.693
torque (MNm)	5.895	4.065
Re_{MAX}	3.32×10^7	9.10×10^6

Table 4.1: Dimensions and operation of the equivalent turbines

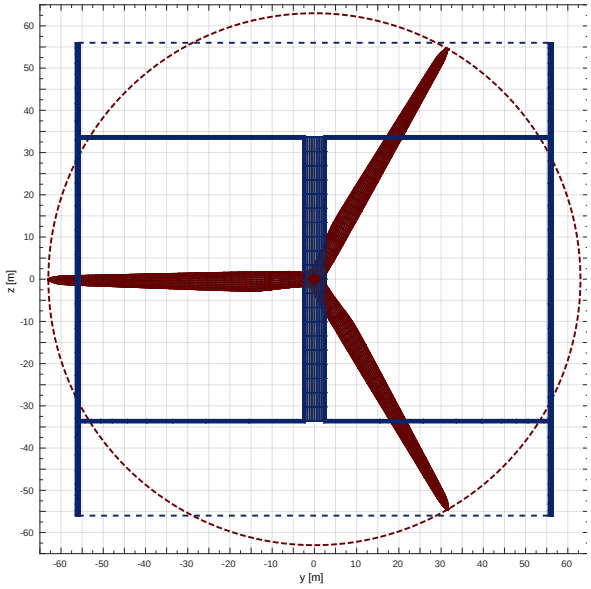

Figure 4.5: Frontal view of VAWT (blue) and HAWT (red), showing the equivalence of the turbines

an HAWT. Given the axial symmetry of the turbine and of the incoming flow, 2D wake models are for HAWT a simple, yet effective, way of describing the flow field behind a turbine. Although the data used in this comparison come from a 3D LES simulation as described in Anderson *et al.* (2015), the authors reduced the 3D flow to 2D flows in radial planes, or simpler radial profiles at specific downstream locations.

In the case of VAWT, the axial symmetry is not present and 3D flows cannot be reduced to 2D flows without loosing relevant details. The comparison of the stream-wise velocity deficit between HAWT and VAWT should either be done on the full 3D flows, or on the 2D flow extracted at specific downstream locations.

With the idea of keeping the comparison straightforward to 1D profiles at specific downstream positions, as the one shown in section 4.3.1, we introduce 2 new quantities: the Equivalent Velocity Profile (EVP) and the Equivalent Kinetic Energy (EKE). For the VAWT, the EVP is computed as the average in the vertical direction between $z = -H/2$ and $z = H/2$ of the stream-wise component of the velocity, while the EKE is the integral of the stream-wise component of the kinetic energy performed over a squared area of a similar downwind turbine (S_D) with center in X_D, Y_D. Both quantities are normalized with respect to the free stream velocity and the domain of integration. For a VAWT wake the following relations hold:

$$EVP(\bar{x},\bar{y}) = \frac{1}{H}\frac{1}{V_\infty}\int_{-H/2}^{H/2} V_x(\bar{x},\bar{y},z)\,\mathrm{d}z$$

$$EKE(X_D,Y_D) = \frac{1}{2RH}\frac{1}{V_\infty^2}\iint_{S_D} V_x^2(X_D,y,z)\,\mathrm{d}y\,\mathrm{d}z$$

$$\text{with } S_D : x \in \left[\frac{-H}{2},\frac{H}{2}\right], y \in [Y_D - R, Y_D + R]$$

For the HAWT, the EVP is equal to the axial velocity profile, while the EKE is calculated as for the VAWT, except that the integration area (S_D) is a circle. Hence for a HAWT wake the following relations are valid:

$$EVP(\bar{x},\bar{y}) = V_x(\bar{x},\bar{y},0)/V_\infty$$

$$EKE(X_D,Y_D) = \frac{1}{\pi R^2}\frac{1}{V_\infty^2}\iint_{S_D} V_x^2(X_D,y,z)\,\mathrm{d}y\,\mathrm{d}z$$

$$\text{with } S_D : (y - Y_D)^2 + z^2 = R^2$$

In this way two 2D quantities are obtained and, at specific downstream locations, a set of 1D profiles can be compared. Such comparison is presented in figs. 4.6 and 4.7 for the VAWT (black continuous lines) and the HAWT (red dashed lines) at 6 different downstream locations ($x/R = 1, 2, 4, 6, 8$, and 12). The VAWT profiles include error bands (shown at selected y/R locations) computed as the max variations of the running averages after convergence as explained in section 4.2.2.

The first consideration to be made concerns the shape of the EVP profiles in fig. 4.6. The VAWT wake profiles show an initial deep U shape caused by the blade extracting

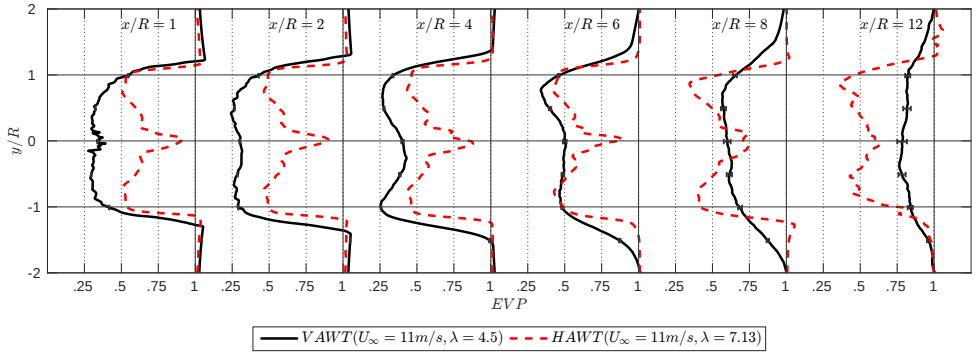

Figure 4.6: Comparison of Equivalent Velocity Profiles for VAWT (black) and HAWT (red) equivalent turbines.

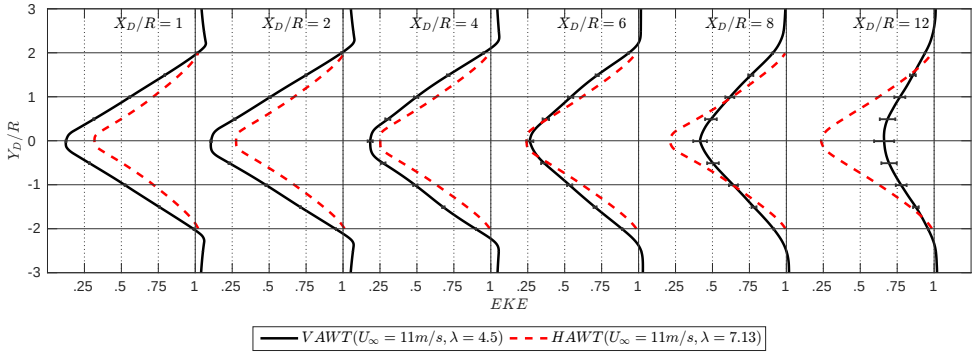

Figure 4.7: Comparison of Equivalent Kinetic Energy for VAWT (black) and HAWT (red) equivalent turbines

most of the energy around $y/R = 0$. The profiles gradually change into a W shape, as a consequence of the vertical contraction of the wake around $y/R = 0$ which decreases the average velocity deficit. Finally the profiles tend to flatten out due to the ceased vertical motion and continuous horizontal expansion (as explained in sections 4.2.3 and 4.3.4). The inherent asymmetry of the VAWT wake observed in section 4.2.3 and other studies (Dixon, 2008; Ferreira, 2009; Scheurich *et al.*, 2011; Tescione *et al.*, 2014) is still visible, but softened by the averaging in the z direction. The vertical motion of the vortices implies more energetic flow at $z/H = \pm 0.5$ but also a greater induction at $z/H = 0$, and these two effects cancel out to a certain extent.

The HAWT wake profiles show the typical W shape caused by the circulation distribution of the blade and the presence of the root vortices. Moreover such shapes are fundamentally symmetric through all the observed extension (though in the LES results for the HAWT slight asymmetries are observed as well).

In fig. 4.7 the values of the EKE are shown as a function of wake distance (X_D) and sideways displacement of the integration area (Y_D). The reader is reminded that the EKE is a measure of the available kinetic energy in the wake over an area equal to the frontal area of the wind turbine. The comparison shows how the VAWT experiences a higher

energy deficit in the near wake (up to 2 diameters) with a minimum energy content of 12% and 11% at $X_D/R = 1$ and 2 respectively. Thanks to the entrapment of kinetic energy following the vertical contraction, the VAWT wake experiences an increase in energy content starting from $X_D/R = 4$. The minimum values of the EKE are indeed $18\% \pm 2\%$, $26\% \pm 2\%$, $42\% \pm 5\%$ and $66\% \pm 7\%$ at wake locations $X_D/R = 4, 6, 8$ and 12.

The minimum energy content of the HAWT wake instead shows a steady decrease from 32% at $X_D/R = 1$ to 21% at $X_D/R = 8$ where the wake starts to recover to a minimum energy content of 24% at $X_D/R = 12$.

For the VAWT it is worth mentioning that the results of the present analysis are the product of a numerical model which has been validated against experimental results until $x/R = 6$ and then extended further downstream. The higher initial velocity deficit and the increase in the EVP are therefore observed also in the experimental data, and the numerical results further downstream conserve the observed trend. The shift from a model turbine to a 5-MW machine, with its higher Re_c, does not influence the confidence of the results from a numerical method based on a potential flow solver.

Attention should be given to the fact that the comparison between HAWT and VAWT wakes is done based on results from different numerical models. The vortex method used for the VAWT wake does not include a viscous diffusion model (only a viscous vortex core model), and is therefore not able to reproduce the energy recovery of the wake due to diffusion. The increase in the energy content showed in fig. 4.7 is only due to the geometric deformation of the wake and is hence a conservative estimation of what would happen if diffusion was included. The LES method used for the HAWT wake does include viscous diffusion, and partially also numerical diffusion, although the use of a fine grid minimizes the latter.

4.3.4. WAKES SPATIAL EXTENSION

In the present section, the spatial extension of the wake of the HAWT and VAWT is considered. The wake boundaries affect the extent of the partial wake operation, as often occurs in wind farms.

Figure 4.8 shows the limits of the two turbines wakes computed as the points where the stream-wise velocity reaches 99% of the free-stream value. For the VAWT both the maximum horizontal limits (black lines) and minimum vertical limits (blue lines) are shown, while for the HAWT, given the axial symmetry, the radial limits (red lines) are shown. The analysis shows how the radial expansion of the HAWT wake lies in between the horizontal and the vertical extension of the VAWT wake. In the horizontal plane the VAWT wake expansion is almost two times the one of the HAWT, with an increase of 23%, 52% and 84% for the former and of 14%, 33% and 49% for the latter at $x/R = 2, 6$ and 12. In the vertical plane the VAWT wake presents a maximum contraction of 25% at $x/R = 4$,followed then by a slight expansion as observed also in section 4.2.3.

To account for the combined vertical and horizontal different extensions of the VAWT wake, fig. 4.9 shows the limit of the two turbines wakes computed as the points where the EKE level reaches 99% of the free-stream value. As the EKE is computed as the integral of the kinetic energy over the frontal area of a second turbine (with its center in X_D, Y_D), its extension is larger than that of fig. 4.8 as a second turbine located on the limit of the upwind turbine wake would still be in partial wake conditions, and is hence taken into

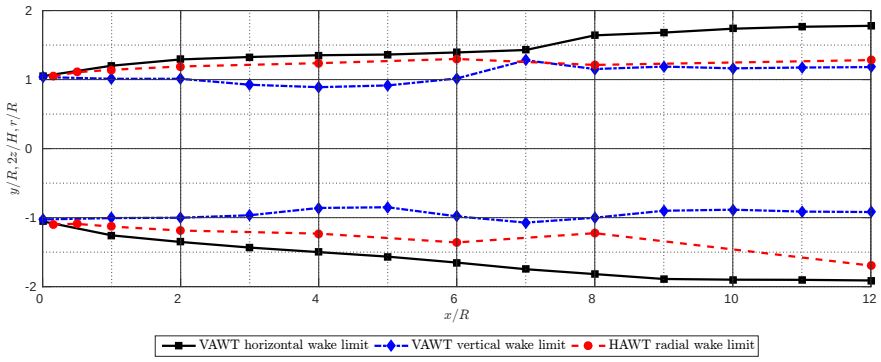

Figure 4.8: Comparison of the wake extension based on local velocity: horizontal VAWT (black), vertical VAWT (blue) and radial HAWT (red).

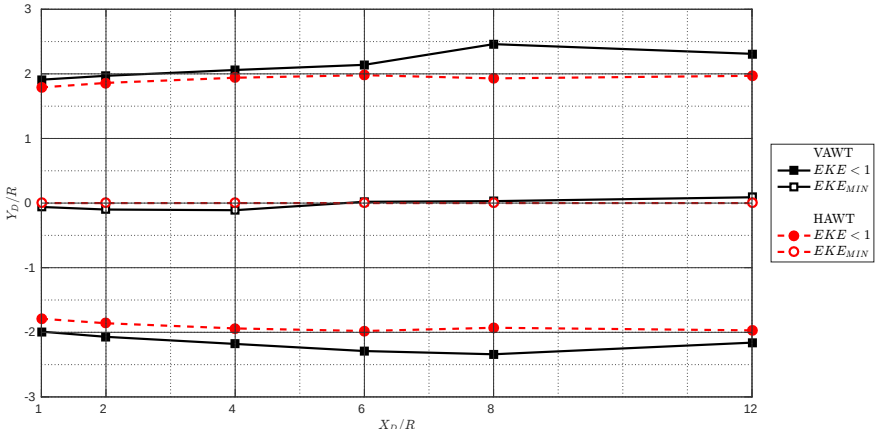

Figure 4.9: Comparison of the wake extension based on EKE levels: VAWT (black), HAWT (red)

account. Figure 4.9 represents the cross-stream spacing between turbines in a cluster for no wake interaction. The results show an area of influence of the HAWT extending to 86%, 98% and 97% while that of the VAWT to 102%, 122% and 124% at $X_D/R = 2, 6$ and 12.

4.4. CONCLUSIONS

The increasing deployment of wind turbines in clusters has shifted the focus of the research to wake aerodynamics and made the development of accurate wake models fundamental for wind farm planning and operation. The recent interest in VAWT for floating offshore devices finds a lack of dedicated wake models with the consequence that HAWT wake models are used with little consideration of their different characteristics.

The current paper presents a numerical analysis of the wake of a 5-MW H-VAWT and compares the results to that of the NREL 5-MW HAWT available in literature. The comparison is made on the lateral expansion and the mean velocity profiles of the two wakes,

and also by considering the kinetic energy available to a second turbine placed in the wake of the first.

The analysis shows the vortical structures responsible for the vertical contraction of the VAWT wake with the associated transport of outer energetic flow inside the area swept by the downwind turbine.

Differently from the case of HAWT, the axial velocity profiles at the symmetry plane cannot be used for VAWT as a tool to predict the output of a downwind turbine. These profiles would, in fact, take into account only the horizontal expansion, which is almost double that of a HAWT, and not consider the vertical contraction. The EVP introduced here is a suitable way to compare HAWT and VAWT wake profiles by performing an average in the vertical direction of the velocity.

Moreover, the EKE provides an adequate way of determining the energy available for extraction of a second similar wind turbine in the wake of an upwind turbine. By comparing the EKE profiles it is shown how the energy content in the wake of a VAWT exceeds that of a HAWT after 3 diameters, with an increase of 20% after 4 diameters and 40% after 6 diameters. At the same time the spatial extension of the perturbed flow behind a VAWT is 25% larger than that of a HAWT. For the studied H-VAWT the stream-wise spacing can be considerably reduced and the cross-stream spacing needs to be slightly increased with respect to a conventional HAWT.

Optimization of wind farms cannot rely solely on the aerodynamic efficiency of rotors but need to include the dynamics of their wakes as well. The present study showed how the use of a VAWT, with its reduced inter-turbines spacing, can be advantageous.

Dedicated wake models, able to include the relevant 3D effects from different VAWT configurations, are needed if proper economical analysis of the different systems in a wind farm scenario is to be performed.

CHAPTER REFERENCES

Ainslie, J.F. 1988. Calculating the flowfield in the wake of wind turbines. *Journal of Wind Engineering and Industrial Aerodynamics*, **27**, 231–224.

Anderson, E.W., Chow, R., & van Dam, C.P. 2015. A comparison of the NREL 5-MW wake characteristics using both SOWFA and OVERFLOW2. *In: 33rd Wind Energy Symposium, AIAA ScitTech, Kissimmee, FL.*

Churchfield, M., & Lee, S. 2015. *NWTC Information Portal (SOWFA).* [https://nwtc.nrel.gov/SOWFA. Last modified 2015-03-31; accessed 2015-12-17].

Dixon, K.R. 2008. *The Near Wake Structure of a Vertical Axis Wind Turbine.* M.Phil. thesis, Delft University of Technology.

Ferreira, C. 2009. *The Near Wake of the VAWT, 2D and 3D Views of the VAWT Aerodynamics.* Ph.D. thesis, Delft University of Technology.

Jonkman, J., Butterfield, S., Musial, W., & Scott, G. 2009. *Definition of a 5-MW Reference Wind Turbine for Offshore System Development.* Tech. rept. NREL/TP-500-380606. National Renewable Energy Laboratory (NREL).

Oweis, G.F., & Ceccio, S.L. 2005. Instantaneous and time-averaged flow fields of multiple vortices in the tip region of a ducted propulsor. *Experiments in Fluids*, **38**, 615–636.

Scheurich, F., Fletcher, T.M., & Brown, R.E. 2011. Simulating the Aerodynamic Performance and Wake Dynamics of a Vertical-Axis Wind Turbine. *Wind Energy*, **14**(2), 159–177.

Tescione, G., Ragni, D., He, C., Ferreira, C., & van Bussel, G.J.W. 2014. Near Wake Flow Analysis of a Vertical Axis Wind Turbine by Stereoscopic Particle Image Velocimetry. *Renewable Energy*, **70**, 47–61.

Tescione, G., Ferreira, C., & van Bussel, G.J.W. 2016. Analysis of a free vortex wake model for the study of the rotor and near wake flow of a vertical axis wind turbine. *Renewable Energy*, **87**, 552–563.

5

CONCLUSIONS AND RECOMMENDATIONS

ONE of the first and main contributions to the aerodynamic research of a VAWT wake of the work of this dissertation comes from the experimental results presented in chapter 2, where the wake dynamics of a model H-VAWT have been documented in detail. The novelty lies in both the detail and the extent of measurements, with the production of phase-locked three-dimensional velocity and out-of-plane vorticity fields in the equatorial plane and on several vertical planes until three rotor diameters from the tower.

The impact of the experimental database created is twofold. From one side it gives researchers the insight into the wake flow phenomena needed to understand the dynamics involved. The use of the Particle Image Velocimetry (PIV) technique, providing simultaneous measurements of instantaneous velocity fields in 2D planes is of great value. Secondly, it creates the basis for validation of advanced numerical models by providing local flow quantities instead of integral parameters that might have hidden cancellation of opposite velocities.

Both aspects have been exploited in the present work, and the conclusions of the research are then conveniently organized in three parts, following the structure of the research questions in section 1.3: a phenomenological description of the flow dynamics from experimental observations, a consideration on the use of a vortex method for the analysis of a VAWT wake, and the conclusions of the numerical analysis extended to a 5-MW VAWT wake and compared with that of a HAWT. Finaly some recommendations for future research topics are given.

5.1. ON THE TOPOLOGY & VORTEX DYNAMICS IN THE WAKE OF VAWTS

In the discussion of the conclusions the division of the vorticity in the wake into a component parallel (*shed vorticity*) and one perpendicular (*trailing vorticity*) to the vertical axis is retained. This distinction is convenient to explain the wake creation and evolution since the two components are caused by distinct physical processes and have dynamics which evolve in different dimensions.

The shed vorticity is a consequence of the change of circulation around the rotating blade and develops in the horizontal planes: it is mainly 2D and a direct consequence of the energy extraction. The trailing vorticity is caused by the finite span of the blades, it rolls up in a system of tip vortices with a strong three-dimensional dynamics.

Different dominant behaviors can be observed if one looks at the horizontal equatorial plane or at the vertical stream-wise planes. However, it is important to stress how there is an underlying strong connection between different views, and the wake is characterized by a complex vorticity system with strong mutual interactions.

THE SHED VORTICITY AND THE EDGE VORTICES

The cycloidal sheet of varying shed vorticity in the equatorial plane is organized in a system of contra-rotating coherent vortical structures at the edges of the wake. The locations of the Blade-Wake Interactions (BWIs) act as *foci* for such roll-up, by both creating an initial deformation of the existing wake geometry and by superimposing a newly shed non-parallel vortex sheet.

Such transition marks the passage from the near-wake, where the individual blade wakes are clearly visible, to the mid-wake, where the edge vortices are the only relevant structures and the wake is characterized by a smooth induction field. For the experiment performed ($\lambda = 4.5$ and $Re_c = 1.7 \times 10^5$) such transition happens after three radii from the shaft. It is hypothesized that tip speed ratio and diffusion effects have an influence on the transition point, however this was not quantified.

In the measured volume ($x/R \leq 4.5$) the edge vortices travel at the horizontal boundaries of the wake, clearly distinct, with no mutual interactions and with a constant speed. They undergo a continuous outward horizontal motion; the windward system of edge vortices, with a rotation opposite to the turbine, is characterized by a more pronounced expansion and a stronger vorticity.

THE TRAILING VORTICITY AND THE TIP VORTICES

H-shaped VAWTs (H-VAWTs) are characterized by a complex system of tip vortices emanated on a cycloidal path with a convex segment released by the upwind blade passage and a concave one released by the downwind passage. Due to the blade rotation and the wake motion, the two parts intersect at different blade azimuth positions with varying angles. Due to the change in pressure/suction sides between the upwind and downwind blade passage, the tip vortices are co-rotating with varying vorticity. The result is

a very unstable system of structures with varying strength and spacing which undergo mutual pair-wise interactions followed by a strong stretching and a rapid diffusion. In the $Re_c = 1.7 \times 10^5$ experiment performed the structures are no longer distinguishable at $x/R \approx 3$.

For all the vertical planes measured the start of the mutual induction marks a change in the vertical motion of the tip vortices. For the central part of the wake an inward motion is observed, while the leeward and windward sides experience a decrease in their rate of outward motion.

THE WAKE TOPOLOGY AND INDUCTION FIELD

The 3D wake of H-VAWTs is characterized by different evolutions in the horizontal and vertical planes and a general asymmetry in both directions. The asymmetry of the wake geometry and of its velocity field increases for the whole range of measurements, suggesting how its origin is not localized at the rotor but transported in the wake.

In the horizontal direction a continuous expansion is observed, with a higher cross-stream velocity at the windward side, while in the vertical direction a contraction in the middle part and an asymmetric expansion at the edges, more pronounced at the windward side, can be seen. Stream-wise velocities are lower at the windward side; the minimum is reached in the equatorial plane, closer to the rotor in the middle of the wake and more downstream for the wake edges. The vertical velocities are almost null at the equatorial plane, indicating a span-wise symmetric flow.

Signs of wake velocity recovery are observed at three radii from the turbine shaft in the central part of the wake and further downstream for both the windward and leeward sides, up to six radii downstream. The velocity recovery proceeds gradually from the vertical edge of the wake towards the center, with the equatorial plane being the place where velocity recovery is later achieved.

5.2. ON THE USE OF A VORTEX METHOD FOR VAWT WAKE ANALYSIS

Given the high content of vorticity in the wake of Vertical Axis Wind Turbines (VAWTs) a Vortex Element Method (VEM) proved to be a very effective tool for aerodynamic simulation, giving accurate detailed instantaneous information on the wake structure and the induction field while avoiding the use of a grid with the associated numerical dissipation and increase in computational time. Recent progress in computer technology, with the development of scientific computations with General Purpose GPU (GPGPU) computing, make VEM of high interest for their high parallelization potential. Although in the present research no complete algorithm optimization was conducted, a simple straightforward Graphic Processing Unit (GPU) parallelization of the wake-to-wake and wake-to-body induction functions led to a speed increase of 25× of the numerical model.

Since the simulation starts with no wake, a transient exists before the wake builds up its induction field and a periodical stationary solution is reached. Convergence is reached at later stage moving downstream the domain. A study on the induction field showed a converged solution after seven rotations in the rotor volume and after 25 rotations up to six diameters in the wake. A non converged solution led to higher Angle of Attack (AoA) perceived by the blade, higher velocities and lower expansion in the wake.

Large scale oscillations are found in the far wake with increasing energy in the lower frequencies with distance. While it is not clear if the numerical solution represents physical wake meandering, the occurrence of periodicity different from the blade passage has to be considered in the averaging process.

The study on the spatial discretization of the blade and on the temporal discretization, both leading to a different grid spacing in the wake lattice structure, showed little sensitivity of the solution. A medium discretization of 30 span-wise and 60 chord-wise panels on the blades and a 5 degrees azimuth step leads to a converged solution and discretization refinements lead to marginal changes in the output.

The numerical uncertainty derives from the discretization error and from the level of coherence of the periodic solution. While the first is constant through all the domain and bounded to 1.5% of V_∞, the latter increases with the downstream distance reaching a level of 7.5% of V_∞ at 6 diameters from the shaft.

All important vortex dynamics are qualitatively well captured by the model, both the vortex roll-up in the horizontal planes and the tip vortex evolution. Quantitatively, the model is capable to accurately predict the near wake evolution in the central part and leeward side. There is a tendency to underestimate the wake expansion at the windward side (both horizontal and vertical) leading to a decrease in the wake asymmetry.

5.3. ON THE COMPARISON BETWEEN VAWT AND HAWT WAKES

In the wake of an H-VAWT the horizontal expansion and the central vertical contraction leads to the characteristic $\infty-$shape, while the near wake of Horizontal Axis Wind Turbines (HAWTs) is characterized by a continuous radial expansion. Contrary to the HAWT wakes, where the axial symmetry allows the reduction to 2D flow in the radial plane, in the case of VAWTs, the highly 3D flow cannot be represented by the 2D flow in the equatorial plane without loosing relevant details. For the same reason the use of a 2D numerical model for the VAWT wake is unsuitable if one is interested in the far wake development, as it would only account for the horizontal wake expansion.

In order to perform a comparison between the two wakes, new quantities have been introduced by integrating the time-averaged stream-wise velocity or the kinetic energy in the vertical direction and in the frontal area of an hypothetical downwind turbine of same dimensions. The equivalent kinetic energy profiles take into account the mechanical transport of the outer flow into the area of the downwind turbine.

A second downwind turbine would experience a less energetic inflow in the first six radii in the wake of a VAWT with respect to the wake of a HAWT. After this distance, in the case of the VAWT wake, the energy content for a downwind turbine is greater than for the HAWT case, with an increase of 20% and 40% at eight and 12 radii. This is the product of the vertical contraction of the VAWT wake which brings undisturbed flow in the downwind turbine's swept area.

At the same time the wake of a VAWT has a 25% larger expansion in the horizontal direction than the wake of a HAWT. The increase in the horizontal wake expansion would rise to almost 50% if one considers only the equatorial plane of the VAWT wake.

The different wake behavior needs to be considered for wind farm optimization and operation. The use of VAWTs in a wind farm could potentially decrease the stream-wise spacing between the turbines and the associated land and electrical grid costs. At the same time the cross-stream spacing needs to be increased to account for the slight increase of wake expansion.

This research proved the inapplicability of HAWT wake models to the case of VAWT wakes, as well as the use of simplified 2D models for far wake analysis. In order to perform a proper evaluation of the wake effects, VAWT wakes need a new model capable of taking into account all the 3D dynamics, the vertical transport of flow and the inherent asymmetry.

5.4. RECOMMENDATIONS FOR FURTHER RESEARCH TOPICS

During the present research a number of interesting topics and further improvements have been identified which are recommended for future research:

- During the experimental activity one of the most interesting and unexpected results was the strong interaction between the upwind-generated and downwind-generated vortex curve and how this led to an earlier vortex breakdown and vertical contraction of the wake. More investigation on this phenomenon is recommended, especially exploring the possibility to use the tip speed ratio as a design parameter to control such instability and the wake recovery.

- A further experimental follow-up involves the interaction between the edge vortices and the tip vortices in terms of transfer of vorticity that the present research could not address properly. The use of full volumetric experimental techniques, such as Tomographic PIV, might be required for this.

- As the title of this dissertation suggests, this is the study of A vertical axis wind turbine wake aerodynamics, specifically a straight blade H-VAWT. The possibility to extend the findings to different VAWT configurations in terms of wake development and underlying physics is compelling and requires further experiments and modeling efforts. Although the author believes the extension of the vortic-

ity dynamics in the horizontal plane to be rather straightforward, the tip vortex evolution and the 3D wake topology will differ considerably for different rotor geometries. Furthermore parameters as tip speed ratio, number of blades and blade solidity or rotor aspect ratio were not addressed and need further study.

- From the numerical point of view, the use of a vortex method for VAWT wake aerodynamics holds great potential but brings also major challenges. A sequence of refinements that were initially considered did not find the necessary resources and are left to future development. The stability of the wake lattice for long simulations, the implementation of viscous diffusion and a higher order handling of the BWI are the main improvement areas. In view of the latter, and also of the initial generation of vorticity, the use of an hybrid Lagrangian-Eulerian method is probably the most interesting and promising improvement.

- The spectral analysis of the numerical simulation of the up-scaled 5-MW turbine for longer wake extension showed an increasing amount of energy at frequency smaller than N/Σ. It was not possible to conclude if such oscillations were the effect of the numerical model or represented a physical phenomenon, and more experimental activity is needed to address such issue.

About the Author

Giuseppe Tescione was born in Rome, Italy, on the 20th of May 1981. He completed a M.Sc in Aeronautical Engineering from the Università La Sapienza of Rome in 2009. He was first introduced to Wind Energy during his exchange year at the faculty of Aerospace Engineering of the University of Technology of Delft, the Netherlands He then returned to TUDelft at the end of his M.Sc. as a guest researcher in the department of Wind Energy to work on his experimental thesis on the blade flow of an horizontal axis wind turbine.

He was later on offered a position in the same department for a doctoral research on the Aerodynamics of the wake of a vertical axis wind turbine, presented in this dissertation. He now works as an applied aerodynamicist specialist in the wind energy industry in Denmark.

Besides being a researcher, an experimentalist, an applied aerodynamicist and a convinced supporter of wind energy, he is also a musician and a great music lover, a photographer (both digital and film photography), a tireless traveler, a motorcyclist and a rock climber.

LIST OF PUBLICATIONS

7. **G. Tescione**, C. Ferreira, and G. van Bussel, *A Comparison of the Wake Evolution for 5-MW Vertical and Horizontal Wind Turbines*, Journal of Wind Engineering and Industrial Aerodynamics, *under review* (2016).

6. **G. Tescione**, C. Ferreira, and G. van Bussel, *Analysis of a Free Vortex Wake Model for the Study of the Rotor and Near Wake Flow of a Vertical Axis Wind Turbine*, Renewable Energy, **87**, 552-563 (2016).

5. D. Castelein, D. Ragni, **G. Tescione**, C. Ferreira, and M. Gaunaa, *Creating a benchmark of Vertical Axis Wind Turbines in Dynamic Stall for validating numerical models*, 33rd ASME Wind Energy Symposium, AIAA SciTech (AIAA 2015-0723).

4. **G. Tescione**, D. Ragni, C. He, C. Ferreira, and G. van Bussel, *Near Wake Flow Analysis of a Vertical Axis Wind Turbine by Stereoscopic Particle Image Velocimetry*, Renewable Energy **70**, 47-71 (2014).

3. **G. Tescione**, D. Ragni, C. He, C. Ferreira, and G. van Bussel, *PIV-Based Analysis of 2D and 3D Flow Phenomena of Vertical Axis Wind Turbine Aerodynamics*, 32nd ASME Wind Energy Symposium, AIAA SciTech (AIAA 2014-1080).

2. B. Akay, C. Ferreira, G. van Bussel, and **G. Tescione**, *Experimental Investigation of the Wind Turbine Blade Root Flow*, 48th AIAA Aerospace Sciences Meeting (AIAA 2010-641).

1. B. Akay, C. Ferreira, G. van Bussel, and **G. Tescione**, *Experimental and Numerical Investigation of the Effect of Rotor Blockage on Wake Expansion*, 3rd EWEA Conference, Torque (2010).